Glass Filters Made from Capillary Suspensions

Zur Erlangung des akademischen Grades eines
DOKTORS DER INGENIEURWISSENSCHAFTEN (DR.-ING.)

von der KIT-Fakultät für Chemieingenieurwesen und Verfahrenstechnik des
Karlsruher Instituts für Technologie (KIT)
genehmigte

DISSERTATION

von

M. Sc. Kevin Tedjokusuma

aus Surabaya, Indonesien

Tag der mündlichen Prüfung:	09.10.2025
Erstgutachter:	Prof. Dr. Norbert Willenbacher
Zweitgutachter:	Prof. Dr. Harald Horn

Preface

This dissertation is primarily based on research conducted as part of the project “Development of innovative glass membranes based on capillary suspensions” and was funded by the German Federation of Industrial Research Associations under grant no. 20866 N / 1 and the German Federal Ministry of Economics and Climate Protection based on a resolution of the German Bundestag. Experimental work was conducted at the Institute of Mechanical Process Engineering and Mechanics (MVM) at KIT. This dissertation is mainly grounded in the following publication: K. Tedjokusuma, W. Lauth, N. Willenbacher, Manufacture and filtration performance of glass filters made from capillary suspensions, Separation and Purification Technology 329 (2024) 125097 [1].

Acknowledgement

This dissertation would not have been possible without the support, expertise, and collaboration of many individuals to whom I would like to express my deep appreciation.

First and foremost, I would like to express my sincere gratitude to Prof. Dr. Norbert Willenbacher for providing me with the opportunity to pursue my doctoral studies within his group. His guidance throughout the project — from insightful scientific discussions to his support in my research — has been instrumental in the successful completion of this work. I am also deeply appreciative of the trust he placed in me and the academic freedom he allowed during my research. I would also like to thank Prof. Dr. Harald Horn for kindly taking on the role of second reviewer for this thesis.

I am grateful to Werner Lauth of Weingut Lauth & Sohn for sharing his expertise in filtration processes, which significantly contributed to the experimental aspects of this study. I also extend my thanks to Rudi Flegler, Ralph Hörner, and Manuel Roth of DWK Life Sciences GmbH for their valuable insights into glass manufacturing and their support with the mechanical testing in this research. Their contributions have been deeply appreciated.

I would also like to express my gratitude to Dr. Bernhard Hochstein for his support with technical and organizational matters. My sincere thanks go to Dr. Claude Oelschlaeger for his advices, his positive spirit, and the many uplifting moments. I am also thankful to Thomas Lebe and Volker Zibat for their valuable contributions in the field of electron microscopy, which played an important role in the analytical part of this work. In addition, I acknowledge Klaus Hirsch, Astrid Huber, and Regina Mall for their support with particle preparation and characterization. My appreciation also goes to Karsten Sasso and Olaf Jörg for their technical assistance, which was indispensable for the successful completion of my experiments.

During the course of this doctorate, I had the pleasure of working alongside a number of colleagues whose presence contributed to a collegial, open, and motivating environment. I would like to thank Annika H., Ophélie, David, and Marianne for the many enriching conversations and for sharing the day-to-day of office life. I am also grateful to Kasia, Yiliang, Bo, Max, Karim, Katrin, Hongye, Jonas, Moritz, Annika V., Ronald, and Tillman for the time spent together — both in and beyond the lab — and for their support, team spirit, and the collaborative atmosphere that shaped our work environment. A special thanks goes to Bruna and Felipe, with whom I shared not only many everyday conversations but also reflections and perspectives beyond academic matters.

I would also like to thank the group of students who actively contributed to the experimental work of this project: Torben Sträßner, Beicao Feng, Dilara Örtel, Anubhav Vats, and Doménica Paz. Their commitment and hands-on contributions were an essential part of many successful experiments.

Finally, I would like to express my deepest gratitude to my family. To my parents, Sukanto and Liliek, whose principles and values have always been a guiding force in my life and who have consistently inspired and motivated me. To my sister, Sabrina, for her unwavering support, encouragement, and warmth. Their belief in me has been an essential source of strength throughout this journey.

Abstract

Glass filters are open-pore materials designed to separate particles from liquids or gases. Its function is to trap certain particles either on the filter surface or within the porous structure while allowing the fluids/gases to pass through the pore. Glass is a well-suited material for filters due to its chemical inertness, high temperature resistance and mechanical stability. There are many methods for producing porous glass, including leaching, sol-gel processes, and sintering. Sintering, based on finely ground glass powder, is one of the simplest methods. The process can be either wet or dry. In the dry process, the powder is formed, pressed and partially sintered to increase the mechanical stability. In the wet process, the powder is dispersed into a slurry, formed, dried, and partially sintered at the end.

A special approach for the production of glass filters is the use of capillary suspensions as precursors in a wet process with subsequent sintering. Capillary suspensions are three-phase systems consisting of solid particles and two immiscible liquids. The process begins by suspending particles in a primary liquid to which a small amount of a secondary liquid is added. Upon mixing, a self-organized particle network forms, resulting in significant changes in flow properties. Depending on the type and amount of secondary liquid, the texture of the suspension can vary from liquid or weakly viscoelastic to an elastic gel-like or paste-like consistency. This pasty material is particularly advantageous for forming stable, complex structures. The particle network in capillary suspensions is particularly robust and retains its structure throughout the drying and sintering processes. This results in a final product with a high porosity and a defined, stable pore structure.

Previous research on sintered porous glass filters made from capillary suspensions has demonstrated their potential for achieving high porosity, with pore sizes ranging from 1 to 50 microns [2]. These filters exhibited significantly high permeability for both air and liquids, attributed to their smooth, rounded pore structures. However, some areas are still unexplored. This study extends previous work with a focus on in depth investigation of the manufacturing processes and a thorough examination of filtration performance. In this study, borosilicate glass 3.3, commonly used in laboratories for its superior chemical resistance, low coefficient of thermal expansion, and excellent thermal shock resistance, serves as the material for the filters. The study is divided into two main parts: the first focuses on the manufacturing process, including an investigation of shrinkage behavior and porosity gradient, while the second examines the filtration performance of the glass filters.

In the production of glass filters from capillary suspensions, the drying process, which is accompanied by shrinkage, is crucial. Controlling shrinkage is essential for maintaining

dimensional accuracy and preventing defects, such as cracks, which can significantly affect the structural integrity of the filters. This study investigated dimensional changes in the molded paste throughout the drying and sintering processes. Notably, capillary suspensions can reduce green body shrinkage during drying by 20% compared to those made from pure suspensions. Shrinkage during sintering, primarily driven by particle consolidation, is mainly influenced by the sintering temperature rather than the composition of the suspension. Additionally, capillary suspensions enhance shape accuracy during the debinding process, promoting isotropic shrinkage in all directions.

The pore structure of sintered glass filters produced from capillary suspensions is primarily influenced by the paste composition and key manufacturing parameters, particularly the sintering process. This study examined how two crucial aspects—pore size and porosity—depend on these factors. Pore size is largely controlled by the particle size of the glass powder, while porosity is determined by the solids content of the capillary suspension, sintering activity, and particle size. Additionally, during sintering, a porosity gradient may form due to spatially uneven heat transfer, resulting in localized regions of higher sintering activity. This variation leads to greater solidification and denser pore structures in certain areas, as observed in cross-sectional image analysis of the filters. The porosity gradient intensifies with longer sintering times, affecting the uniformity of the final pore structure. The pore architecture of filters is essential to filtration performance, directly influencing both permeability and mechanical strength. Water permeability is significantly affected by pore size and open porosity, with larger pores and higher porosity yielding greater permeability. Mechanical strength, on the other hand, is primarily a function of porosity and is hardly affected by pore size, particle type or specific manufacturing methods.

Building on previous findings, crack-free glass filters with a uniform porosity gradient, high permeability, and small pore sizes suitable for microfiltration were successfully developed. The second part of the study involved solid-liquid filtration experiments using well-defined spherical polystyrene particles as a model, along with Oenococcus oeni, a lactic acid bacterium which play a key role in the winemaking process. The tests included turbidity and flux measurements during filtration, employing both dead-end and cross-flow setups. The investigation showed that filtration efficiency and flux are strongly influenced by pore size and open porosity.

Alongside monolithic sintered glass filters, asymmetric glass membranes with enhanced permeability have been developed. These membranes consist of a thin functional layer supported by a coarse-pored, thick substrate for mechanical stability. Development focused on optimizing manufacturing parameters to achieve crack-free functional membranes. This involved adjusting the thickness of the membrane layer and optimizing the paste composition.

The resulting asymmetric membranes were characterized for their filter properties and compared with the filtration performance of monolithic sintered filters.

Finally, benchmarking of the filtration performance of capillary suspension-based glass filters against commercially available filters was conducted. The results indicated that the capillary suspension glass filters, made from the same glass powder, exhibited larger pore sizes and higher permeability. Capillary suspension filters with comparable pore size and porosity to the benchmark filter showed significantly higher filtrate flux, demonstrating the competitiveness of this innovative approach for fabrication of glass filters.

Zusammenfassung

Glasfilter sind offenporige Materialien, die dazu dienen, Partikel von Flüssigkeiten oder Gasen zu trennen. Ihre Funktion besteht darin, bestimmte Partikel entweder auf der Filteroberfläche oder innerhalb der porösen Struktur zurückzuhalten, während die Flüssigkeiten/Gase durch die Poren hindurchtreten können. Glas ist aufgrund seiner chemischen Inertheit, hohen Temperaturbeständigkeit und mechanischen Stabilität ein gut geeignetes Material für Filter. Es gibt viele Methoden zur Herstellung von porösem Glas, darunter Auslaugen, Sol-Gel-Verfahren und Sintern. Das Sintern, bei dem fein gemahlenes Glaspulver verwendet wird, ist eines der einfachsten Methoden. Das Verfahren kann entweder nass oder trocken durchgeführt werden. Beim Trockenverfahren wird das Pulver geformt, gepresst und teilweise gesintert, um die mechanische Stabilität zu erhöhen. Beim Nassverfahren wird das Pulver in einer Slurry dispergiert, geformt, getrocknet und am Ende teilweise gesintert.

Ein spezieller Ansatz für die Herstellung von Glasfiltern ist die Verwendung von Kapillarsuspensionen als Vorprodukte in einem Nassverfahren mit anschließendem Sinterprozess. Kapillarsuspensionen sind Dreiphasensysteme, die aus festen Teilchen und zwei nicht mischbaren Flüssigkeiten bestehen. Der Prozess beginnt mit der Suspendierung von Partikeln in einer Hauptflüssigkeit, der eine kleine Menge einer Sekundärflüssigkeit zugesetzt wird. Beim Mischen bildet sich ein selbstorganisiertes Teilchennetzwerk, was zu erheblichen Veränderungen der Fließeigenschaften führt. Je nach Art und Menge der Sekundärflüssigkeit kann die Textur der Suspension von flüssig oder schwach viskoelastisch bis hin zu einer elastischen, gelartigen oder pastenartigen Konsistenz variieren. Dieses pastöse Material ist besonders vorteilhaft für die Formgebung stabiler, komplexer Strukturen. Das Partikelnetzwerk in Kapillarsuspensionen ist besonders robust und behält seine Struktur während des gesamten Trocknungs- und Sinterungsprozesses bei. Das Ergebnis ist ein Endprodukt mit hoher Porosität und einer definierten, stabilen Porenstruktur.

Frühere Studien zu gesinterten porösen Glasfiltern, die aus Kapillarsuspensionen hergestellt wurden, haben gezeigt, dass sich mit dieser Methode eine hohe Porosität mit Porengrößen von 1 bis 50 Mikrometern erzielen lässt [2]. Diese Filter wiesen eine signifikant hohe Durchlässigkeit sowohl für Luft als auch für Flüssigkeiten auf, was auf ihre glatten, abgerundeten Porenstrukturen zurückzuführen ist. Einige Aspekte sind jedoch noch unerforscht. Diese Studie erweitert frühere Arbeiten mit dem Schwerpunkt auf einer umfassenden Untersuchung der Herstellungsprozesse und einer ausführlichen Bewertung der Filtrationsleistung. In dieser Studie wird Borosilikatglas 3.3, das aufgrund seiner hohen chemischen Beständigkeit, seines niedrigen Wärmeausdehnungskoeffizienten und seiner

ausgezeichneten Temperaturwechselbeständigkeit häufig in Laboratorien verwendet wird, als Material für die Filter verwendet. Die Studie besteht aus zwei Hauptteilen: Der erste konzentriert sich auf den Herstellungsprozess, einschließlich der Untersuchung des Schrumpfverhaltens und des Porositätsgradienten, während der zweite die Filtrationsleistung der Glasfilter untersucht.

Bei der Herstellung von Glasfiltern aus kapillaren Suspensionen ist der Trocknungsprozess, der mit Schrumpfung einhergeht, entscheidend. Die Kontrolle der Schrumpfung ist wesentlich, um die dimensionale Genauigkeit zu gewährleisten und Defekte wie Risse zu verhindern, die die strukturelle Integrität der Filter erheblich beeinträchtigen können. Diese Studie untersuchte dimensionale Veränderungen in der geformten Paste während des Trocknungs- und Sinterprozesses. Bemerkenswert ist, dass kapillare Suspensionen die Schrumpfung des grünen Körpers während der Trocknung um 20 % im Vergleich zu solchen, die aus reinen Suspensionen hergestellt werden, reduzieren können. Die Schrumpfung während des Sinterns, die hauptsächlich durch die Konsolidierung der Partikel verursacht wird, wird hauptsächlich durch die Sintertemperatur beeinflusst, nicht jedoch durch die Zusammensetzung der Suspension. Darüber hinaus verbessern kapillare Suspensionen die Formgenauigkeit während des Entbinderungsprozesses, was eine isotrope Schrumpfung in alle Richtungen fördert.

Die Porenstruktur von Sinterglasfiltern, die aus Kapillarsuspensionen hergestellt werden, wird in erster Linie durch die Pastenzusammensetzung und wichtige Herstellungsparameter, insbesondere den Sinterprozess, beeinflusst. In dieser Studie wurde untersucht, wie zwei entscheidende Aspekte - Porengröße und Porosität - von diesen Faktoren abhängen. Die Porengröße wird weitgehend durch die Partikelgröße des Glaspulvers bestimmt, während die Porosität durch den Feststoffgehalt der Kapillarsuspension, die Sinteraktivität und die Partikelgröße bestimmt wird. Darüber hinaus kann sich während des Sinterns aufgrund der räumlich unterschiedlichen Wärmeübertragung ein Porositätsgradient bilden, der zu lokalisierten Bereichen mit höherer Sinteraktivität führt. Diese Variation führt zu einer stärkeren Verfestigung und dichteren Porenstrukturen in bestimmten Bereichen, wie in der Querschnittsbildanalyse der Filter zu beobachten war. Der Porositätsgradient verstärkt sich mit längerer Sinterzeit, was sich auf die Homogenität der endgültigen Porenstruktur auswirkt. Die Porenarchitektur von Filtern ist für die Filtrationsleistung von wesentlicher Bedeutung, da sie sowohl die Permeabilität als auch die mechanische Festigkeit direkt beeinflusst. Die Wasserpermeabilität wird maßgeblich von der Porengröße und der offenen Porosität beeinflusst, wobei größere Poren und eine höhere Porosität zu einer höheren Permeabilität führen. Die mechanische Festigkeit hingegen ist in erster Linie eine Funktion der Porosität und wird durch Porengröße, Partikelart oder spezifische Herstellungsverfahren kaum beeinflusst.

Aufbauend auf früheren Erkenntnissen wurden rissfreie Glasfilter mit gleichmäßigem Porositätsgradienten, hoher Durchlässigkeit und kleinen Porengrößen, die für Mikrofiltration geeignet sind, erfolgreich entwickelt. Der zweite Teil der Studie umfasste Experimente zur Fest-Flüssig-Filtration unter Verwendung von wohldefinierten sphärischen Polystyrolpartikeln als Modell, zusammen mit *Oenococcus oeni*, einem Milchsäurebakterium, das bei der Weinherstellung eine Schlüsselrolle spielt. Die Tests umfassten Trübungs- und Durchflussmessungen während der Filtration, wobei sowohl Dead-End- als auch Cross-Flow-Anordnungen verwendet wurden. Die Untersuchung zeigte, dass die Filtrationseffizienz und der Durchfluss stark von der Porengröße und der offenen Porosität beeinflusst werden.

Neben monolithischen Sinterglasfiltern wurden auch asymmetrische Glasmembranen mit erhöhter Permeabilität entwickelt. Diese Membranen bestehen aus einer dünnen funktionellen Schicht, die von einem grobporigen, dicken Substrat getragen wird, das für mechanische Stabilität sorgt. Die Entwicklung konzentrierte sich auf die Optimierung der Herstellungsparameter, um rissfreie Funktionsmembranen zu erhalten. Dazu gehörten die Anpassung der Dicke der Membranschicht und die Optimierung der Pastenzusammensetzung. Die resultierenden asymmetrischen Membranen wurden hinsichtlich ihrer Filtereigenschaften charakterisiert und mit der Filtrationsleistung von monolithischen Sinterfiltern verglichen.

Abschließend wurde ein Benchmarking der Filtrationsleistung von Glasfiltern auf Kapillarsuspensionsbasis mit handelsüblichen Filtern durchgeführt. Die Ergebnisse zeigten, dass die Kapillarsuspensions-Glasfilter, die aus demselben Glaspulver hergestellt wurden, größere Poren und eine höhere Durchlässigkeit aufwiesen. Kapillarsuspensionsfilter mit vergleichbarer Porengröße und Porosität wie der Benchmark-Filter zeigten einen deutlich höheren Filtratfluss, was die Wettbewerbsfähigkeit dieses innovativen Ansatzes für die Herstellung von Glasfiltern unterstreicht.

Contents

1 Introduction

Microfiltration is an essential technique in various scientific and industrial applications, particularly for the separation of particulate matter from liquids. The process is effective for particles ranging from 0.1 to 10 µm in size [3,4], making it widely applicable in many fields. For example, microfiltration is widely used in drinking water purification [5,6], pharmaceutical manufacturing [7,8], food and beverage processing [9,10] and wastewater treatment [11,12]. A wide range of materials are used in the manufacture of filters and membranes, which can be broadly categorized into organic and inorganic types [13,14]. Organic membranes are typically polymer-based. Notable examples include polyvinylidene difluoride (PVDF) and polyethersulfone (PES), both of which offer specific advantages in terms of flexibility, cost, and ease of fabrication. In contrast, inorganic materials, such as ceramics and glass, are recognized for their superior chemical stability and mechanical robustness. These properties allow ceramic and glass-based filters to withstand higher pressures and provide longer service life compared to polymeric membranes. Common ceramic materials used in filtration include aluminum oxide (Al_2O_3), titanium dioxide (TiO_2), silicon carbide (SiC), and various types of glass. Among inorganic materials, borosilicate glass has attracted considerable interest for filtration applications. In particular, its superior chemical resistance, low coefficient of thermal expansion, and excellent thermal shock resistance [15–17] make it particularly well-suited for use in harsh filtration environments characterized by chemical exposure, rapid temperature changes, and mechanical stress. These properties motivated the selection of borosilicate glass as filter material for this study.

Filter possesses an open porous structure with interconnected pores, allowing fluids to flow through while removing particle from fluids. There are various established methods to manufacture open porous glass. The glass fiber filter found normally in the laboratory is made through a process similar to woven fabric production and also paper production. Monolithic glass filter can be produced through leaching of phase-separated glass [18,19], sol-gel process [20,21] and sintering of glass powder [22], among others. Due to the simple and cost-effective processes, the sintering process is widely used for the production of open-pore glasses for filtration applications. For this method, glass powder is first produced by grinding or milling. The glass powder can be further processed either in the dry or wet state. For the dry processing route, the glass powder is shaped with a mold, possibly also compressed to increase the stability, and finally sintered. The glass is partially sintered so as to achieve a sufficiently high stability without significantly reducing the pore volume. In wet processing route, the glass powder is homogeneously mixed with additives and binders. The mixed powder can be formed then by using various techniques such as cold pressing, slip casting as well as extrusion or 3D printing. The resulting green body is debinded to remove

organic matter and finally partially sintered. The pore structure can also be adjusted by adding inert material or salt as pore forming agent to the glass powder, which can be washed or leached at low temperature afterwards [19,23]. An alternative approach for adjusting pore structure is the foam replica method [24,25], which uses a foam template immersed in a glass particle slurry to coat the foam struts. During thermal treatment, the foam decomposes while the glass particles sinter, resulting in a porous structure that mimics the original foam's architecture. Compared to dry processing, wet processing can better control particle–particle interactions and increase the homogeneity of particle packing. Lesser and smaller defects can be expected in the final microstructures, as compared with dry processing [26].

In this work, wet processing methods based on capillary suspensions were employed to manufacture porous glass filters through a sintering approach. Capillary suspensions [27] serve as versatile precursors to produce sintered porous materials that exhibit both high porosity and mechanical strength [28]. This method allows for the production of sintered materials with open porosity exceeding 50% and pore sizes ranging between 0.1 and 10 µm, a characteristic that is exclusively accessible via this route [2,29]. Capillary suspensions consist of three phases: a primary liquid, dispersed solid particles, and a small amount of secondary liquid, which is immiscible with the primary liquid. To prepare these suspensions, the solid particles are first dispersed into the primary liquid and homogenized by mixing. The secondary liquid is then added and mixed, inducing the formation of a self-organized particle network throughout the system, regardless of whether the secondary liquid preferentially wets the particles [27]. When the secondary fluid preferentially wets the particles in the atmosphere of the primary liquid, pendular bridges of the secondary fluid form, connecting adjacent particles within the particle network. Conversely, if the secondary fluid does not wet the particles well, the system seeks to minimize its free energy, leading to the entrapment of secondary fluid droplets within particle clusters. These clusters then self-assemble into a percolating network. The strength of the network in capillary suspension is governed by factors such as particle size, the interfacial tension between the liquids, and the three-phase contact angle of the secondary liquid on the particle surface in the presence of the primary liquid. These capillary forces significantly alter the bulk rheological behavior of the suspension, transforming it from a predominantly viscous or weakly elastic state (as seen in suspensions with only a primary liquid and dispersed particles) to a highly elastic or gel-like state with a notable increase in yield stress upon the addition of the secondary liquid [27]. The high yield stress of capillary suspensions ensures excellent green body stability and high precision in molding, allowing for the fabrication of complex geometries [30]. After shaping, the green body undergoes debinding to remove most of the liquid, leaving primarily the solid particles. The debinded body is then finally partially sintered to enhance mechanical stability. A key feature of this method is that the particle network formed within

the capillary suspension largely remains intact even after liquid removal and sintering. Additionally, the sintered body derived from the capillary suspension exhibits significantly less shrinkage compared to those made from conventional pastes. Both aspects contribute to the formation of a highly porous structure in the final sintered material [2,29,30].

During the manufacturing process of glass filters derived from capillary suspensions, control of shrinkage behavior is critical to ensure dimensional accuracy and prevent defects such as cracks [31–34]. Excessive stress induced by shrinkage can significantly compromise the structural integrity of the final product. The drying and debinding phases inherent in the wet processing route, including the capillary suspension method, are particularly associated with shrinkage. During this process, liquid is gradually removed from the system. The reduction in liquid content leads to the formation of menisci and the build-up of capillary pressure, which collectively exert a contractile force on the particles, resulting in shrinkage [33]. In addition, the subsequent sintering process, which densifies the particle structure, may also cause shrinkage. In general, shrinkage can be mitigated by strategies such as increasing solids content and achieving a broad particle size distribution [35,36]. A comprehensive understanding of shrinkage behavior is essential not only to prevent defects, but also to ensure the dimensional stability of the glass filters throughout the manufacturing process.

The pore structure, specifically the porosity and pore size of the capillary suspension filter, is determined by both the material composition and the manufacturing process. A fundamental understanding of these factors is essential to effectively control the pore structure of the final product. Material composition is a variable that includes the specific glass powder used and the ratio of each component within the precursor paste mixture. Another important determining factor is the sintering conditions. Key parameters such as the heating rate, holding time at the sintering temperature, and the sintering temperature itself have a significant effect on the densification process and thus the pore structure. In addition, a phenomenon known as a porosity gradient may also occur during the sintering process [37–41]. This gradient results from a spatially inhomogeneous temperature distribution across the green body, leading to locally varying sintering kinetics. Since sintering kinetics are highly temperature dependent, regions with elevated temperatures undergo accelerated sintering, resulting in denser, less porous structures. Consequently, this phenomenon contributes to an inhomogeneous particle structure in the final sintered body. Heat transfer plays a critical role in determining the temperature profile within the furnace, which directly affects the pore structure of the sintered material. Controlling the pore structure by effectively managing the above factors - such as the composition of the capillary suspension and the sintering conditions - is crucial, since the permeability and filtration performance are strongly dependent on the pore structure.

Due to its versatility, capillary suspension has been also used in thin film coating applications. In the past, a functional alumina filtration membrane made of capillary suspension in an asymmetric arrangement has been successfully developed by thin film coating process [42]. This so-called asymmetric membrane consists of a very thin layer of fine-pore membrane serving as the functional filter, supported by a coarse-pore thick layer underneath to stabilize the thin filter membrane. The thickness of the thin membrane layer is responsible for the higher filtration flux and lower filtration resistance compared to conventional monolithic filters. However, this reduced thickness also makes it more susceptible to structural instability, which is why the coarse-pored support layer is incorporated underneath. The coarseness of the support layer's pore structure is essential to prevent the substrate from interfering with the filtration performance. It is important to note that thin suspension films are prone to cracking and defects during the drying process [43–46]. As the wet suspension film loses liquid, the distance between particles decreases, leading to the gradual formation of capillary bridges. The resulting capillary forces exert internal stress, which can ultimately cause crack formation. During sintering, additional cracks may occur if there is a mismatch in the thermal expansion coefficients of the layers [47]. Cracks in asymmetric membranes can lead to a loss of functionality, as small particles may pass through these large cracks and contaminate the filtrate. The use of a capillary suspension for thin film coating can significantly suppress crack formation [42]. This is due to the fact that the capillary bridges formed by the secondary liquid between particles reduce particle mobility and promote a more homogeneous distribution of pore sizes, which helps prevent the strong anisotropic stress differences that often lead to cracking.

Sintered porous glass filters prepared from capillary suspensions have been the subject of previous research [2], demonstrating the potential to achieve high porosity with pore sizes ranging from 1 to 50 microns. These filters are characterized by relatively high air and liquid permeability, primarily due to their smooth, rounded pore structures. Despite these advances, certain areas require further investigation. This study aims to build upon existing research by focusing on two key aspects: a detailed investigation of the manufacturing process of sintered porous glass filters and a comprehensive filtration testing in solid-liquid separation. In the first part of this study, the influence of material composition and process parameters on the pore structure of the filters was investigated. In addition, the shrinkage behavior of monolithic glass filters and the formation of porosity gradients during the sintering process were analyzed. In this work, asymmetric glass-based membranes were also developed as a viable alternative to monolithic sintered glass filters to improve filtration performance. Particular emphasis was placed on optimizing the manufacturing process to produce crack-free asymmetric membranes, as well as characterizing their structural properties and filtration behavior. Based on the results obtained in the first part of the study, low-shrinkage, porosity-gradient-free glass filter discs and crack-free asymmetric glass

membranes were prepared. These were then subjected to comprehensive filtration tests in the second part of the study. Initially, all filters and membranes were characterized, and key filter parameters such as pore size, porosity, permeability, and flexural strength were determined and analyzed. Subsequently, filtration tests were conducted to evaluate their performance. Spherical polystyrene particles were selected as a reference model for evaluating filtration performance due to their well-defined and consistent size and shape. These particles provided a controlled baseline for understanding the behavior of the glass filters under specific conditions. In practical applications such as drinking water purification, pharmaceutical manufacturing, food and beverage processing, and wastewater treatment, biological particles like microorganisms are often present. Unlike rigid particles, microorganisms exhibit compressibility and flexibility, allowing them to pass through filter pores smaller than their typical rigid size. To simulate these real-world conditions, the bacterium Oenococcus oeni, a common lactic acid bacterium with an ellipsoidal form found in the wine industry, was used as a second model particle in the filtration tests. Filtration efficiency was evaluated through turbidity measurements and flow monitoring using both dead-end and cross-flow filtration setups at constant pressure. Finally, the performance of the capillary suspension-derived glass filters was compared with that of commercial filters of similar pore size and porosity. This benchmarking exercise assessed the effectiveness and competitiveness of the filters.

2 Theoretical Background

This chapter presents a comprehensive review of the theoretical concepts and principles underlying this study. It begins with an overview of the fundamental properties of glasses, which are integral to the materials studied in this research. The discussion then moves to open porous materials, highlighting their importance in filtration applications. Various methods of manufacturing porous glasses are reviewed to provide an insight into the state of the art in this field. Special emphasis is placed on the production of sintered porous glass from glass powder. In addition, capillary suspension filters and glass filtration membranes are analyzed in detail, providing insight into their underlying principles, concepts, and theoretical frameworks. The chapter concludes with an overview of the sintering process, followed by a review of the filtration principles that are essential for evaluating the performance of the manufactured filters.

2.1 Glasses

Glasses are dense (non-fractal), isotropic, and homogeneous non-crystalline solids characterized by the absence of internal phase boundaries [48]. They exist in a glassy or vitreous state, lacking long-range atomic order [15]. Notably, glasses are recognized for their significant brittleness and high transparency in the visible spectrum, particularly in the case of oxide glasses, allowing light within this range to pass through with minimal absorption or scattering.

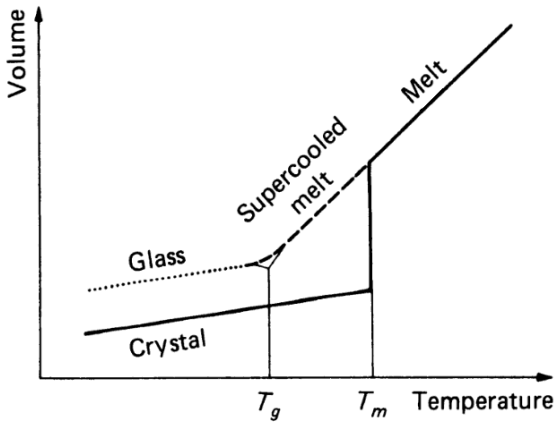

Figure 1 Schematic diagram of the temperature dependence of volume for glass and crystal [49].

Unlike crystals, glasses do not have a distinct melting point but instead soften gradually over a range of temperatures known as the glass transition temperature (T_g) [49]. Figure 1 illustrates this phenomenon. When a melt cools, its volume typically decreases, and crystallization occurs at the melting point (T_m), resulting in a drop in volume and a sharp decrease in the expansion coefficient. If crystallization is prevented, as in rapid cooling, the melt enters a supercooled state, maintaining a metastable equilibrium. In this state, thermodynamic equilibrium is not evident and the glasses exhibit such an extremely high viscosity that the atoms or molecules cannot arrange themselves into a crystalline structure, resulting in a "frozen" amorphous solid. [49]

The process by which a substance transforms into glass, forming a non-crystalline amorphous solid, is known as vitrification. Many techniques have been developed for this purpose, including melt-quenching, sol-gel, hot-pressing of gels, physical vapor deposition, chemical vapor deposition or spark plasma sintering, among others [48,50]. In industry, the most widely used method for glass production is melt-quenching. In this process, raw materials such as silica (sand), soda ash and limestone are melted to produce molten glass. After melting and refining, the glass is rapidly cooled or quenched. The quenching process consists of subjecting the molten glass to controlled cooling, typically achieved by passing it through a series of coolers or placing it in contact with a cool surface. Rapid cooling prevents the formation of a crystalline structure and facilitates the formation of an amorphous, glassy structure. Determining the cooling rate during quenching is critical to the resulting glass properties due to the sensitivity of mechanical properties, thermal expansion coefficient, and glass transition temperature (T_g) to the thermal history of the glass [51]. After quenching, the glass is annealed. Rapid cooling by quenching can result in the retention of internal stresses and an uneven structure in the glass. Annealing is used to relieve these stresses and ensure uniformity of structure.

There are numerous families of glasses, including silicate, borate, chalcogenide, fluoride, germanate, halide, phosphate, tellurite, and combinations of these components, as well as other inorganic oxide glasses. In addition, glasses can be categorized based on their components into organic, metallic, and ceramic glasses. [48,50]. Prominent examples of organic glasses include polymeric glasses such as polymethyl methacrylate (PMMA), commonly referred to as acrylic glass or plexiglass, and polycarbonate (PC). These materials are characterized by long-chain macromolecules that are entangled in an amorphous state. Notably, almost all commercially important glasses originate from the silicate family [52]. A representative example of this family is soda-lime-silicate glass, which has been known since ancient times. The main components of soda-lime-silica glass are SiO_2 (71-75%), Na_2O (12-16%), and CaO (10-15%) [52,53]. This type of mass-produced glass serves as the basis for a wide range of commercially important products in the flat glass industry, including

architectural windows and glass containers used as packaging materials [54,55]. Over 90% of the world's glass production is soda-lime-silica glass [55].

Another special type of glass based on silicate glass is called of borosilicate glass, which is also used in this work. The main composition of borosilicate glass is silica (SiO_2) and boric oxide (B_2O_3) [48,50,52,54]. Borosilicate glass is a significant contributor to the global glass production landscape [56], with an estimated 3 million tons produced in the EU-27 in 2009, representing approximately 10% of the region's total glass production [57]. This importance is further underscored by an additional estimated annual production of 1.25 million tons of frits in 2005 within this geographical area [53]. These versatile glasses find applications across various industries, including common household and laboratory glassware, fiberglass, bulbs in high-wattage electronic lamps and tubes, liquid crystal displays, glass wool, glazes and enamels for aesthetic and protective coatings, industrial piping, glass-to-metal sealing, and nuclear waste storage [54,56,58]. The numerous applications of these glasses are due to their characteristic properties, the most important of which are excellent chemical resistance, high light transmission, low coefficient of thermal expansion and high resistance to thermal shock [15–17,48,50,59].

Borosilicate glasses include several subtypes that are distinguished by their composition: non-alkaline earth borosilicate glasses, alkaline earth borosilicate glasses, and high borate borosilicate glasses [50,52,60]. Non-alkaline earth borosilicate glasses are characterized by B_2O_3 and SiO_2 concentrations typically in the range of 12-13% and >80%, respectively. These glasses exhibit distinctive properties such as exceptional chemical resistance, high light transmission, and minimal thermal expansion, making them widely used in both laboratory and industrial glassware applications. A prominent example in this category is borosilicate glass 3.3, standardized under DIN ISO 3585 and used in this study, featuring a thermal expansion coefficient of approximately $3.3 \times 10^{-6}\ K^{-1}$ at 20°C [61]. This low coefficient translates into a reduced susceptibility to cracking or fracture when exposed to abrupt temperature changes. In contrast, soda-lime glass has a coefficient of thermal expansion about three times higher, typically about $9.0 \times 10^{-6}\ K^{-1}$ at 20°C [52]. Alkaline earth borosilicate glass, or low borate borosilicate glass, typically consists of 75% SiO_2, 8-12% B_2O_3, up to 5% alumina (Al_2O_3) and alkaline earth elements like calcium and magnesium. This composition provides high chemical resistance and a thermal expansion coefficient of 4.0 to $5.0 \times 10^{-6}\ K^{-1}$. Its lower viscosity makes it ideal for molding and forming applications, such as in the production of lamps, tube envelopes [50], and liquid crystal displays [54].On the other hand, high borate borosilicate glasses are characterized by a higher B_2O_3 content, typically in the range of 15-25%, along with 65-70% SiO_2. These glasses may also contain small amounts of alkalis and alumina (Al_2O_3), resulting in low softening points and low coefficients of thermal expansion. These properties make them ideal for glass-to-metal seals [50,60]. In addition, high electrical insulation capability is another notable feature. The increased B_2O_3 content

in high-borate borosilicate glasses comes at the expense of reduced chemical resistance, which distinguishes them from non-alkaline and alkaline earth borosilicate glasses [60].

2.2 Open porous materials as filter

Mechanical filtration uses filter media with defined structural properties, particularly open porous materials. These materials consist of interconnected networks of pores that allow fluids to pass through while trapping solid particles. The open porous structure is essential to ensure fluid flow and particle retention. Glass is a common material used in filtration because of its chemical inertness, mechanical strength, and thermal stability. Its resistance to chemical degradation and ability to withstand high temperatures make it particularly suitable for demanding filtration environments.

2.2.1 Various manufacturing methods of porous glass

Open porous glass can be produced through several manufacturing methods. Notable techniques include the production of glass filters made from glass fibers, leached phase-separated glass, the sol-gel method, sintered porous glass, and capillary suspension-derived porous glass. Sintered porous glass and capillary suspension-derived porous glass, in particular, will be discussed in greater detail in chapters 2.2.2 and 2.2.3, respectively,

A glass fiber filter is a type of filtration medium made from fine strands of glass fibers. There are two types of glass fiber filters: woven and nonwoven. The manufacturing process for woven fiberglass filters, as described in [62], involves several steps. It begins with mixing raw glass materials, which are melted in a furnace to create molten glass. From this, two main types of fibers are made: continuous filament and staple fibers. Continuous filaments are formed by drawing the molten glass through orifices, where they are tapered into fine filaments and wound onto packages with a sizing material applied. Staple fibers are created by pulling molten glass with air jets, then gathering the filaments onto rotating drums. Both types of fibers are treated with binders to facilitate their processing. These fibers are then twisted, plied, and woven into fabric using textile looms. After weaving, the fiberglass fabric undergoes finishing treatments to stabilize the fabric due to the inherent poor abrasion resistance of glass fibers [63]. The fiberglass fabric is heat treated in a furnace at approximately 650°C for a controlled period of time. This process removes the binder, relieves tension and stress, and heat-set the fabric.

Nonwoven glass fiber filters are produced using a wet-laid process similar to papermaking [64,65]. First, glass fibers are broken down and dispersed in an aqueous solution containing acid to form a slurry. To enhance the structural integrity and mechanical strength of the resulting filter, binders are added to the mixture. The slurry is then conveyed to a

papermaking machine where the pulp suspension is deposited onto a fine mesh screen in a continuous wet-laid process. Using a series of vacuum mechanisms, excess water is then removed. Water repelling chemicals and binding chemicals are applied just before the final vacuum, which pulls them through the entire depth of the paper as it is being formed [64]. The dried finished filter media is then rolled into flat sheet form. Typical pore sizes of such filters range from 1 to 50 µm [66,67].

Porous glasses can be produced by leaching phase-separated alkali borosilicate glasses. This process begins by subjecting alkali borosilicate glasses with an appropriate composition to heat treatment at 500–580 °C, inducing phase separation (liquation) [18,68]. The phase separation generates two interconnected phases: an alkali-rich borate phase, which is soluble in acids, water, or alcohols, and a secondary phase consisting primarily of silica. Upon leaching, the alkali-rich borate phase dissolves, creating a porous structure. Depending on the glass composition and the conditions of phase separation, colloidal silica may deposit within the pores during leaching, influencing the pore structure. These deposits determine the pore size, correlating with the gaps between the silica particles [68,69]. To increase pore size, the colloidal silica can be removed by subsequent treatment with a dilute alkaline solution, resulting in macroporous structure [18]. Porous glasses formed through this method exhibit a wide range of pore sizes, from 0.3 to 1000 nm [68], depending on the composition, leaching conditions, and the duration and temperature of phase separation [69–72]. Figure 2 illustrates the porous glass structure throughout the process.

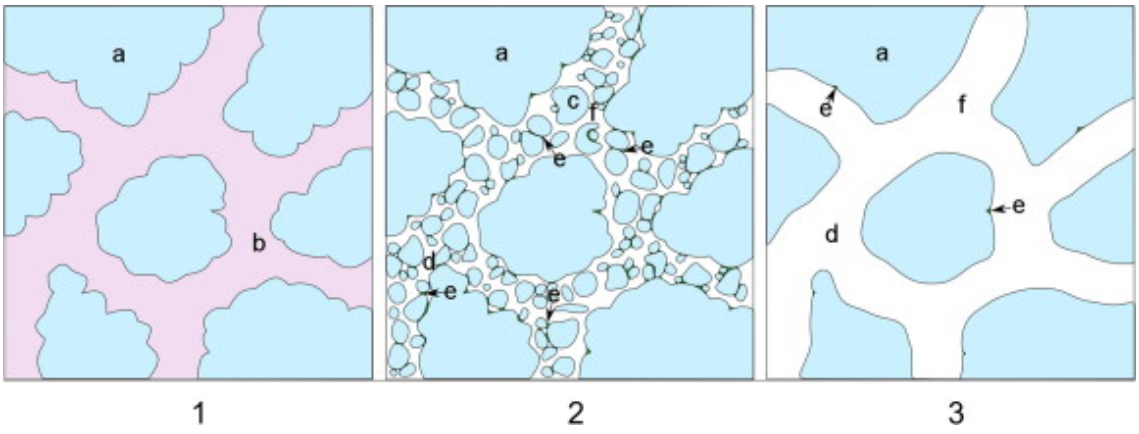

Figure 2 **Production of porous glasses by leaching phase-separated alkali borosilicate glasses [69].** **Figure 2.1** shows the phase-separated glass after liquation, with silica (**a**) and alkali-rich phases (**b**). After leaching, a porous structure is formed, as depicted in **Figure 2.2**. Depending on the glass composition and phase separation conditions, secondary silica globules (**c**) may form in liquation channels (**d**). **Figure 2.3** illustrates a wide-pore glass after alkali treatment. Micropores (**e**) are the contact areas between the globules themselves and with the walls of liquation channels. Mesopores (**f**) are the free space regions in liquation channels, not occupied with colloidal silica.

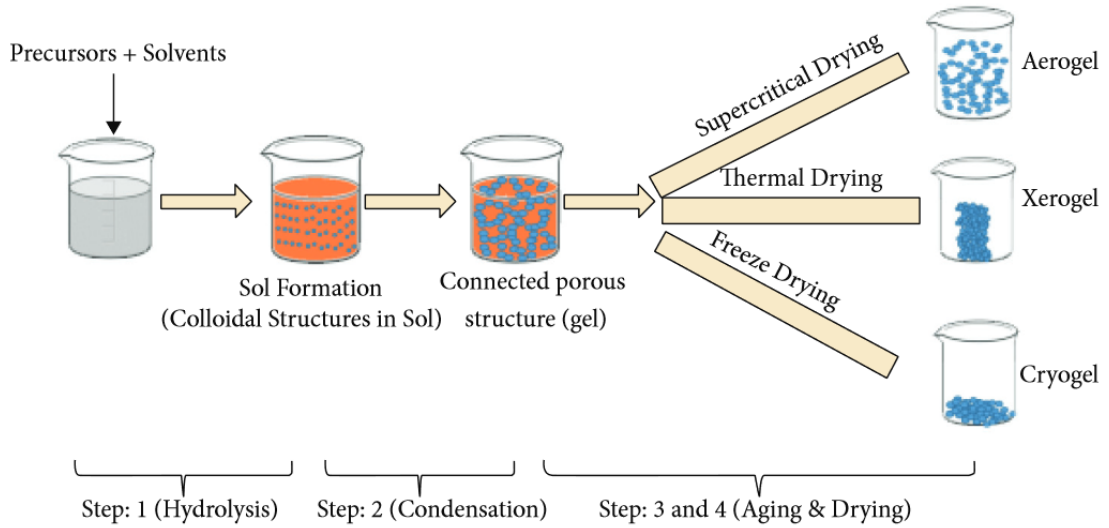

Figure 3 Schematic of different stages of sol-gel process [78].

The sol-gel process is a wet chemistry-based synthesis technique, which is visually depicted in Figure 3. This method can be utilized to produce porous glass. In a typical process, this entails the sequential hydrolysis and polycondensation of alkoxy silicon derivatives (e.g., tetraethyl orthosilicate (TEOS) or tetramethyl orthosilicate (TMOS)) in the presence of aqueous acid or base catalysts. This process is extensively discussed in the literature [73–75]. The initial stage of the process yields a sol, which is defined as a stable suspension of colloidal solid particles within a continuous liquid medium. This transformation occurs as precursor molecules undergo controlled hydrolysis and condensation reactions, leading to the formation of the sol [74,76–78]. In the subsequent phase, the sol evolves into a gel through further condensation of its particles, a process referred to as polycondensation. This process results in the formation of a rigid, highly interconnected, three-dimensional (3D) network, known as the gel, comprising discrete particles or polymer chains [74,76,77,79]. The gel structure can be conceptualized as a porous network embedded within a liquid medium. The structural attributes of the resulting gel are profoundly influenced by the catalyst utilized, which dictates the relative rates of hydrolysis and condensation reactions [74,80]. Subsequent to gelation, the drying stage is initiated. The deformation and shrinkage that occur during this process exert a considerable influence on the pore-forming process [81]. Depending on the selected method, xerogels are obtained through the evaporation of the liquid, while aerogels are typically generated by removing solvents under hypercritical conditions. Alternatively, cryogels are produced through freeze-drying. To consolidate the network structure following drying, the glass can undergo controlled partial sintering. The final product resulting from the sol-gel synthesis process exhibits a

distinctive mesoporous structure inherent to sol-gel materials, as elucidated in the literature [75,82].

2.2.2 Sintered porous glass from glass powder

Sintering glass powder is a widely used and cost-effective method for producing porous glass. This approach allows for precise control of pore size and overall porosity by adjusting the particle size and shape of the glass powder. Such control is crucial for applications requiring specific permeability, mechanical strength, or thermal properties. A variety of glass powders, including soda-lime, borosilicate, and specialty glasses, are commercially available, enabling tailored compositions to meet particular application needs. Sintering glass powder is well-established in the glass industry, particularly for manufacturing porous glass filters.

The manufacturing process of glass powder involves selecting suitable raw materials, crushing and grinding them to achieve the desired particle size, and then classifying the powder to ensure a uniform particle size distribution. The powder is washed to remove impurities and dried to ensure it is free of moisture. Glass powder can be processed in either a dry or wet state (see Figure 4). In the dry processing route, the powders are shaped into the desired form, potentially compressed to enhance stability, and subsequently sintered to consolidate the structure and impart greater mechanical strength. For filtration purposes, the glass powder is subjected to partial sintering in order to attain sufficient stability, while avoiding a significant reduction in the pore volume, as this can impair the permeability of the filter.

In the wet processing route, glass powder is uniformly mixed with additives and binders to form a slurry. This involves incorporating specific liquids as binders into the glass powder to create the slurry, allowing for further tuning of the porous glass structure after sintering and enabling the fabrication of more complex shapes, as slurry can be shaped more

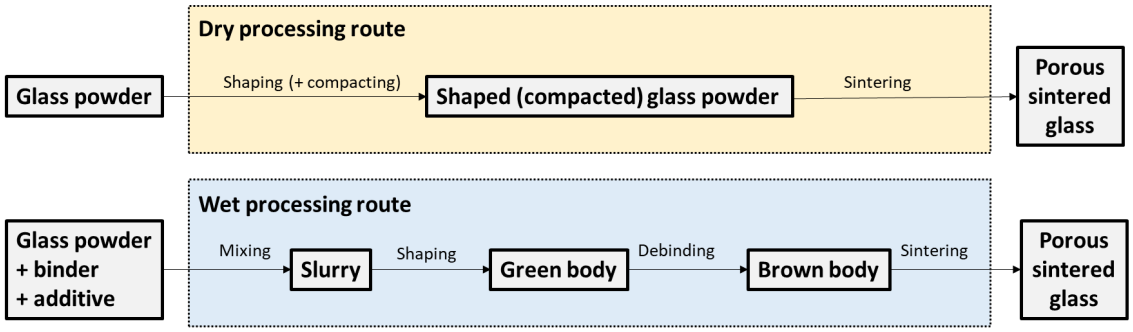

Figure 4 **Dry and wet processing route in the process of manufacturing porous glass from sintering glass powder.**

effectively than loose powder. Various shaping techniques, including cold pressing, slip casting, and extrusion, may be utilized. Subsequently, the resulting green body is subjected to debinding, which involves the removal of organic matter, and is then sintered. Compared to dry processing, wet processing may offer superior control over particle interactions and enhances the homogeneity of particle packing, resulting in fewer and smaller defects in the final microstructure [26].

An extension method for producing porous glasses integrates the filler principle with the sintering process, where inorganic salts, organic salts, or polymers act as pore-generating agents [19,23,83–85]. In this method, glass powder, such as sodium borosilicate glass, is typically combined with filler salts, such as potassium sulfate or sodium chloride. This is complemented by a binder, which enhances the mechanical stability of the resulting material [19,83]. The mixture is thoroughly mixed via stirring and then uniaxially pressed into the desired shapes. Following shaping, the structures undergo drying and subsequent sintering. Post-sintering, the inorganic salt is leached out with water to reveal the pore system. The morphology of these pores can be fine-tuned by manipulating the grain sizes and volume fractions of the filler salt [19]. The compression force significantly impacts the resultant pore characteristics [19]. Higher pressures promote denser particle packing and reduce glass particle sizes due to heightened shear forces, leading to a reduction in additional pore volume. Pore sizes resulting from this methodology typically fall within the range of 20 to 200 μm [84].

Another wet processing route involves using foam as a template. The foaming replica method offers an approach for manufacturing porous glass structures by replicating the porous design of sacrificial templates [24,25]. This method involves immersing a foam template into a slurry containing glass particles suspended in a binder solution to achieve a uniform coating on the foam struts. A variety of materials can be employed as a foam template, including synthetic polymeric foam [86] and natural materials such as marine sponges [87]. Subsequently, the foam template is subjected to thermal treatment, which decomposes the foam and sinters the glass particles in the coating. The resulting porous glass structures exhibit microporous, open-cell, interconnected pores, and hollow struts, replicating the original template's design [25,86]. By adjusting various parameters, including immersion frequency, slurry composition, and sintering conditions, the final product's characteristics, such as mechanical properties, permeability, and porosity, can be finely tuned [24,88].

Manufacturing porous materials using the wet processing route presents challenges, notably excessive shrinkage. Well-controlled shrinkage is critical to maintaining dimensional accuracy and preventing defects such as cracks [31–34]. Shrinkage during manufacture can be divided into debinding and sintering shrinkage. During debinding, the liquid binder is

gradually removed from the green body. For low-viscosity binders, this can be accomplished by mechanical debinding, in which the liquid binder is absorbed by a porous substrate, or by thermal debinding, in which the remaining binder components are burned at high temperature. As the process proceeds, the liquid content decreases, menisci form, and capillary pressure builds up, causing the particles to contract and shrink [33]. Furthermore, a concentration gradient of the liquid phase can be developed within the green body which can induce internal stresses. This potentially promote crack formation, the extent of which increases, the larger the part [32,34]. For thermal debinding, appropriate temperature control depending on the material system used and a gentle process with a slow heating rate are favorable for good dimensional stability and avoidance of abrupt shrinkage and thus cracking [89,90]. The sintering process is always accompanied by densification of the particle structure, resulting in sinter shrinkage. The amount of shrinkage can be reduced by a high solids content and a wide particle size distribution [35,36].

2.2.3 Capillary suspension derived filters

Porous glass filters made from capillary suspensions are produced using a sintering method with a wet processing route [2], the complete processes of which are schematically illustrated in Figure 5. The process begins with the preparation of a capillary suspension as a precursor. Capillary suspensions are three-phase systems comprising a main liquid, dispersed solid particles, and a small amount of a secondary liquid that is immiscible with the main liquid. These suspensions are characterized by their sample-spanning particle network, formed due to capillary forces in the ternary system controlled by the interfacial tension between the liquids and the three-phase contact angle Θ of the secondary liquid on the particle surface. The structure of this particle network depends on the wettability of the particles by the secondary liquid in the presence of the primary liquid, leading to the differentiation between the pendular and capillary states [27,91,92], the structures of which are shown in Figure 6. In the pendular state, where the secondary liquid wets the particles well (Θ < 90°), the particles are individually connected by liquid pendular bridges formed by the secondary liquid. Conversely, in the capillary state (Θ > 90°), where the secondary liquid

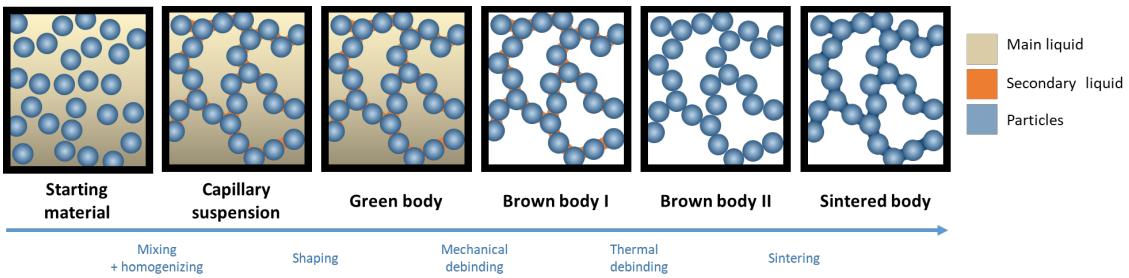

Figure 5 **Process route for the production of glass filters made from a capillary suspension.**

does not wet the particles well, then the secondary fluid is separated from the bulk fluid inside the interstitial volume of particle clusters, thus lowering the free energy of the system [91]. These clusters then self-assemble into a sample spanning network [92]. The formation of capillary bridges or clusters requires that the secondary liquid droplets be approximately the same size as or smaller than the particles, typically achieved through mixing. The capillary suspensions used in this work are exclusively in the pendular state. The formation of the particle network within capillary suspensions significantly alters the bulk rheological behavior of the suspension, transforming it from predominantly viscous or weakly elastic to highly elastic or gel-like, with a substantial increase in yield stress by orders of magnitude [27]. Capillary suspensions also exhibit a strongly shear-thinning flow behavior [93]. The particle network present in capillary suspensions is robust and can be effectively utilized to stabilize particle suspensions against sedimentation, which is particularly beneficial for suspensions containing relatively large particles that are prone to sedimentation due to gravitational forces.

The incorporation of a small amount of surfactant into a capillary suspension might additionally modify their properties, presenting both advantages and challenges. Surfactants may reduce the interfacial tension between the immiscible fluids in the suspension or change the contact angle between the solid particles and the fluids. A reduction in suspension strength can be anticipated, with an associated decline in yield stress. This is attributed to a partial trapping of the secondary fluid within surfactant micelles [93]. In addition, surfactants may be beneficial in reducing particle agglomeration and increasing particle dispersion, thereby improving the homogeneity of the suspension. This effect is particularly useful for suspensions containing smaller particles, which are more prone to agglomeration due to van der Waals forces. Surfactants may adsorb onto the surfaces of the particles, providing steric or electrostatic barriers that prevent the particles from aggregating, thus

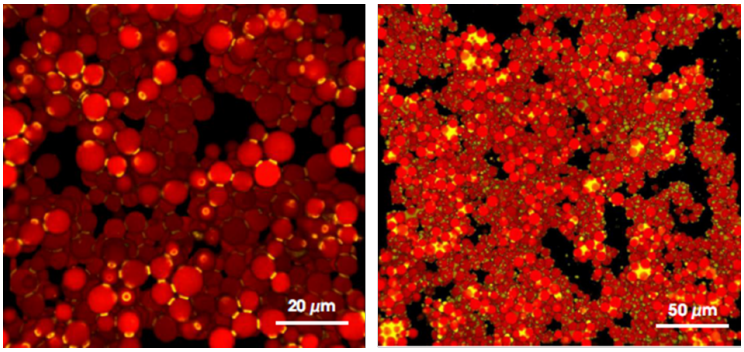

Figure 6 **The particle network in a capillary suspension [92].** Three-dimensional reconstructions of confocal images of capillary suspensions show non-porous particles (red) and the added secondary fluid (yellow). The left image shows the particle network in the pendular state, while the right image shows the capillary state.

maintaining a more uniform particle distribution within the suspension. Moreover, the reduction in yield stress due to the presence of surfactants facilitates easier mixing of the suspension, which further enhances its homogeneity. This is particularly advantageous in the case of suspensions with high particle loads.

The subsequent manufacturing step involves the shaping of the suspension into the desired green body. The modification of rheological properties, such as yield stress, in capillary suspensions due to the formation of a particle network is highly beneficial for shaping. The increased yield stress enhances the stability of the suspension, facilitating easier handling and accurate shaping into complex and intricate designs. A variety of shaping techniques can be utilized for capillary suspensions, encompassing conventional approaches such as molding [2,28] and extrusion [30] and emerging methodologies like 3D printing [94,95].

The shaped green body is then subjected to debinding, a process that removes the liquid and any organic content from the particle structure. This process can be divided into two distinct stages: mechanical debinding and thermal debinding. During mechanical debinding, the wet green body is placed on a dry, fine-pored substrate. In this step, most of the liquid from the capillary suspension is absorbed by the substrate due to capillary forces. The removal of the liquid creates interspaces between the particles, forming pores. The duration of this process can vary from a few hours to several days, depending on factors such as the size of the green body, the composition of the capillary suspension, and the pore characteristics of the absorbing substrate. The pore size of the resulting porous structure should be within the same range as, or smaller than, the voids left by the fluid during mechanical debinding. This is essential to ensure that the capillary forces generated by the porous substrate are adequate to effectively absorb the fluid from the green body. If the pores are too large, the capillary forces may be insufficient to draw out the fluid. Following mechanical debinding, the green body is subjected to thermal debinding. This process involves heating the mechanically debinded body in a furnace to a high temperature, but below the sintering temperature, in order to burn off any remaining liquid and organic materials. The thermal debinding phase is crucial for ensuring that the debinded body is free of any residual substances inside the pores. The debinding process, particularly mechanical debinding, is critical because the removal of liquid exerts capillary forces on the structure, leading to shrinkage. The formation of a stable particle network in capillary suspensions is beneficial for the debinding process, as it promotes more homogeneous shrinkage throughout the body, which results in better shape accuracy and more uniform drying stress within the debinded body [30]. This significantly helps to avoid cracks and achieve defect-free drying [42].

After thermal debinding, the sample remains fragile as it consists of loosely bound particles. Therefore, sintering is required to consolidate the porous structure. Sintering is conducted at temperatures above the glass transition temperature, allowing the particles to fuse

together sufficiently until the desired mechanical strength and porosity are achieved. Importantly, the particle network present in the capillary suspension is well preserved even after sintering [2,29]. Dittmann et al. demonstrated the correlation between the precursor suspension and the resulting particle structure after sintering for suspensions with varying secondary liquid contents [29]. This study identified three distinct regimes based on the amount of secondary liquid added. Regime I comprises binary suspensions without added secondary fluid or including only a very small fraction of secondary liquid. Sintered bodies produced from these suspensions exhibit densely packed and homogeneously distributed particles, with interactions predominantly governed by van der Waals forces. Regime II involves the addition of a sufficient amount of secondary liquid, significantly increasing the yield stress of the suspension and indicating the formation of a robust particle network, as mentioned earlier in this chapter. In the pendular state liquid bridges form, bonding the particles together in a sample-spanning network. After sintering, the particle structure in

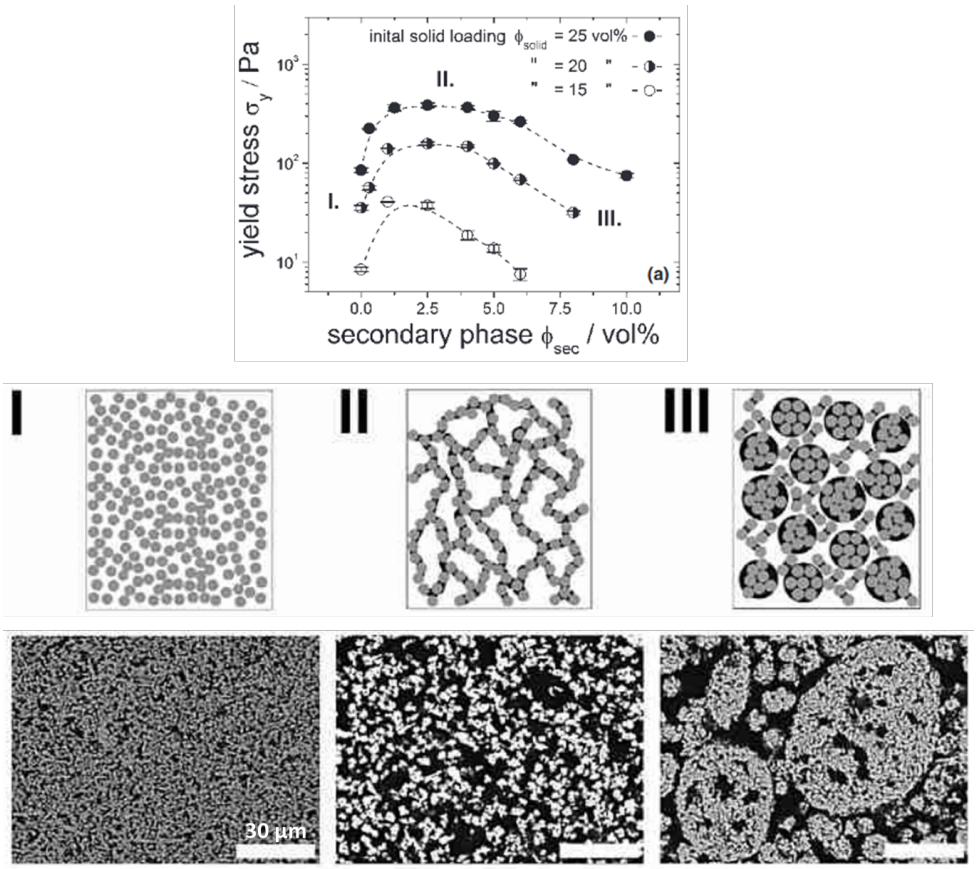

Figure 7 **Particle structure of capillary suspensions in the pendular state [29].** The diagram at the top shows the yield stress of the capillary suspension at varying secondary fluid contents, illustrating a three-regime model. In the middle, three images represent the idealized model of the wet state, corresponding to these regimes. At the bottom, SEM images of polished surfaces of sintered parts are shown, corresponding to each regime.

this regime is characterized by a more open and porous structure compared to sintered bodies made from Regime I. Within Regime II, further increases in the secondary liquid do not significantly affect the yield stress or the microstructure, suggesting a stable particle network is maintained. Regime III occurs when the amount of secondary liquid exceeds a critical threshold, causing the yield stress to decrease with increasing secondary liquid content, indicating oversaturation. This oversaturation leads to the formation of aggregates, and the particle structure after sintering displays a uniformly flocculated network. The critical amount of secondary liquid required to transition from Regime II to Regime III increases with higher solids content, as more particle-particle contacts need to be saturated before reaching Regime III. Porous sintered bodies made from these capillary suspensions typically exhibit pore sizes ranging from 0.5 to 100 µm, with open porosities exceeding 50% [2,29].

2.2.4 Glass filtration membranes made from capillary suspensions

A filtration membrane is a discrete, thin material layer that serves as a selective barrier, permitting certain chemical species to pass while blocking others. It is designed to be thin in order to provide higher filtration flux and lower filter resistance compared to normal filters, as these are dependent on the thickness of the filter. The most common materials used to manufacture filtration membranes are polymer-based. These membranes offer flexibility, cost effectiveness, and relative ease of manufacture. However, they have limitations in harsh environments such as high temperatures or exposure to aggressive chemicals. To overcome these challenges, glass membranes are emerging as effective alternatives. They are versatile and suitable for various applications due to their high thermal and chemical stability, as well as their excellent mechanical strength.

There are numerous methods for manufacturing glass membranes, some of which were derived from techniques previously described in section 2.2.1. For instance, Fuchigami et al. developed a thin macroporous membrane through a sol-gel process followed by sintering and grinding, resulting in a membrane thickness of 1 mm [96]. Enke et al. produced porous glass membranes from sodium borosilicate glass through phase separation, combined with acid and alkaline leaching processes [18,97]. This method involves thermal treatment to initiate phase separation in the borosilicate glass, which is then sawed into ultrathin layers and subsequently leached to create membranes with thicknesses ranging from 100 to 300 µm and pore sizes between 1 and 120 nm. However, due to their thinness, these standalone membranes are delicate and have limited mechanical strength, rendering them less suitable for filtration applications, especially those requiring high pressure. The incorporation of an asymmetric structure can address this issue. Glas membranes with asymmetric structure are based on ceramic membrane processing techniques. In this approach, effective membranes are built on a thick supporting substrate, providing structural stability to the thin

membrane layer. The so-called asymmetric membranes utilize a coarse-pored structured substrate, which is essential for filtration applications since this substrate allows for less interference with the filtration performance of the fine-pored thin membrane. The manufacturing process involves a series of steps. Initially, the substrate is prepared, and then it is coated with a glass or ceramic suspension slurry. A variety of techniques may be employed to apply the slurry to the substrate, including tape casting [98,99], dip and spin coating [47,100,101], and filtration coating [102]. After coating, the substrate is dried and sintered to finalize the membrane.

Ensuring the compatibility of the substrate and the membrane is essential during the manufacturing of asymmetric membranes. This compatibility is crucial to guarantee adherence and prevent delamination of the thin layer during coating [47,101]. Adjusting the pore size and surface roughness of the substrate can enhance the adherence of the wet suspension slurry, thereby preventing delamination and preserving the membrane's functionality. The drying process of thin suspension films plays a critical role in the formation of cracks and defects [43–46]. Cracks in the membrane can lead to the passage of small particles into the filtrate, compromising its integrity. During the drying process, as the wet suspension film loses its liquid content, the distance between particles decreases, and capillary bridges gradually form. The resulting capillary forces exert internal stress, which can lead to crack formation. Therefore, the drying process of thin films must be carefully controlled to avoid crack formation. Gentle drying conditions, such as regulated humidity and drying temperature, along with increasing the pore size and surface tension of the liquid, can help reduce crack sensitivity and further mitigate crack formation [103]. Crack formation can also occur during thermal treatment due to a mismatch in the thermal expansion coefficients of the substrate and the thin layer [47]. Different materials expand differently during heating, which can build internal stress and lead to defects. Using the same material for both the substrate and the membrane is beneficial in this case, as it ensures thermal compatibility. If the chemical composition of the substrate and the membrane differs significantly, incorporating an intermediate layer as a buffer between the membrane and the substrate can alleviate the degree of mismatch and prevent defects during the manufacturing process [47].

Capillary suspension is a beneficial precursor for the manufacturing of asymmetric membranes. Schneider et al. investigated the crack formation in asymmetric membranes for filtration made from capillary suspension and assessed the filtration performance of such membranes [42]. They compared Al_2O_3 suspensions with a secondary liquid (capillary suspension) and without a secondary liquid (pure suspension), both having the same wet film thickness, which were coated on a porous ceramic surface, dried, and sintered. The pure suspension shrank and compacted more, resulting in a denser and thinner film than that made from the capillary suspension. This density arises from the settling of particles in the weak particle network of pure suspensions during debinding and sintering. Conversely, the

thin film made from capillary suspension exhibited a significant reduction in cracks during the manufacturing process compared to the thin film made from pure suspension. This improvement is attributed to the capillary bridges formed by the secondary liquid between particles, which reduce particle mobility and provide a more homogeneous distribution of pore sizes. These bridges prevent the strong anisotropic stress differences that cause cracking. The reduction in cracking is also crucial for the filtration performance of the sintered asymmetric membrane. Membranes with cracks showed similar permeability to the substrate due to bypass flow, preventing efficient particle filtration as particles could pass through the cracks and enter the filtrate unfiltered.

2.3 Sintering

Sintering is a process where powder particles are consolidated and densified into a more compact form through controlled heating. This method is widely employed to enhance the mechanical stability and produce stronger materials from powder precursors. The primary driving force for sintering is the reduction of surface energy. Small particles have a high surface area relative to their volume, resulting in high specific surface energy. The smaller the particles, the higher their specific surface energy. During sintering, the system aims to minimize this energy by reducing the surface area through particle coalescence. As the particles bond, porosity is reduced, leading to the densification of the material and consequently an increase in mechanical strength. The sinter process can be improved, such as by applying external pressure to increase sinter activity and promote further densification.

The densification process during sintering can be characterized by changes in relative density or porosity. Relative density ρ_{rel} is defined as the ratio of the actual density of a porous material to the density of the same material in its fully dense state. Porosity or total porosity ε, on the other hand, is the percentage of the total volume of a material that is occupied by pores or voids. These pores can be either interconnected and accessible from the surface or isolated and not accessible from the surface. Open porosity ε_o refers specifically to the volume of interconnected pores, while total porosity ε combines both open and closed porosity. The relationship between relative density and porosity is given by the equation.

$$\rho_{rel} = 1 - \varepsilon \tag{1}$$

The sintering densification can be divided into three distinct stages (Figure 8) [104]: the initial stage, the intermediate or shrinkage stage, and the final stage. Each stage is characterized by specific changes in the microstructure and density of the material. In the initial stage of sintering, particle bonding begins and initial necks form at the contact points

between particles. The powder undergoes a slight densification, typically around 5%. The intermediate stage is where the most significant densification occurs, and it is often referred to as the shrinkage stage. As the sintering necks grow further, the particles continue to coalesce and grow together, resulting in a decrease in the overall volume of the system and an increase in density. The final stage of sintering occurs at high relative densities, typically when the material has already achieved substantial densification. During this phase, the remaining open pores gradually close, transforming into isolated, closed pores.

As previously stated in Chapter 2.1, glass, as an amorphous material, undergoes a gradual transition from a solid to a softened state over a range of temperatures known as the glass transition temperature (T_g). Sintering of glass typically occurs above T_g, where the material's viscosity is significantly reduced. This reduction in viscosity facilitates coalescence, enabling glass particles to bond together through viscous flow mechanisms [104–106]. In contrast to typical diffusion mechanisms in the sintering of crystalline materials, viscous flow affects the material in bulk. As the glass material flows, the densification occurs.

There are various models to describe the mechanism of viscous sintering, with Frenkel's model being one of the most notable [107]. Frenkel developed a model to elucidate this behavior, starting with the assumption of two identical spherical droplets contacting each other at a single point. The reduction of surface energy between the liquid and gas phases initiates coalescence and neck growth through viscous flow. Frenkel's energy balance equation equates the rate of energy dissipation through viscous flow to the rate of energy gained by reducing the surface area of the pores [108]. His model accurately describes the initial sintering stage, during which significant neck growth occurs between the spheres. Frenkel's model is linear and valid for the initial shrinkage stage of sintering, typically up to a linear shrinkage of 10%. [109]. Frenkel's linear shrinkage can be described by the equation (2),

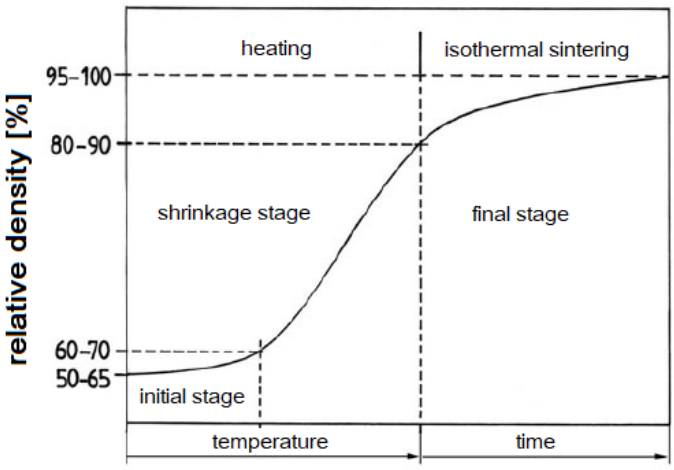

Figure 8 Schematic densification process with sintering stages [104].

where Δl represents the linear shrinkage after a sintering time t. In this equation, l_0 is the initial length, γ_{lv} is the surface tension between the glass and vapor, η is the viscosity of the glass, and r is the particle radius.

$$\frac{\Delta l}{l_0} = \frac{3}{8}\left(\frac{\gamma_{lv}}{\eta\, r}\right) t \tag{2}$$

As densification progresses and the neck radius grows to a size comparable to the particle size, the kinetics of densification diverge from Frenkel's initial concept. Scherer developed a model based on Frenkel's energy-balance principle to describe the subsequent densification stage [110]. This model depicts the microstructure of a sintering compact as a cubic arrangement of intersecting cylinders, with the cylinder radius representing the average particle radius. As densification progresses, the cylinders become shorter and thicker. Scherer's model, with its cubic array of intersecting cylinders and interconnected pores, is applicable over a wide range of relative densities up to the final stage [108]. Towards the final stage of sintering, densification has progressed significantly, resulting in more pores being isolated and converted to closed pores. Mackenzie and Shuttleworth developed a theory for the viscous sintering of glass based on a simple model of isolated spherical pores of uniform size within a dense glass matrix [111]. Their analysis is particularly applicable to this final stage of sintering with a relative density greater than 94% [110]. The densification rate of Mackenzie and Shuttleworth model is given in equation (3) where ρ_{rel} is the relative density and a_0 is the initial pore radius.

$$\frac{d\rho_{rel}}{dt} = \frac{3}{2}\left(\frac{\gamma_{lv}}{\eta\, a_0}\right)(1 - \rho_{rel}) \tag{3}$$

The sintering process of glasses is influenced by several parameters. Assuming a proportionality between particle size and pore size, equations (2) and (3) suggest that densification during sintering is inversely related to both particle size and glass viscosity. Smaller particles result in increased specific surface area, which leads to higher surface energy. Since surface energy acts as a driving force for sintering, this increase in surface energy results in increased sintering activity and, consequently, a higher sintering rate [112–114]. In addition, irregularly shaped particles, which have a greater specific surface area compared to spherical particles of the same size, typically exhibit accelerated sintering rates. The viscosity of the glass also plays a critical role in the sintering process. Lower viscosity increases the viscous flow of the glass, thereby promoting the densification process. Importantly, viscosity is a temperature dependent property; as temperature increases, viscosity decreases, which in turn accelerates the densification process.

Sintered objects can exhibit porosity gradients formed during the sintering process [37–41]. The distribution of pores within the material can vary, resulting in regions of different porosity. This variation could be due to spatially heterogeneous temperature distributions across the sample during sintering. These temperature variations lead to localized differences in sintering kinetics, as the sintering rate is highly temperature dependent. Regions experiencing higher temperatures will exhibit accelerated sintering rates, resulting in a locally denser and less porous structure. Consequently, this non-uniform sintering behavior results in an inhomogeneous particle structure in the final sintered body. Heat transfer into and within the sample plays a critical role in shaping the temperature profile within the sample and thus the resulting microstructure of the sintered material. Heat transfer is controlled by several factors, including the thermal properties of the material such as thermal conductivity and heat capacity, the initial porosity of the green body, the dimensions of the sample, and the design of the furnace including the heating elements. Controlling the porosity gradient is critical in the production of sintered glass filters, as the filtration performance and properties of the filter are closely related to the pore structure.

2.4 Filtration

Filtration is a mechanical separation process that involves the segregation of phases, typically separating dispersed particles from a liquid or gas. This is achieved by forcing the carrier fluid—either gas or liquid—through a porous medium. As the fluid passes through the filter medium, the particles are retained either on the surface or within the medium itself. The driving force behind this process can vary, originating from differences in gas pressure, mechanical pressure, hydraulic pressure, hydrostatic pressure, or centrifugal forces. In this work, the focus is specifically on filtration processes that remove solid particles from liquids, using pressure differentials as the primary driving force.

The filtration efficiency of porous materials as filter media is largely determined by their structural characteristics, including pore size distribution, porosity, and pore connectivity. Pore size determines the ability of the filter to retain particles, which directly affects the separation efficiency. Fine control of pore size is necessary to meet specific filtration requirements, ensuring that particles above a certain size are effectively retained. A critical aspect of filtration performance is the balance between porosity and mechanical strength. High porosity improves fluid permeability, allowing for higher flow rates. However, increased porosity generally results in reduced mechanical strength, making the material more susceptible to structural failure under operating conditions. Therefore, it is important to optimize both parameters to achieve sufficient fluid flow without compromising the mechanical integrity of the filter.

In membrane technology, filtration processes are categorized by pore size into microfiltration, ultrafiltration, nanofiltration, and reverse osmosis (Figure 9). Each category is tailored to address specific separation requirements depending on the size of particles or solutes targeted for removal. Microfiltration, with pore sizes ranging from approximately 100 nanometers to 10 micrometers, effectively removes larger particles such as suspended solids, cells, and microorganisms from liquids. Ultrafiltration, which operates with pore sizes between 2 nanometers and 100 nanometers, is designed to filter out smaller particles, including viruses, large proteins, and macromolecules. Nanofiltration and reverse osmosis utilize even smaller pore sizes to remove finer particles, such as dissolved salts, ions, and small organic molecules. Conventional filtration, microfiltration, and ultrafiltration can be classified as mechanical separation processes. In these methods, particles are separated from a fluid based on their size relative to the pore size of the filter medium. Larger particles are retained on the surface of the filter, while particles that are similar in size to the pores may block or clog them. Smaller particles can pass through the pores, potentially becoming trapped within the pore structure or moving through to the filtrate. In contrast, nanofiltration and reverse osmosis involve not only size exclusion but also additional molecular interactions between the solutes and the filtration medium. These processes can separate particles and solutes based on their chemical properties and molecular size, involving more complex interactions beyond simple mechanical sieving. As the pore size decreases, from conventional filtration to microfiltration, ultrafiltration, and further to nanofiltration and reverse osmosis, the resistance to fluid flow increases. This heightened resistance necessitates higher operational pressures to maintain effective separation and achieve the desired flux.

The filtration performance is largely determined by the interactions between the particles and the filter. Factors such as particle size, size distribution, shape, surface properties of the particle in the fluid environment, and electrostatic charges play a critical role in the filtration process [115]. On the filter side, critical properties that affect performance include the pore structure, particularly pore size, size distribution, porosity, pore shape, pore length, and tortuosity [116]. As particles are captured, they gradually accumulate on the filter surface or within its pores, leading to a phenomenon known as fouling. Fouling significantly impacts the efficiency of filtration by reducing the flow rate and increasing the operational

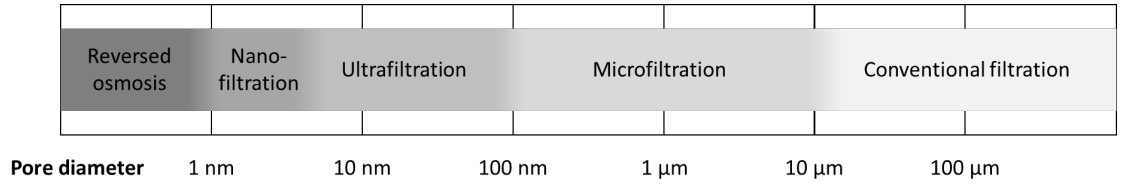

Figure 9 Classification of filtration processes by pore size in membrane technology.

pressure required to maintain performance. The process of fouling can be described by four primary models: cake filtration, complete blocking, intermediate blocking and standard blocking [117–119]. The four models of fouling mechanisms are illustrated in Figure 10.

In cake filtration, particles are deposited on the surface of the filter medium, progressively forming a porous, permeable layer known as the "cake." This process typically occurs when the particles are larger than the pore size of the filter. However, it can also happen with smaller particles, especially in suspensions with high solids content or where particles tend to agglomerate. These smaller particles can create a stable structure, or "bridge," across the pore entrances. Over time, additional particles accumulate on this bridge, causing the cake layer to thicken as the filtration process continues. This accumulated cake layer functions as an additional filter medium, further trapping incoming particles.

Complete blocking, also referred to as sieve filtration, involves particles completely sealing the pore entrances, thus preventing any flow through them. In this model, each particle contributes to the blockage of some pores, leading to a reduction in the open flow area. This type of fouling is commonly observed when particles are similar in size to the pores. Intermediate blocking describes a scenario where some particles partially seal the pore entrances, while additional particles deposit on top of these partially blocked pores.

Lastly, standard blocking, which is commonly encountered in depth filtration processes, involves the deposition of particles within the pore system. This type of fouling typically occurs when particles are significantly smaller than the pores, such as in highly diluted slurries containing very fine particles. Within the pore network, particles are deposited on the pore walls through several transport mechanisms. Inertial impaction causes particles to deviate from their flow path due to their inertia, leading them to collide with and adhere to the

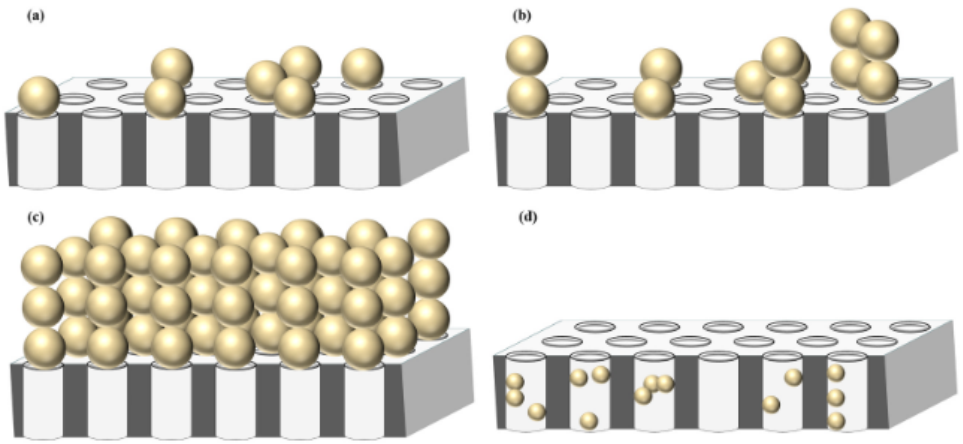

Figure 10 **Schematic representation of fouling mechanisms [119].** (**a**) complete pore blocking, (**b**) intermediate pore blocking, (**c**) cake filtration and (**d**) standard pore blocking

pore walls. Van der Waals forces, which are electrostatic interactions between the particles and the pore surfaces, may also facilitate particle adhesion to the pore wall. Diffusion, driven by Brownian motion, causes very small particles to move erratically, resulting in their collision with and subsequent deposition on the pore walls. Lastly, interception occurs when particles are captured and deposited in pores smaller than their own size within the pore system. As particles accumulate within the pores, they reduce both the effective pore size and the overall pore volume. This accumulation leads to a gradual decrease in flow rate over time, as the filter's ability to transmit fluid diminishes.

It is important to note that all of these fouling mechanisms are modeled under the simplifying assumption that all pores are cylindrical, uniform in size, and parallel to each other, and that the particles are uniform and not deformable or compressible. In reality, however, the filtration process is more complex and often involves a combination of these mechanisms, especially since both pore and particle sizes typically exhibit a wide range of distributions.

In filtration processes, the fluid flow relative to the filter medium can be classified into two main types: dead-end filtration and cross-flow filtration. In dead-end filtration, the fluid flows perpendicularly to the filter medium, meaning all the fluid is forced directly through the filter at a 90-degree angle. This process tends to require periodic cleaning or replacement of the filter as fouling increases over time, reducing efficiency. In contrast, cross-flow filtration involves the feed stream flowing parallel to the surface of the filter medium. Only a portion of the fluid, known as filtrate, passes through the filter, while the remainder, referred to as retentate, continues flowing along the surface. This tangential flow helps sweep away particles that accumulate on the filter, reducing the rate of fouling. The shear forces generated by the flow help dislodge particles from the membrane surface, which enhances the filtration efficiency and prolongs the filter’s lifespan.

3 Materials and Methods

This chapter provides an overview of the materials and experimental procedures used in the study. It begins by detailing the fabrication processes used to produce both symmetrical cylindrical glass filters and asymmetric glass membranes. After discussing the fabrication steps, the focus shifts to the various characterization techniques employed throughout the study. These techniques include a wide range of analyses, starting from the characterization of the glass powder, such as particle size distribution and composition, to the methods used to evaluate the paste that serves as a precursor for the glass filter production. Special emphasis is placed on the characterization methods used to determine the critical properties of the glass filters-such as porosity, pore size distribution, and permeability-as these parameters are critical to evaluating the performance of the filters. The chapter concludes with a description of the procedures used to perform filtration tests on the manufactured filters, focusing on key metrics such as filtrate flux and turbidity.

3.1 Manufacturing processes

The manufacturing process includes the method of producing a glass filter from capillary suspensions. The process starts with the preparation of capillary suspensions as precursors. Subsequently, a series of steps including shaping, debinding and sintering methods are applied to obtain a symmetrical cylindrical porous sintered glass filter. Specific parameters used in the preparation of glass filters for various investigations are then outlined, including studies on the shrinkage ratio and porosity gradient. Finally, the method for preparing asymmetric cylindrical glass membranes is described.

3.1.1 Raw materials

Borosilicate glass 3.3 glass powder was used to manufacture the glass filters. The key physical and technical properties of borosilicate glass 3.3 are provided in Table 5 in the appendix. P4 and P5 borosilicate glass 3.3 glass powder fractions, supplied by DWK Life Sciences GmbH, Wertheim, Germany, were employed as received. By fractionation using an air classifier (Hosokawa Alpine Multi-Plex 100 MZR, Hosokawa Alpine AG, Augsburg, Germany), two glass powder fractions, designated F1 and F2, were extracted from P5. By adding the fractionated glass powders to the P4 or P5 glass powder, three powder mixtures were prepared: P4+20F1 (80 vol% P4 + 20 vol% F1), P4+50F1 (50 vol% P4 + 50 vol% F1) and P5+30F2 (70 vol% P5 + 30 vol% F2). Figure 11a and Figure 11b show the particle size distribution of all glass powders used. The particle shape of glass powders P4 and P5 are shown

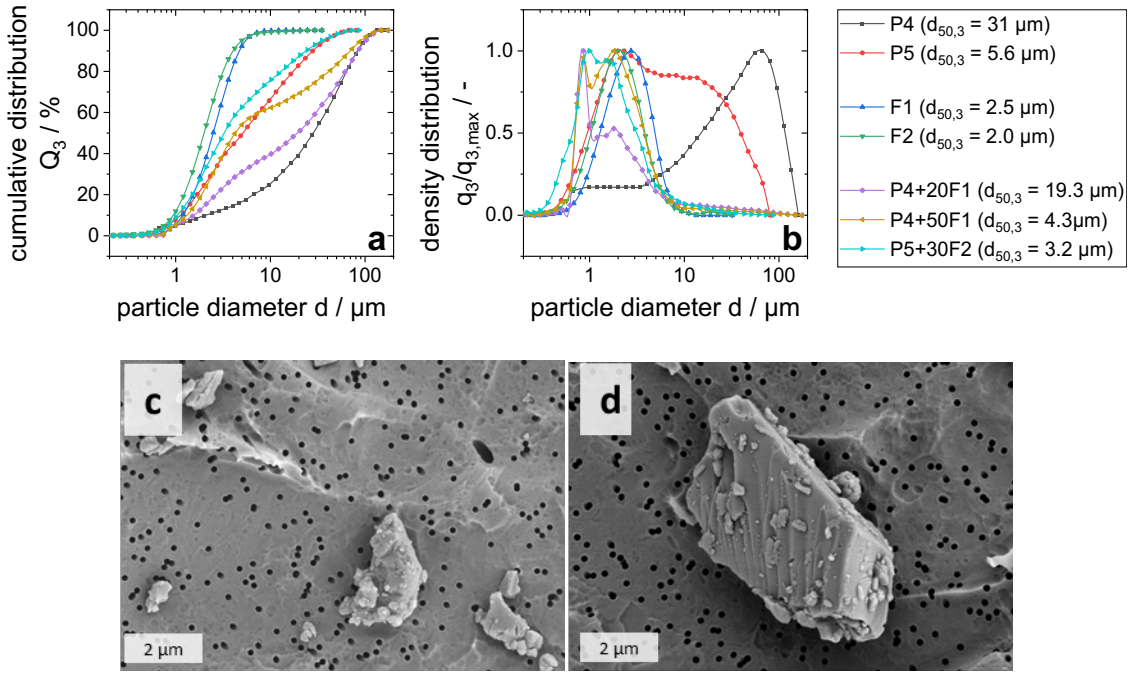

Figure 11 **Glass powder used to prepare the capillary suspensions.** Cumulative (**a**) and density (**b**) distributions of the glass particle sizes as obtained from Fraunhofer diffraction. Scanning electron micrographs (SEM) of glass powders P5 (**c**) and P4 (**d**). To prepare the sample for SEM, the particles were dispersed in ethanol and subjected to ultrasonication to break up the agglomerates. The ethanol was removed by vacuum filtration using a polycarbonate nuclepore membrane with a pore diameter of 200 nm. The membrane with the particles on top was then placed in the SEM. The pores of these membranes are visible as black circles in the SEM images shown above.

in the scanning electron microscopy (SEM) images in Figure 11c and Figure 11d. Both glass particles are fairly isometric and have rounded edges. The capillary suspension filters prepared in this work were labelled according to the name of glass powder used.

To prepare the capillary suspensions, odorless mineral spirits (Merck KGaA, Darmstadt, Germany) with a boiling range between 179 °C – 210 °C, a flash point of 67 °C and a viscosity of 1.33 mPa·s was employed as the main liquid. Its high volatility ensures a gentle removal of the liquid during the debinding processes. D(+)-sucrose (Carl Roth GmbH + Co. KG, Karlsruhe, Germany) was dissolved in distilled water to produce a 50 vol% sucrose solution, which serves as secondary phase. The interfacial tension of sucrose solution with mineral spirits and viscosity of the sucrose solution are 45.3 mN/m and 85 mPa·s, respectively. The three-phase contact angle of a sucrose solution droplet on borosilicate glass 3.3 in the presence of mineral spirits is $\Theta = 52.9°$. Since the sucrose solution, as the secondary fluid, wets the glass better than the mineral spirits as the main liquid, the system can be classified as a capillary suspension in the pendular state (see Chapter 2.2.3). Nonionic surfactant polysorbate 20 (Tween 20, Merck KGaA, Darmstadt, Germany) were used as additive to homogenize the paste and prevent agglomeration.

3.1.2 General processing route

For the preparation of capillary suspensions, a planetary centrifugal mixer (Speedmixer, Hauschild GmbH & Co. KG, Hamm, Germany) was employed. In the first step, a pure suspension was prepared by mixing the glass powder with mineral spirits and a small amount of surfactant polysorbat 20 for four minutes at 2000 rpm. The solids content Φ_{sol} was varied between 20 vol% and 40 vol%. The surfactant volume fraction Φ_{sur} relative to the main liquid is less than 0.7 vol% depending on the solids content. In the second step, sucrose solution as secondary liquid was added drop by drop and the mixture was then mixed for another three minutes. Depending on the solids content and the study being conducted, the secondary liquid content was varied up to a maximum of 8 vol%. The rotational mixer's speed ranged from 1000 rpm to 15000 rpm, adjusted based on the mixture's consistency. Pastes with high yield stress were subjected to higher speeds to enhance homogeneity. The addition of the secondary liquid with the subsequent mixing induced the formation of the particle network, and accordingly the texture of the mixture became paste-like.

Immediately after preparation, the paste was molded by hand into metal templates with different shape depending on the intended experiments. If not otherwise specified, the template was cylindrical with a diameter d of 30 mm and a height h of 6 mm. The resulting green bodies were placed onto a porous substrate and left at room temperature for at least one day. During the so called mechanical debinding, most of the main liquid was removed from the green bodies by absorption into the porous substrate and evaporation.

Afterwards, the resulting brown body was subjected to thermal debinding in a debinding muffle furnace (LHT 04/17, Nabertherm GmbH, Lilienthal, Germany). The debinding process was carried out at temperatures ranging from room temperature to 220 °C, using a gentle heating rate $r_{deb,0}$ = 2 °C/min to delicately remove organic matter. Subsequently, to incinerate any remaining organic residues, the temperature was further increased from 220 °C to 600 °C at a rate of r_{deb} = 7 °C/min, with a final hold time $t_{hold,deb}$ = 5 min. The samples were then gradually cooled to room temperature in the furnace before proceeding to the sintering step.

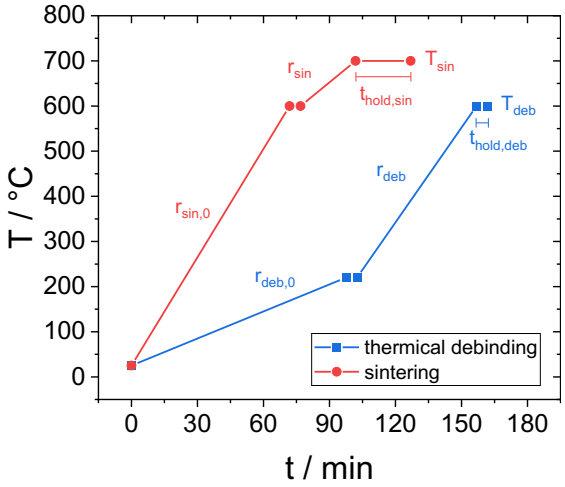

Figure 12 **Temperature profile in the furnace for manufacturing glass filters from capillary suspensions.**

Sintering was performed in a sintering muffle furnace (LVT 05/11, Nabertherm, Lilienthal, Germany). Starting from room temperature, the temperature in the sintering furnace was raised to 600 °C at an initial heating rate of $r_{sin,0}$ = 8 °C/min. The temperature was then further increased to the sintering temperature T_{sin}, which varied between 620 °C and 750 °C. Since the glass transition temperature of borosilicate glass 3.3 is 525 °C [60], the chosen sintering temperature is significantly higher, ensuring that sintering occurs. By default, the heating rate r_{sin} and holding time $t_{hold,sin}$ during this phase were 4 °C/min and 3 min, respectively. After sintering, the furnace was turned off and the samples were allowed to cool to room temperature inside the furnace. The complete temperature profiles in both furnaces are shown in Figure 12. Unless otherwise specified, the thermal debinding and sintering parameters mentioned here apply.

3.1.3 Investigation of shrinkage behavior

Investigation of the volumetric shrinkage due to both debinding and sintering processes were employed. P5 glass powder was used for this purpose. Cylindrical template (d = 45 mm, h = 5 mm) were employed to shape the capillary suspension. The samples were sintered at r_{sin} = 2 °C/min and $t_{hold,sin}$ = 1 h. The optical examination of sample shrinkage was conducted by analyzing the change in diameter and height, thereby assessing the volume changes of the filters. Employing a digital microscope (VHX-950F, Keyence Deutschland GmbH, Neu-Isenburg, Germany), the dimensions of the cylindrical samples were determined. The cylindrical samples are carefully placed on the sample stage. Side-view images of the samples were then captured by tilting the microscope's camera to 90° (see Figure 13). The height, diameter, and consequently the volume of the samples were measured at different stages of the process. The indices "bbII" and "sb" refer to the brown body II (the sample

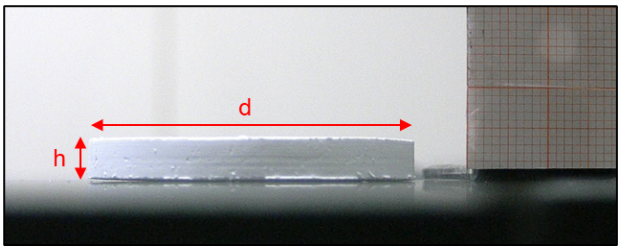

Figure 13 **Determination of cylindrical sample dimensions using a digital microscope.** The samples were placed on a flat surface, and the microscope camera was tilted to capture a side view of the samples. A millimeter scale reference was placed next to the cylindrical samples, ensuring it was positioned at the same distance from the camera as the center of the samples. Using this scale, the diameter (d) and height (h) of the samples were measured.

after thermal debinding, as shown in Figure 5) and the sintered body, respectively. The index "mold" represents the dimensions of the cylindrical metal template used for molding, representing the initial dimensions after molding. The indices “V”, “d”, and “h” denote volume, radius, and height, respectively. The debinding, sintering and total shrinkage ratios were then calculated using following formula:

$$r_{V,shrink,debinding} = 1 - \frac{V_{bbII}}{V_{mold}} = 1 - \frac{{d_{bbII}}^2 * h_{bbII}}{{d_{mold}}^2 * h_{mold}} \quad (4)$$

$$r_{V,shrink,sintering} = 1 - \frac{V_{sb}}{V_{bbII}} = 1 - \frac{{d_{sb}}^2 * h_{sb}}{{d_{bbII}}^2 * h_{bbII}} \quad (5)$$

$$r_{V,shrink,total} = 1 - \frac{V_{sb}}{V_{mold}} = 1 - \frac{{d_{sb}}^2 * h_{sb}}{{d_{mold}}^2 * h_{mold}} \quad (6)$$

$$r_{h,shrink,debinding} = \frac{h_{bbII}}{h_{mold}} \quad (7)$$

$$r_{h,shrink,sintering} = \frac{h_{sb}}{h_{bbII}} \quad (8)$$

$$r_{h,shrink,total} = \frac{h_{sb}}{h_{mold}} \quad (9)$$

$$r_{d,shrink,debinding} = \frac{d_{bbII}}{d_{mold}} \quad (10)$$

$$r_{d,shrink,sintering} = \frac{d_{sb}}{d_{bbII}} \quad (11)$$

$$r_{d,shrink,total} = \frac{d_{sb}}{d_{mold}} \quad (12)$$

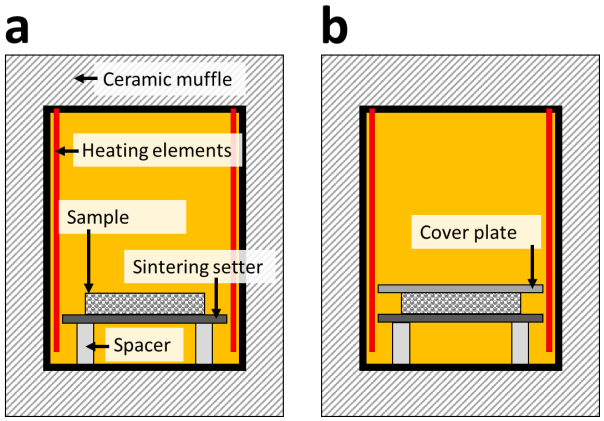

Figure 14 **Setup of the sintering muffle furnace (LVT 05/11, Nabertherm, Lilienthal, Germany).** Samples were sintered on sintering setter without (**a**) or with (**b**) cover plate. The cover plate has the same material and dimensions as the sintering setter used and serves to shield the specimens from the heat that came mainly from the top of the open chamber.

3.1.4 Investigation of porosity gradient

P5 glass powder was employed for the investigation of the porosity gradient. The capillary suspensions were molded in two different shape: cube with side length l = 10 mm and cylinder with d = 45 mm, h = 5 mm. During sintering, the sample was placed on a thin, porous sintering setter. Two types of setters were used: a porous alumina plate (Keralpor 99, Kerafol, Eschenbach in der Oberpfalz, Germany) and a quartz frit (G00, MICQ Shanghai Wechance Industrial Co., Ltd, Shanghai, China). The properties of the corresponding sintering setters are found in Table 1. Unless otherwise stated, an alumina plate was used by default as sintering setter in this investigation.

Table 1 **Properties of the sintering setters.** Information marked with an asterisk (*) is provided by the manufacturer.

	Alumina plate	Quartz frit
Plate thickness / mm	2	3
Total porosity / %	34	35
Material	99.5 % Al_2O_3*	> 99.99 % SiO_2*
Specific heat capacity of the material / J/kg/°C	775 [49]	670*
Thermal conductivity of the material / W/m/°C	30-40 [49]	1,4*

To avoid direct contact with the bottom of the furnace chamber, cylindrical ceramic spacers were placed between the sintering setter and the bottom of the furnace chamber. The location of the heating rods was lateral across the total height (h = 150 mm) of the furnace. The sample was mainly heated from above since it was in the lower part of the furnace chamber (ca. 40 mm above the base). Two setups of the sintering furnace, which differed in the covering of the sample, are shown in Figure 14. While the top surface of the sample in the first setup was in direct contact with the air (Figure 14a), it was covered with the same plate as the sintering setter in the second setup (Figure 14b). Unless otherwise indicated, the first setup without covering is to be assumed.

For determination of the extent of the porosity gradient, cross-sections were made in the center part of the sintered specimens by precise cutting and grinding. The position of the cross-section taken is indicated in Figure 15a. With the aid of a scanning electron microscope (S-4500, Hitachi High-Technologies Europe GmbH, Krefeld, Germany), images of the pore structure were taken over the total height of the sample (Figure 15b). Using image analysis software ImageJ (Rasband, W.S., ImageJ, U.S. National Institutes of Health, Bethesda, Maryland, USA), the acquired SEM images were despeckled to minimize image grain and then binarized, resulting in binarized images (Figure 15c). Porosity was manually

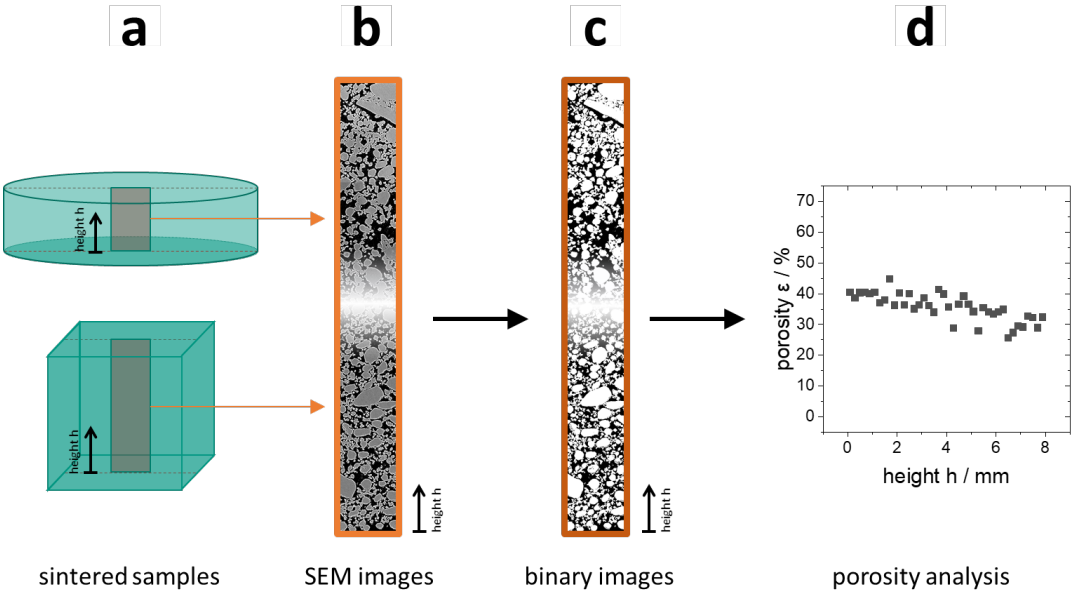

Figure 15 **Porosity gradient analysis method.** (**a**) shows the cross-sectional area, shown in gray, used for porosity gradient analysis. Note that the height scale starts from the lower part of the sample contacting the sintering setter. (**b**) shows exemplary the cross-section of samples made from capillary suspension with Φ_{sol} = 40 vol%, Φ_{sec} = 8 vol% and Φ_{sur} = 0.2 vol% sintered using quartz frit as sintering setter at r_{sin} = 4 °C/min, T_{sin} = 745 °C and $t_{hold,sin}$ = 3 min taken by SEM microscopy over the full height of the sample. The processed and binarized image (**c**) was then analyzed using image analysis software to determine porosity as a function of sample height (**d**).

determined at 0.2 mm height intervals by calculating the ratio of black (representing pores) to the total image area at each image interval.

3.1.5 Asymmetric membrane

The asymmetric membranes presented in this project consist of two layers with different particle structures: a thin layer with a fine pore structure and an underlying, thick and coarse-pored substrate. The asymmetric membranes were manufactured in two steps: Fabrication of the substrate and the subsequent coating of the already sintered substrate with a thin membrane layer. Capillary suspensions made of P4 and F2 glass powder were used for the substrate and the coating, respectively. Both glass powders have the same material, which is beneficial to reduce thermal expansion mismatch during sintering, since this can promote cracking [47]. To manufacture the substrate, capillary suspension (Φ_{sol} = 35 vol% and Φ_{sec} = 5 vol%) was molded into a cylindrical template (d = 45 mm, h = 6 mm), mechanically and thermally debinded, and afterwards sintered at T_{sin} = 700 °C and $t_{hold,sin}$ = 15 min. Other process parameters for mixing, molding, mechanical and thermal debinding and sintering are the same as those described in Chapter 3.1.2.

Prior to coating, the substrate thus produced was prepared by grinding and polishing on the coating side using sandpapers with ascending grit sizes, reaching up to 3000, to ensure a smooth and flat surface. The substrate is then subjected to ultrasonic treatment and distilled water as medium to remove any residual particles or contaminants, and subsequently completely dried prior to coating. Approximately 20 drops of mineral spirits were then carefully pipetted onto the surface to be coated to partially wet the substrate. This prevents excessive absorption of the liquid in the coating paste due to capillary forces induced by the porous substrate during coating process. Coating was done by hand using a stainless-steel stencil and doctor blade. The wet film thickness was controlled by the thickness of the stencil and ranged from 0.2 to 1 mm. Capillary suspensions with Φ_{sol} = 20 – 30 vol% and Φ_{sec} = 3 – 5 vol% were employed for the coating. The coated substrate was then mechanically and thermally debinded. To increase the stability of the coating, the coated substrate was ultimately sintered at T_{sin} = 670 – 680 °C and $t_{hold,sin}$ = 15 min. Any other process parameters for mechanical and thermal debinding as well as sintering are the same as those described in Chapter 3.1.2. Sintering setup without cover plate (Figure 14b) was employed during sintering processes performed in this investigation.

3.2 Characterization methods

The particle size distributions of the glass powders were measured using a laser diffractometer (Helos H0309, Sympatec, Clausthal-Zellerfeld, Germany) equipped with an ultrasonic

wet dispersing unit (Quixel, Sympatec). All SEM images were take using a scanning electron microscope (S-4500, Hitachi High-Technologies Europe GmbH, Krefeld, Germany).

The yield stress of the capillary suspensions was determined using a rotational rheometer (Physica MCR 501, AntonPaar GmbH, Graz, Austria) equipped with a vane geometry ST10-4V-8.8/97.5 and a customized cylindrical stainless-steel sample container with a diameter of 34.8 mm and a depth of 10.2 mm was used to avoid wall slip, especially for paste with high yield stress. Yield stress measurements were conducted by incrementally increasing the shear stress while monitoring the deformation. Plotting the deformation against the shear stress on a double logarithmic scale facilitated the determination of the yield stress using the so-called tangential intersection method. Starting with linear elastic deformation at low stresses, indicative of solid behavior, the deformation increased sharply as the sample began to flow. The yield stress σ_y was determined by finding the intersection of two tangents drawn to the two branches of the deformation vs. stress curve (Figure 16).

Three different methods are used to determine the pore size of the sintered samples: mercury porosimetry, bubble point method and image analysis method using SEM images. Pore size determination by mercury porosimetry was performed using a mercury intrusion porosimeter (AutoPore V, Micromeritics GmbH, Unterschleissheim, Germany). The bubble point measurements were performed according to ISO 4793. Prior to measurement, porous sintered samples were immersed in a 75 vol% aqueous ethanol solution and subjected to vacuum treatment in a desiccator equipped with a vacuum pump for approximately 1 minute. The samples were then left in the ethanol for at least 1 hour to ensure thorough filling of all internal pores. A 75 vol% aqueous ethanol solution was also used as the test liquid for the measurement. To determine the bubble point, the air pressure was gradually increased

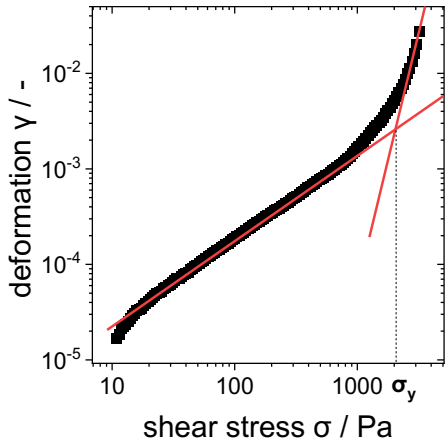

Figure 16 **Tangential intersection method for yield stress determination.** An exemplary plot of deformation versus shear stress for a capillary suspension with Φ_{sol} = 20 vol%, Φ_{sec} = 1.5 vol%, and Φ_{sur} = 0 vol%. The intersection of the two tangent lines indicates the yield stress, σ_y.

from atmospheric pressure until a homogeneous and continuous bubble formation was visibly observed over the entire top surface of the ethanol-covered samples. This pressure represented the bubble point and was used to determine the pore size. In this analysis, the measured pore size is assumed to be the diameter of an ideal spherical pore.

The line intercept method is used to determine pore size by image analysis. Cross-sectional SEM images of epoxy embedded and polished sintered samples were taken for this purpose. The images were then digitally processed to reduce artifacts and grains that could affect measurement accuracy. The images were subsequently binarized. A series of vertical straight lines are systematically superimposed over the image, as shown in Figure 17. The intersection frequency is determined by counting the number of times each line intersects the boundary of a pore. This intersection frequency is then statistically transformed into a pore size distribution following the methodology proposed in [120,121]. For the sake of simplicity, this method assumes that the pores have a circular cross section and the intersection length is equated to the equivalent diameter of a circular pore. All image processing and analysis for this method were performed using MATLAB software (MATLAB 2022a, The MathWorks Inc, Natick, Massachusetts, USA).

The open ε_o and total porosity ε of the sintered samples were determined according to the Archimedean principle following DIN EN 993-1 with distilled water as test medium. It should be noted that porosity determination by image analysis using SEM images, as described in Chapter 3.1.4, was exclusively used in the investigation of the porosity gradient. All other porosity characterizations were conducted utilizing the Archimedean principle.

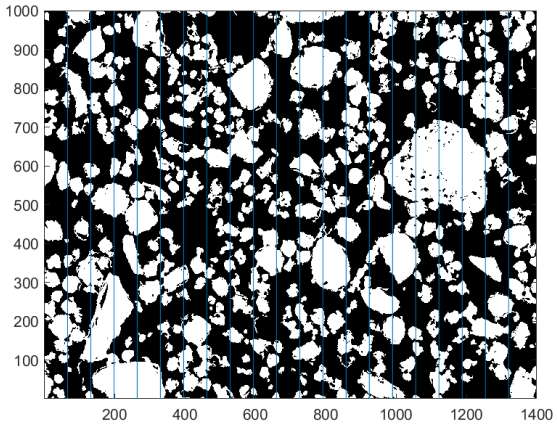

Figure 17 **Line intercept method for pore size determination using SEM images.** SEM cross section of a sintered sample prepared from a capillary suspension with Φ_{sol} = 30 vol%, Φ_{sec} = 5 vol% and Φ_{sur} = 0 vol% and sintered at r_{sin} = 4 °C/min, T_{sin} = 650 °C and $t_{hold,sin}$ = 60 min. The vertical blue lines indicate the locations used to assess the frequency of line intercepts at pore-particle boundaries.

The specific permeability $\varkappa$ was measured with distilled water as test fluid following Darcy's principle according to DIN 30911-6. The measured specific permeability is standardized to the filter thickness. The flexural strength of sintered samples was determined according to DIN EN 1288-5 using a double ring geometry with support and load ring diameters of 20 mm and 4 mm, respectively. The flexural tests were performed using a universal tensile testing machine (TA.XTplus, Stable Micro Systems Ltd, Godalming, United Kingdom).

3.3 Filtration tests

A filtration test is an experimental procedure designed to evaluate the performance of a filtration system under controlled conditions. During the test, a fluid containing a well-defined particle system is passed through a filter and key parameters of the resulting filtrate are measured to evaluate the effectiveness of the filter. A primary focus is on filtrate flux, which measures the rate at which the fluid passes through the filter and provides insight into the capacity and efficiency of the system. Another critical parameter is turbidity, which quantifies the clarity of the filtrate during filtration.

3.3.1 Particle system for filtration tests

Table 2 shows three different particles used for the filtration tests: lactic acid bacteria *Oenococcus oeni* (Lalvin VP41, Lallemand, Montreal, Canada) and two polystyrene particles (micromer plain, micromod Partikeltechnologie GmbH, Rostock, Germany) with a particle diameter of 1 µm and 0.5 µm, as defined by the manufacturer. To prepare the lactic acid bacteria suspension (MSB), the dried powder was dispersed in distilled water and mixed

Table 2. Properties of the suspensions utilized for the filtration tests.

Suspension	MSB	PS1	PS0.5
Dispersed particles	Lactic acid bacteria *Oenococcus oeni*	Polystyrene spheres	Polystyrene spheres
Particle diameter $d_{50,3}$ / µm	0.9	0.9	0.4
Particle shape	ellipsoid	spherical	spherical
Compressible?	yes	no	no
Dispersant	distilled water	distilled water	distilled water
Concentration / µg/L	85	1.2	0.8
Turbidity / ntu	5 ± 0.4	5 ± 0.4	5 ± 0.4

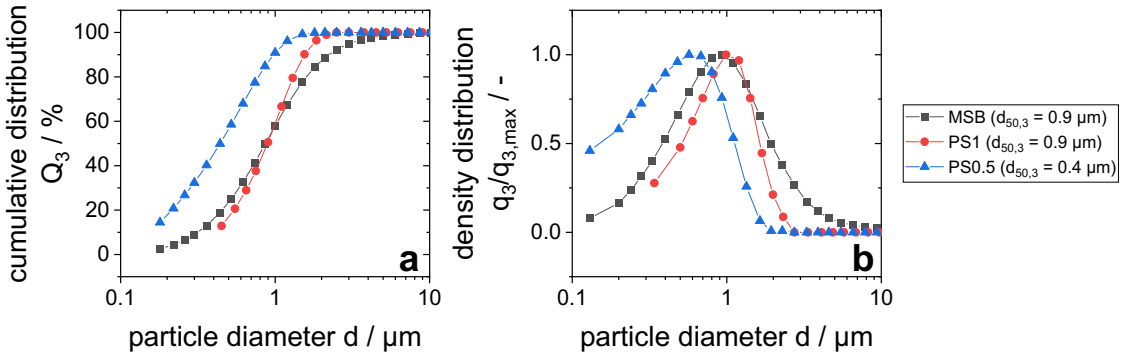

Figure 18 **Particle size of the particles used in filtration tests**. Cumulative (**a**) and density (**b**) distributions of MSB, PS1 and PS0.5, the properties of which are listed in Table 2.

with magnetic stirrer for 20 min at 20 °C. Both polystyrene particles were already dispersed in suspension as manufactured. For the filtration test, the original polystyrene suspensions were diluted in distilled water to the desired concentration and placed in in ultrasonic bath for 15 min to homogenize the suspension. The two polystyrene suspensions are referred to as PS1 and PS0.5. Table 2 summarizes the properties of all suspensions used. The particle size distributions are found in Figure 18.

3.3.2 Filtration performance assessment

To comprehensively evaluate the filtration performance, turbidity measurements and filtrate flux determinations were performed using two different setups, as shown in Figure 19: dead-end and cross-flow filtration. The central component of the setup is the pressurized housing cell containing the suspension. To avoid potential adverse effects of sedimentation, a freshly prepared suspension was used for each filtration test. Compressed air connected to the top of the housing cell provided a constant filtration pressure of 0.8 bar in both configurations. The bottom of the housing cell provided an opening for filtrate flow.

Both dead-end and cross-flow filtrations were performed to assess filtrate flux, which was determined by measuring the filtrate flow rate using an electronic laboratory balance. In the cross-flow setup, additional inlet and outlet openings in the pressurized housing cell facilitated the circulation of the suspension, which was pumped by an air-operated double diaphragm pump (VA25 (HE), Verder Deutschland GmbH & Co. KG, Haan, Germany). The flow rate was maintained constant at 8.3 L/min. To avoid suspension saturation, the concentration in the suspension tank was continuously controlled by manually dilution with distilled water. The cross-flow filtration setup was equipped with a backwash mechanism that could be activated as needed. The backwash, performed with distilled water against the direction of filtration, occurred periodically every 20 minutes for a duration of 2 minutes. The backwash set pressure was 1.6 bar, resulting in an effective transmembrane pressure

of 0.8 bar. Turbidity measurements were performed exclusively in the dead-end setup. For this measurement, every 10 mL of the filtrate was carefully collected in separate containers. The turbidity of each 10 mL filtrate sample was then measured using a turbidimeter (PCE-TUM 20, PCE Deutschland GmbH, Meschede, Germany

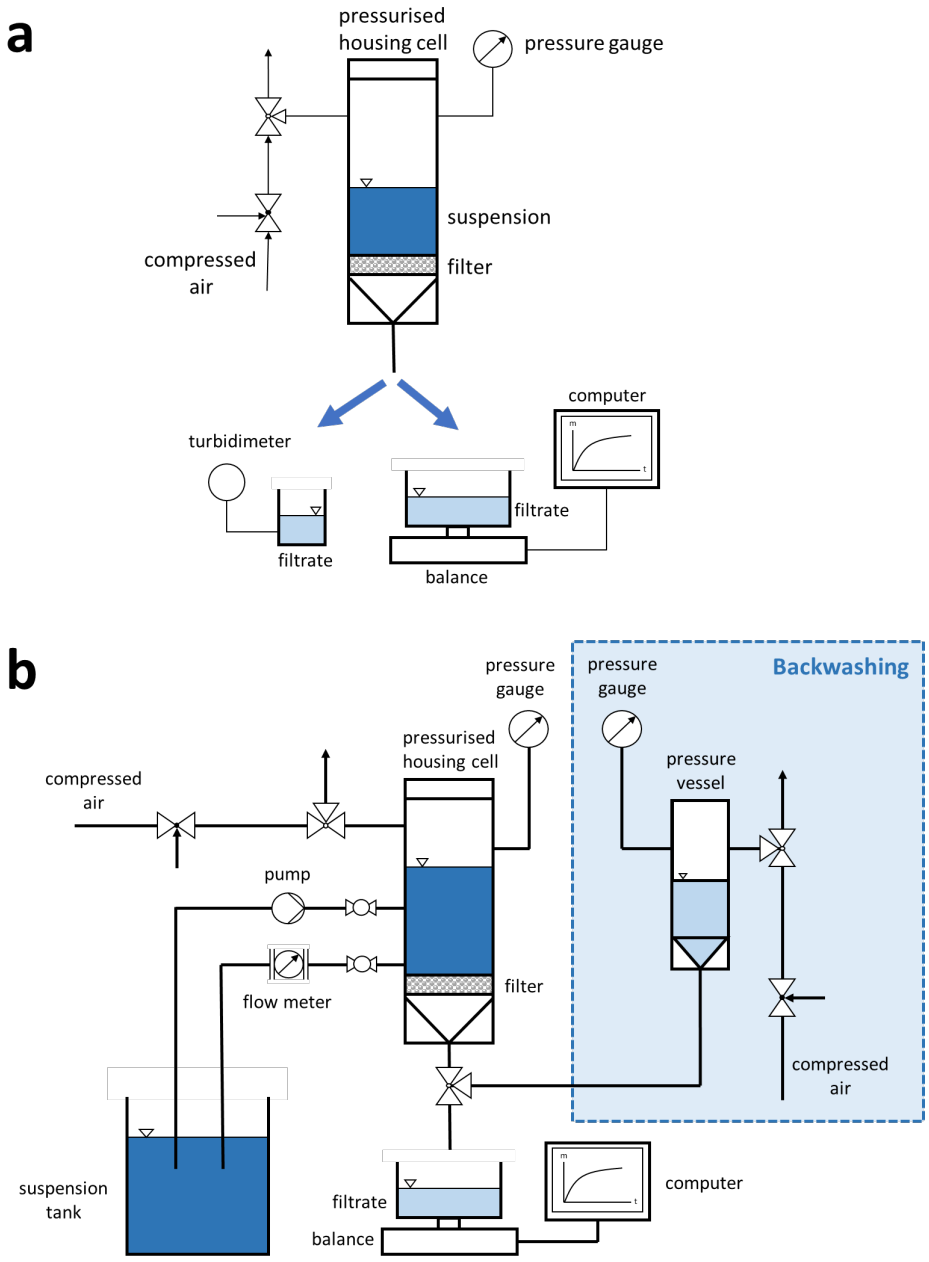

Figure 19 **Setup of the filtration tests.** Dead-end (**a**) and cross-flow (**b**) filtration setup.

4 Manufacturing of glass filters

This chapter addresses the manufacturing processes of glass filters made from capillary suspensions, focusing specifically on shrinkage behavior and pore structure. The manufacturing process, particularly during the debinding and sintering, often results in shrinkage where the samples become more compact. Controlling this shrinkage is critical as uncontrolled shrinkage can lead to defects such as cracks or dimensional inaccuracies. Chapter 4.1 considers the effect of paste composition and sintering conditions on shrinkage behavior and evaluates the dimensional accuracy of the resulting samples. Chapter 4.2 examines rheological measurements to characterize the paste and establish correlations between these properties and the final pore structure. This section examines how variations in paste composition, secondary liquid content, particle size distribution and sintering conditions affect the pore structure of the filters. In addition, Chapter 4.3 discusses the phenomenon of porosity gradients that can occur as a function of sintering conditions. This chapter examines how different sintering parameters contribute to variations in porosity within the filter sample, thereby affecting the overall pore distribution. Understanding these variations is essential as the performance of the filters is closely related to their pore structure.

4.1 Shrinkage behavior

This chapter investigates the shrinkage behavior of porous glass made of capillary suspension. The shrinkage process studied here is divided into debinding and sintering shrinkage. The debinding processes include both mechanical and thermal removal of the organic components. Figure 20 shows that debinding shrinkage is significantly influenced by the solids content of the samples, with lower solids content leading to a higher degree of shrinkage. A higher solids content results in the particles being less mobile, which reduces the extent of shrinkage. Compared to samples from pure suspensions, shrinkage during debinding of capillary suspensions is significantly less pronounced, approximately 20% less, and this is attributed to the strong capillary forces preventing collapse of the particle network.

The shrinkage ratio increases with raising sintering temperature. A higher sintering temperature is correlated with greater sintering activity, resulting in a more pronounced densification of the particle structure. In contrast to debinding shrinkage, sintering shrinkage at a same sintering temperature shows no dependence on solids content. Within the measurement error, there is also no difference between the pure suspensions and the capillary suspensions with respect to sintering shrinkage, as can be seen for samples sintered at 680 °C. The total shrinkage in Figure 20c includes both debinding and sintering shrinkage. As a

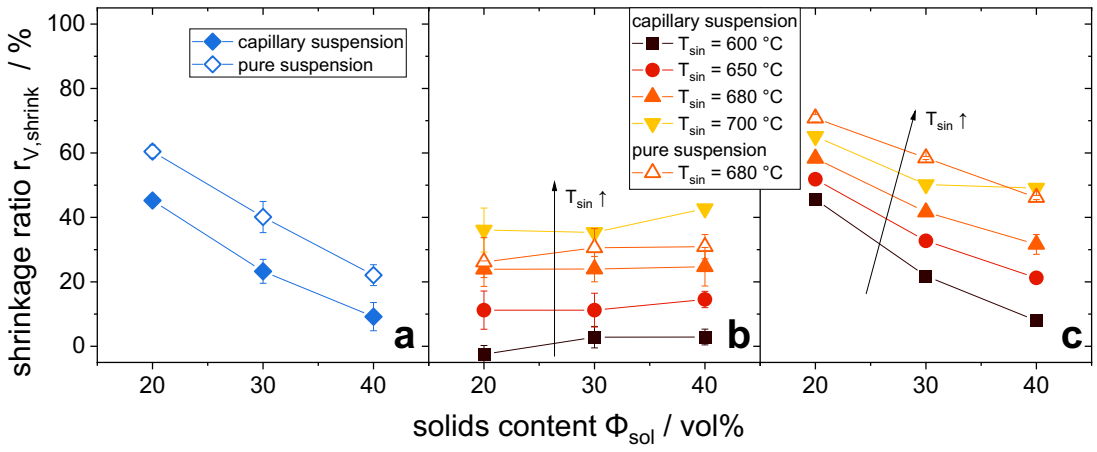

Figure 20 **Shrinkage behavior.** Volumetric shrinkage ratio r_{shrink} of glass filters due to debinding (calculated according to Eq. (4)) (**a**) and sintering (calculated according to Eq. (5)) (**b**) processes as a function of the solids content Φ_{sol}. Heating rate r_{sin} and holding time $t_{hold,sin}$ during sintering are 2 °C/min and 1 h, respectively. The total shrinkage ratio (calculated according to Eq.(6)) (**c**) is composed of the debinding and sintering shrinkage ratios. The capillary suspensions were prepared using P5 glass powder with a secondary fluid content of Φ_{sec} = 3 vol%, Φ_{sec} = 5 vol% and Φ_{sec} = 8 vol% for Φ_{sol} = 20 vol%, Φ_{sol} = 30 vol% and Φ_{sol} = 40 vol%, respectively.

result, the samples shrink as a function of both solids content and sintering temperature. In summary, low shrinkage ratio can be achieved by high solids content and low sintering temperature.

Dimensional analysis is critical for evaluating the dimensional accuracy of the final samples. This analysis was performed by assessing the changes in height and diameter of the cylindrical samples after the debinding and sintering processes. Isotropic shrinkage occurs when shrinkage is uniform in all dimensions. Otherwise, if the shrinkage is uneven and preferentially occurs in a particular direction, it is referred to as anisotropic shrinkage. As mentioned above, the debinding process consists of mechanical and thermal processes. During the mechanical debinding process, two distinct debinding mechanisms take place: absorption and evaporation. When the green body comes into contact with the porous substrate, it immediately and rapidly absorbs the liquid from the samples. However, some of the mineral spirits, which is the main liquid in the samples, also evaporates during this process due to its volatile nature. Moisture gradually escapes from the samples, with the liquid removal rate by evaporation being comparatively lower than that by absorption, particularly at the beginning of the debinding process. While liquid absorption by the porous substrate exerts axial stress in the same direction as the height of the samples, evaporation occurs on all surfaces exposed to ambient air, resulting in both radial and axial stresses. The disk samples used have more area on the top and bottom surface than on the lateral surface, resulting in

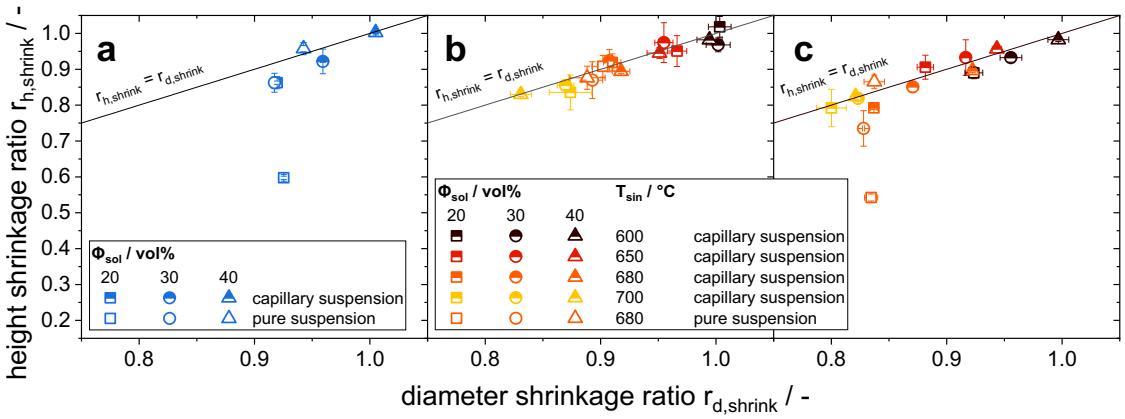

Figure 21 **Shrinkage isotropy.** Dimensional change of the samples after debinding (**a**) and sintering (**b**). The total dimensional change of the samples, which includes both debinding and sintering, is shown in (**c**). The height and diameter shrinkage ratio were calculated according to Eq. (7) - (12). Heating rate r_{sin} and holding time $t_{hold,sin}$ during sintering are 2 °C/min and 1 h, respectively. The capillary suspensions were prepared using P5 glass powder with a secondary fluid content of Φ_{sec} = 3 vol%, Φ_{sec} = 5 vol% and Φ_{sec} = 8 vol% for a solids content of Φ_{sol} = 20 vol%, Φ_{sol} = 30 vol% and Φ_{sol} = 40 vol%, respectively.

more extensive debinding by both absorption and evaporation in the axial direction. As a result, the specimens are susceptible to anisotropic shrinkage, with a preference for shrinkage in the axial direction. Thermal debinding removes residual organic material at high temperature. Since the amount of residual organic material after mechanical debinding and the burning process are negligible and supposedly have little effect on the shrinkage of the samples, it is to be assumed that the debinding shrinkage is primarily due to adsorption and evaporation.

Figure 21a shows the dimensional change of the samples after debinding. The diagonal lines mark the ideal isotropic shrinkage ($r_{h,shrink} = r_{d,shrink}$). It can be seen that both the capillary and pure suspension samples exhibit isotropic shrinkage, except for the pure suspension at lower solids content. The 20 vol% pure suspension sample shows a strong anisotropic behavior, which can be attributed to the absence of a stabilizing particle structure and the excessively low solids content. When comparing the 20 vol% and 30 vol% pure suspensions, both lack the particle network observed in capillary suspension samples. However, the 30 vol% suspension demonstrates better shrinkage isotropy. This enhanced isotropy is likely due to the higher packing density, which increases the number of particle contacts and interactions. These interactions might be useful at mitigating the anisotropic stresses, which are more prevalent in the axial direction, that are generated during the debinding process. As shown in Figure 21b, all samples exhibit isotropic shrinkage behavior during sintering, regardless of solids content, with no observed difference between capillary suspensions and pure suspensions

4.2 Pore structure

The pore structure of a filter is a critical parameter that directly influences its filtration performance. In sintered filters made from capillary suspensions, the pore architecture is a direct result of the particle network established within the capillary suspension [29]. The rheological properties, including the yield stress, of the capillary suspensions can provide information about the particle network in the pastes. Figure 22 shows the correlation between the yield stress and the secondary fluid content for capillary suspension pastes with varying solids content. An increase in solids content is accompanied by a corresponding increase in yield stress. This can be explained by the fact that higher solids content leads to a greater number of particle contacts, resulting in more frequent and pronounced interparticle interactions. The pure suspensions with Φ_{sec} = 0 vol% have the lowest yield stress compared to all other capillary suspensions with the same solids content. With the addition of secondary liquid, the yield stress increases significantly by the order of more than a decade before reaching a plateau at Φ_{sec} > 1.5 vol% and Φ_{sec} > 3 vol% for the samples made from the glass powder P5 and F1, respectively. This behavior corresponds to the typical yield stress increase of capillary suspensions from regime I to regime II investigated by Dittmann et al [29] (see Figure 7). The increase in the yield stress is attributed to the formation of the particle network typical for capillary suspensions [27]. All capillary suspension pastes used to manufacture the glass filters in this work exhibit this behavior. Capillary suspensions with the same solids content have a higher yield stress when the suspended particles are smaller. This can be observed at Φ_{sol} = 30 vol% for both P5 and F1. Smaller particles exhibit a higher number of contacts at a given volume fraction. This result in a denser and more

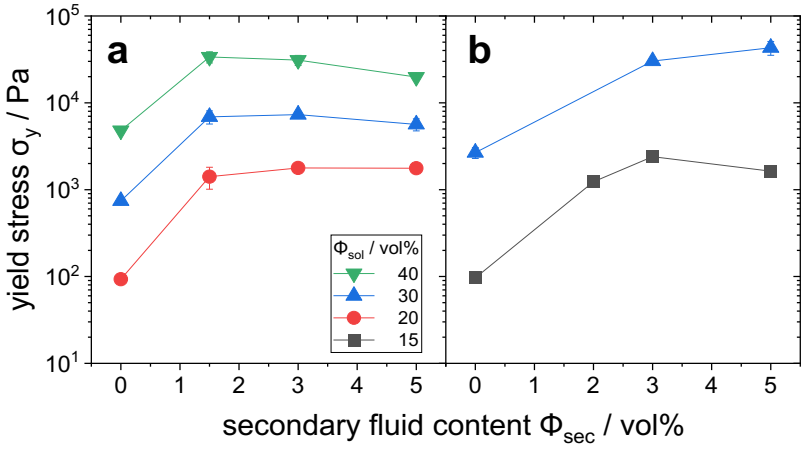

Figure 22 **Rheological properties of the capillary suspension pastes**. Yield stress of capillary suspensions made with glass powders P5 ($d_{50,3}$ = 5.6 µm) (**a**) and F1 ($d_{50,3}$ = 2.5 µm) (**b**) at various solids contents Φ_{sol} as a function of secondary fluid contents Φ_{sec}.

cohesive particle network, requiring more stress to break or deform the network, thus increasing the yield stress of the suspension.

The formation of the particle network in capillary suspension correlates with the increase in porosity of the samples after sintering, which can be clearly observed in Figure 23. It should be noted that the sintered samples in Figure 23 were manufactured using the corresponding pastes measured in Figure 22a. Sintered samples made from capillary suspensions have a significant higher porosity of about 30% than those made from pure suspensions (Φ_{sec} = 0 vol%) with the same solids content. The porosity is also related with the shrinkage behavior, as shown in Figure 20. The shrinkage ratio of pure suspension samples without secondary liquid is higher in comparison to capillary suspension samples with the same solids content. The secondary liquid, which forms capillary bridges between the particles, stabilizes the particle structure in the capillary suspensions during the manufacturing processes. As a result, the densification of the particle structure and the shrinkage are reduced, resulting in a higher porosity of the capillary suspension based sample compared to a sample made from a pure suspension with the same solids content.

For capillary suspension samples with the same secondary fluid content, the porosity depends on the solids content, with the porosity increasing as the solids content decreases. Low solids content is accompanied by lower particle packing density. From the previous results in Figure 20, it can be seen that samples with lower solids content tend to densify and thus shrink more. However, the effect of lowering the solids content to achieve a lower particle packing density is clearly dominating the densification and shrinkage during the

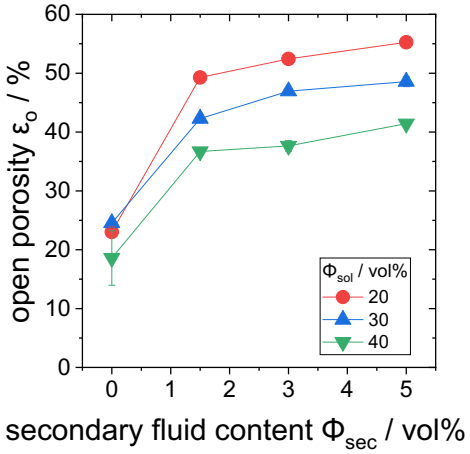

Figure 23 **Open porosity of sintered glass filter**. The influence of the secondary liquid content Φ_{sec} on the open porosity ε_o at different solids content Φ_{sol}. All samples were made from glass powder P5 and sintered with r_{sin} = 2 °C/min at T_{sin} = 680 °C for $t_{hold,sin}$ = 1 h. Yield stress measurements of the capillary suspensions used in the manufacture of these sintered glass filters are shown in **Fehler! Verweisquelle konnte nicht gefunden werden.**a.

manufacturing processes that cause the particle packing density to increase. As a result, samples with lower solids content can achieve higher porosity.

The densification and the porosity of sintered materials can be influenced by adjusting the sintering conditions, such as heating rate r_{sin}, holding time $t_{hold,sin}$ and sintering temperature T_{sin}. In Figure 24 different samples are sintered under different sintering conditions. It is evident that samples made from capillary suspensions have consistently higher porosity than those made from pure suspensions sintered under the same conditions, which is in line with the previous results. Overall, the heating rate exhibits the least influence on the porosity. The porosity is almost constant in the range of r_{sin} = 0.5 – 7 °C/min. Increasing the holding time can influence the porosity by allowing for prolonged particle rearrangement and bonding, resulting in lower porosity. Sintering temperature has the greatest impact on porosity. Higher temperatures directly influence the thermal energy available to the particles being sintered, which enhances the sintering activity, resulting in more pronounced densification and porosity reduction.

In addition to sintering temperature, particle size plays a crucial role in the densification process during sintering, as shown in Figure 25. Under the same sintering temperature, higher solids content results in a reduced porosity, aligning with the results in Figure 23. However, it's important to note that for a constant sintering temperature, the degree of sintering and thus densification are more pronounced when dealing with smaller particles. This phenomenon is clearly exemplified in Figure 25f for samples with Φ_{sol} = 30 vol%. There

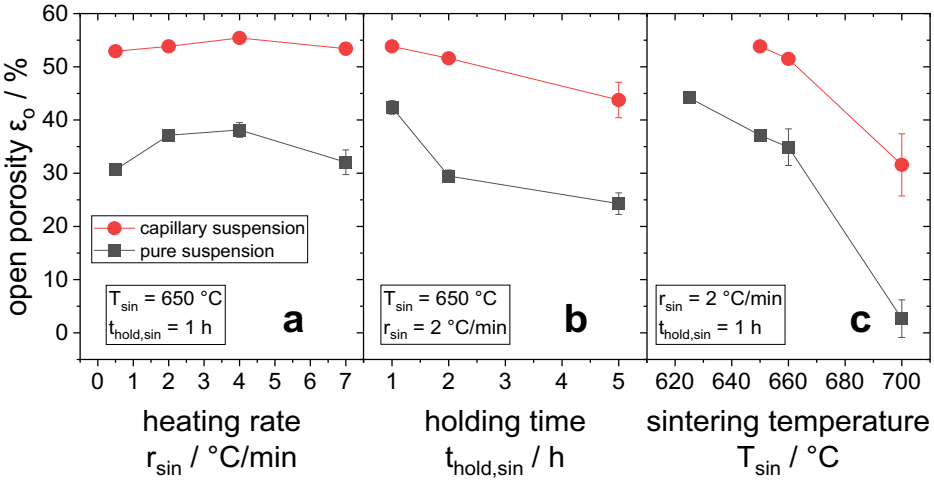

Figure 24 **Influence of sintering conditions on open porosity.** Samples made from glass powder P5 with a solids content of Φ_{sol} = 30 vol% and a secondary fluid content of Φ_{sec} = 5 vol% were subjected to varying sintering conditions: heating rate r_{sin} (**a**), holding time $t_{hold,sin}$ (**b**), and sintering temperature T_{sin} (**c**)."

is a shift of the sintering curve towards lower sintering temperatures for smaller particles. This behavior can be attributed to the fact that smaller particles possess higher specific surface areas, which leads to a higher sintering activity and thus a higher sintering rate [112–114].

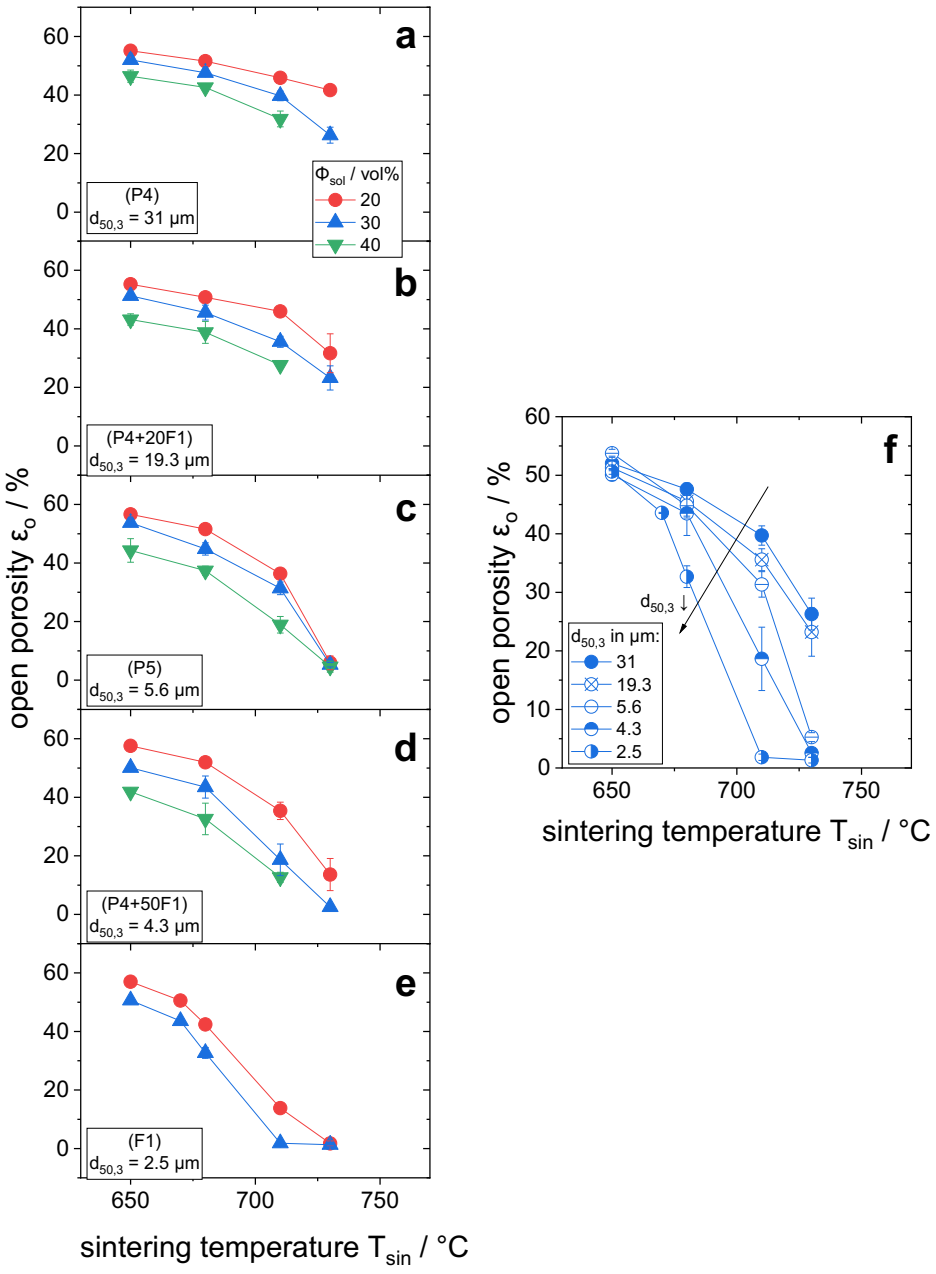

Figure 25 **Influence of particle size on the pore structure of the sintered filter.** The open porosity ε_o is shown for samples prepared using capillary suspensions made from glass powders with different particle sizes: P4 ($d_{50,3}$ = 31 µm) (**a**), P4+20F1 ($d_{50,3}$ = 19.3 µm) (**b**), P5 ($d_{50,3}$ = 5.6 µm) (**c**), P4+50F1 ($d_{50,3}$ = 4.3 µm) (**d**), and F1 ($d_{50,3}$ = 2.5 µm) (**e**). In (**f**), the open porosity ε_o is summarized for all samples with a solids content of Φ_{sol} = 30 vol%. All samples were sintered with a heating rate of r_{sin} = 4 °C/min and a holding time of $t_{hold,sin}$ = 15 min.

In conclusion, this chapter highlights the factors that influence the pore structure and densification of the sintered bodies. The porosity of the sintered bodies correlates with the particle network within the capillary suspensions. Furthermore, it is evident that samples prepared from pure suspensions have consistently lower porosity compared to those prepared from capillary suspensions. This discrepancy is due to the absence of a robust particle network that serves to stabilize the sample during the manufacturing process, mainly during debinding. Among the sintering parameters studied, the sintering temperature is the dominant factor influencing the densification of the sintered body. In particular, the densification of smaller particles commences at lower temperatures compared to larger particles, primarily due to their greater specific surface area.

4.3 Porosity graded structure

A spatially inhomogeneous temperature distribution in a sintered body during the sintering process can lead to locally different sintering activity and thus an inhomogeneous particle structure afterwards, which could express in a porosity gradient. Sintering factors affecting the formation of such porosity gradients are investigated in this chapter.

The morphology of pore structure with porosity gradient is illustrated in Figure 26a – Figure 26e, where the varying degrees of densification in the pore structure at different height positions within a sintered sample are clearly visible. The porosity gradient is gradual, starting from the bottom of the sample at h = 0mm (Figure 26a), where the sample contacts the sintering setter in the furnace, and progressing to the top (Figure 26e), where the sample is exposed to the atmosphere. At h = 0 mm, the pore structure is relatively loose. As the height increases, the structure gradually becomes denser. The smaller particles begin to sinter and coalesce into larger particles. By h = 7.3mm, sintering has advanced to the point where many open pores have transitioned into closed pores. The observed decrease in porosity towards the top of the sample suggests that the temperature in the upper regions of the sample is higher than in the lower regions, leading to increased sintering activity at the top. This thermal gradient is likely due to the low positioning of the samples within the sintering furnace chamber, as illustrated in Figure 14, which causes heat to be predominantly applied from above. While porosity gradients can also arise due to gravitational forces acting on the particles during sintering [38,122], typically resulting in decreased porosity with increasing depth, our findings indicate that thermal effects dominate over gravitational effects. This conclusion is supported by the relatively thin nature of the samples, which limits the impact of gravity compared to thermal influences.

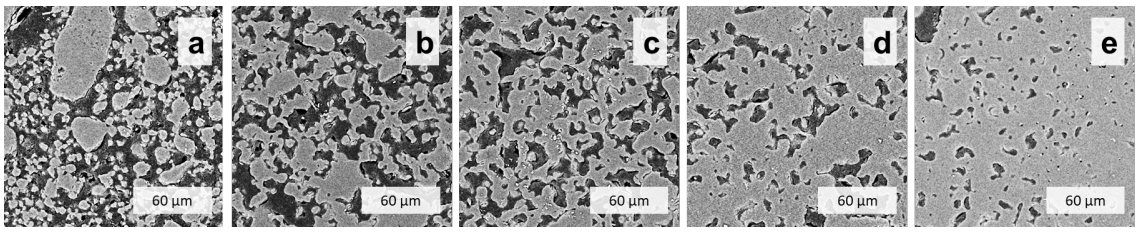

Figure 26 **Morphology of pore structure with porosity gradient.** (**a**) – (**e**) illustrate the gradual change in pore structure at different height positions within a sintered sample: (**a**) h = 0 mm, (**b**) h = 1.9 mm (**c**) h = 3.7 mm, (**d**) h = 5.5 mm, (**e**) h = 7.3 mm. The height position h = 0 mm corresponds to the contact point of the sample with the sintering setter in the furnace. The sample was prepared using capillary suspension made from glass powder P5 with a solids content of Φ_{sol} = 30 vol% and a secondary fluid content of Φ_{sec} = 5 vol%, molded into a cubic shape with an initial side length of 10 mm. The sample was sintered with a heating rate of r_{sin} = 4 °C/min, a sintering temperature of T_{sin} = 710 °C and a holding time of $t_{hold,sin}$ = 15 min.

In order to quantify the extent of porosity gradient developed within sintered samples, the porosity in the middle of the samples is plotted over the total sample's height, as shown in the following graphs (Figure 27 - Figure 29a). All curves were linearly fitted and the slope m is used to assess the extent of porosity gradient formation. A porosity gradient, where porosity decreases with increasing sample height, is present in the majority of samples examined. Figure 27 shows an analysis of how heating rate and holding time affect the formation of porosity gradient. It is obvious that as the heating rate decreases and the holding time increases, the magnitude of the porosity gradient becomes more pronounced. This suggests that extending residence time in the sintering furnace promotes the development of

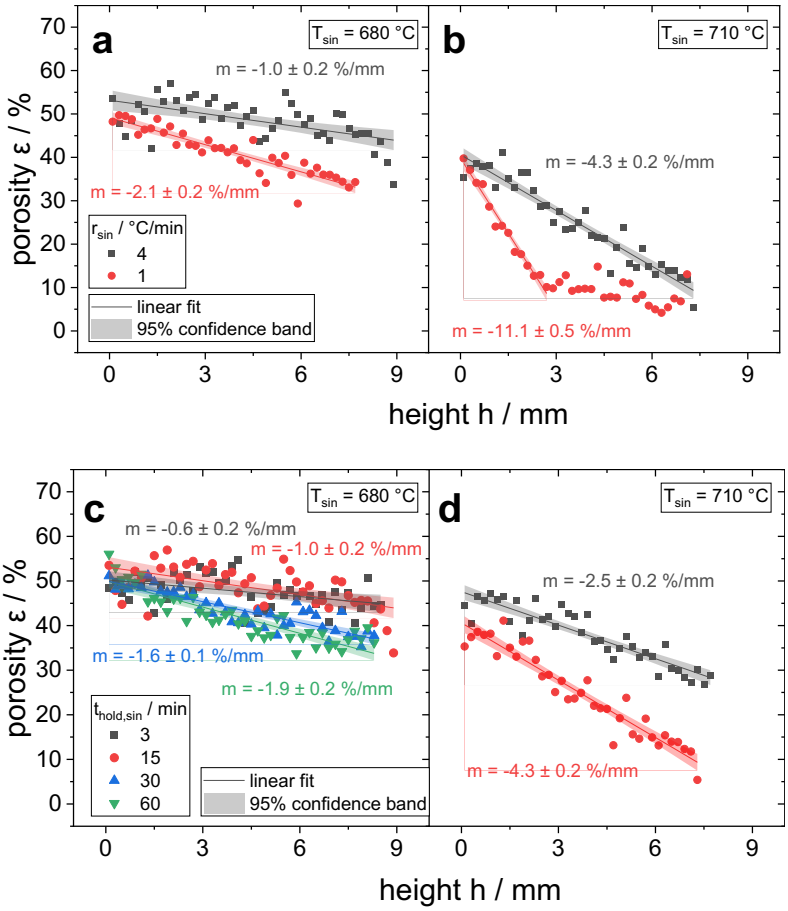

Figure 27 **Influence of sintering parameters on porosity gradient formation.** (**a**) – (**d**) show the porosity profile over the sample height. In (**a**) and (**b**), the samples were sintered at different heating rates with a constant holding time $t_{hold,sin}$ = 15 min. In (**c**) and (**d**), the samples were sintered at different holding time with a constant heating rate of r_{sin} = 4 °C/min. The m value indicates the slope of the curve in the linearly fitted section. All samples were prepared using a capillary suspension of P5 glass powder with a solids content of Φ_{sol} = 30 vol% and a secondary fluid content of Φ_{sec} = 5 vol%, formed into a cubic shape with an initial side length of 10 mm.

porosity gradients. Furthermore, increasing the sintering temperature not only leads to an overall reduction in porosity but also enhances the magnitude of the gradient. For samples sintered at r_{sin} = 1 °C/min, T_{sin} = 710 °C and $t_{hold,sin}$ = 3 min (see Figure 27b), the curve becomes flatter again for h = 3000 µm. This can be attributed to the fact that, at this stage, the porosity at the upper half of the sample is already quite low, causing the sintering activity to slow down significantly as the process progresses, which is typical of the final stages of sintering.

The influence of the sintering setters used in the furnace on the porosity gradient is shown in Figure 28. Two different sintering setters with similar dimensions were employed: porous alumina plate and quartz frit. As can be seen from the diagram, the use of the alumina plate favors the formation of porosity gradients and a slightly lower overall porosity. The two sintering setters have similar properties, except for the thermal conductivity. As shown in Table 1, the thermal conductivity of alumina significantly exceeds that of quartz glass by a factor of approximately 23. It is therefore reasonable to assume that the alumina plate can transfer heat into and out of the sample more quickly during the sintering process, making the temperature distribution within the sample more inhomogeneous.

Figure 29a presents the influence of covering the top part of cylindrical sample during sintering to shield it from the environment, the setup of which is shown in Figure 14b. It is obvious that the covered sample shows no porosity gradient over the total height. By covering the upper part of the specimens, a more homogeneous temperature distribution in the specimen might be achieved, which promotes a more homogeneous pore structure. Cross-

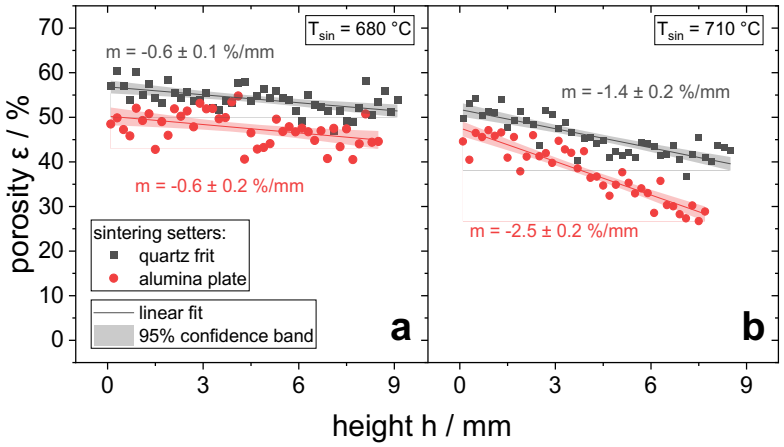

Figure 28 **Influence of sintering setters on porosity gradient formation.** (**a**) and (**b**) show the porosity profile over the sample height for samples sintered at a sintering temperature of T_{sin} = 680 °C and T_{sin} = 710 °C, respectively. All samples were sintered at a heating rate of r_{sin} = 4 °C/min and a holding time of $t_{hold,sin}$ = 3 min and were prepared using a capillary suspension of P5 glass powder with a solids content of Φ_{sol} = 30 vol% and a secondary fluid content of Φ_{sec} = 5 vol%, formed into a cylindrical shape with an initial dimension of d = 45 mm, h = 5 mm.

sectional and surface images of the covered sample were taken using SEM at the upper and lower edge regions (see Figure 29b and Figure 29c). It can be identified that the small particles on the upper side that was in contact with the cover plate are more fused together than on the lower edge region. The sinter necks are more distinctly formed and the particle network appears smoother. This discrepancy confirms again that heat is predominantly

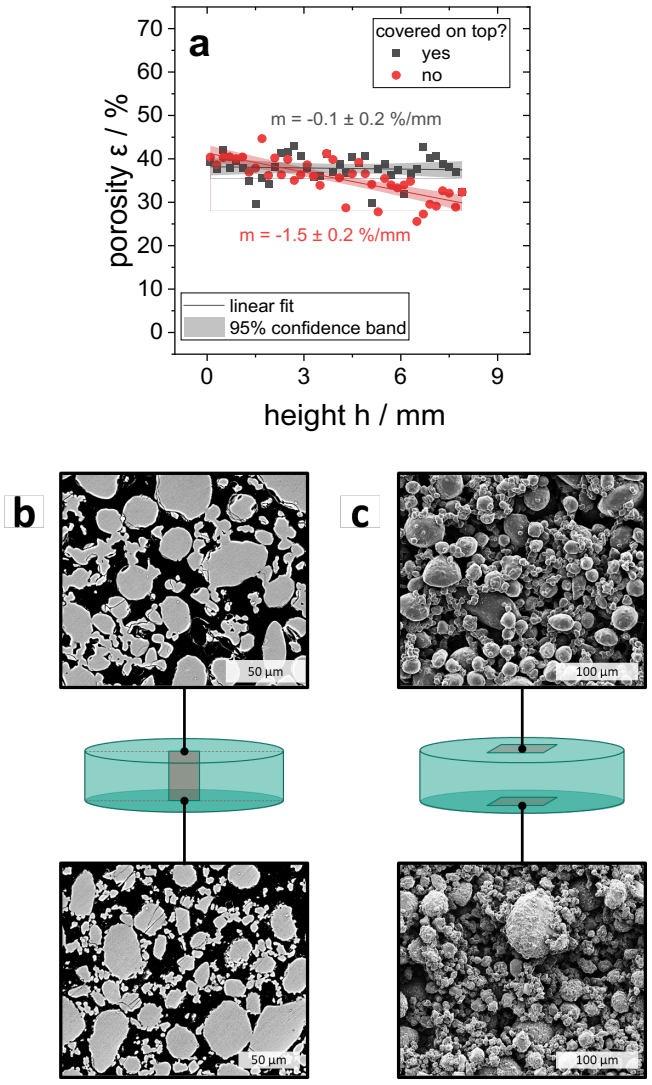

Figure 29 **Influence of covering the top of cylindrical glass filter during sintering on the extent of porosity gradient and the particle structure of such covered samples.** (**a**) Porosity profile of the samples (Φ_{sol} = 40 vol%) over the total sample height. Quartz frits were utilized as setter (and cover) during sintering. The samples were sintered under the following conditions: r_{sin} = 4 °C/min, T_{sin} = 745 °C, $t_{hold,sin}$ = 3 min. (**b**) and (**c**) show the particle structure of the covered sample analyzed using SEM. (**b**) SEM cross-sectional images of the particle structure at the upper and lower edge region. (**c**) SEM surface images of the superfacial particle structure at the top and bottom of the cylindrical sample.

transferred into the sample from the top and consequently there is higher sintering activity at the top than at the bottom.

In conclusion, the magnitude of the porosity gradient can be effectively controlled by regulating the sintering conditions. In particular, several key factors have been identified that influence the formation of this gradient. Reducing the residence time in the sintering furnace, which can be achieved by decreasing the holding time or increasing the heating rate, as well as lowering the sintering temperature have a significant effect on reducing the development of the porosity gradient. Moreover, the selection of sintering setters with thermal properties similar to those of the sintered body can also contribute to mitigating the extent of the gradient. This compatibility ensures more uniform heat distribution during the sintering process. In addition, measures such as shielding the sintered body from direct exposure to heat sources play a positive role in further minimizing the extent of the porosity gradient.

5 Manufacturing of asymmetric glass membrane

Asymmetric membranes offer a unique combination of high filtration efficiency and low filtration resistance. This advantageous profile is achieved through their distinctive construction, featuring a fine-pore, thin membrane layer supported by a coarse-pore substrate beneath. This chapter introduces the manufacturing methods of asymmetric membranes made from capillary suspensions. Finally, the characteristic filter properties, including pore size, porosity and water permeability are presented and compared to their symmetric counterparts.

The challenge in the production of asymmetric membranes lies mainly in avoiding cracking in the thin layer, since this could impair the functionality of the membrane. Crack formation can be suppressed by adjusting the solids content of the capillary suspension. As shown in Chapter 4.1, a higher solids content reduces the degree of shrinkage during debinding and should therefore be preferred to suppress crack formation. Conversely, a lower solids content was found to be beneficial in this investigation. Figure 30a and Figure 30b show the surface of thin films of sintered asymmetric membranes prepared from pastes with different solids contents. While the sample with Φ_{sol} = 30 vol.% shows many agglomerates and defects, the sample with Φ_{sol} = 20 vol.% shows a more homogeneous, nearly crack-free surface. These agglomerates are attributed to insufficient homogenization during paste

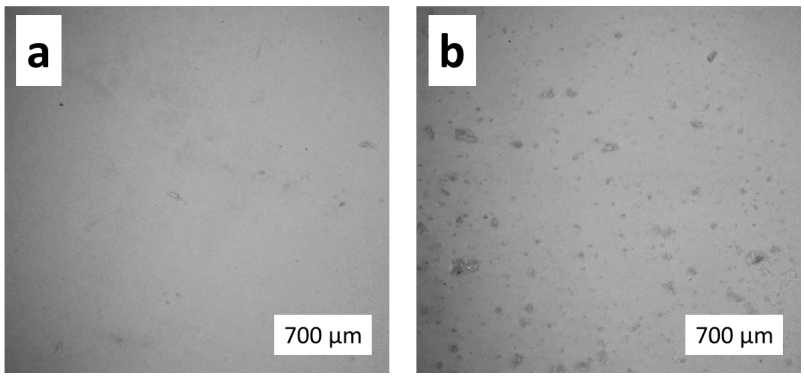

Figure 30 **Surface quality of the thin film in sintered asymmetric membranes.** The thin films were produced from capillary suspensions using glass powder F2 with a solids content of Φ_{sol} = 20 vol% and a secondary fluid content of Φ_{sec} = 3 vol% (**a**), and with a solids content of Φ_{sol} = 30 vol% and a secondary fluid content of Φ_{sec} = 5 vol% (**b**).

preparation due to the higher yield stress of the capillary suspension paste with Φ_{sol} = 30 vol% compared to that with Φ_{sol} = 20 vol%. From these remaining agglomerates, cracks can easily propagate. Crack formation can also be controlled by the thickness of the wet film during coating, since they nucleate spontaneously only above a critical film thickness [42,46,123]. Figure 31a – Figure 31c show that the extent of cracking is more pronounced in samples with higher wet film thickness. The cracks started radially from the edge to the center. The critical wet film thickness for the glass particle paste with Φ_{sol} = 20 vol.% used here is approx. 0.3 mm, below which no cracks are observed.

Using the same material for both the support layer and the thin active layer in asymmetric membrane manufacturing, as implemented in this study, may reduce the risk of cracking during high-temperature processes such as debinding and sintering. Thermal stresses often result from mismatched expansion coefficients between different materials, leading to cracking, delamination, or other defects [47]. A uniform material ensures uniform thermal expansion, minimizing internal stresses and improving structural stability. This might improve not only the reliability of the manufacturing process, but also the long-term durability

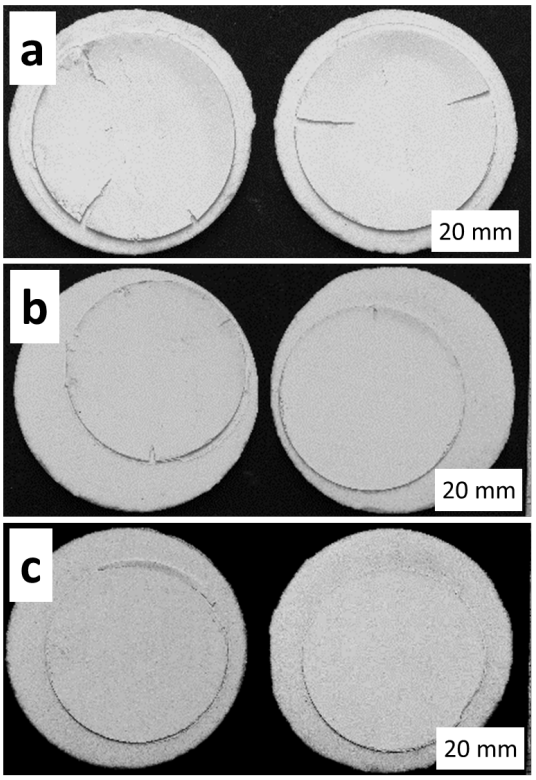

Figure 31 **Crack formation in the thin film of sintered asymmetric membranes:** (**a**)–(**c**) illustrate the quality of the fine-pored, thin filtration layer produced from a paste with a solids content of Φ_{sol} = 20 vol% and a secondary fluid content of Φ_{sec} = 3 vol%, at different wet film thicknesses: 1 mm (**a**), 0.5 mm (**b**), and 0.3 mm (**c**). The wet film thickness was controlled by the stencil thickness used during substrate coating.

and performance of the diaphragm in the operating environment involving fluctuating temperatures.

The SEM cross-sectional image of the asymmetric membrane in Figure 32 shows the particle structure at the transition between the substrate and the thin layer. It is obvious that there is a clear separation between the two layers and the fine particles do not penetrate the coarse-pored underlying substrate. Adsorption of the fine particles in the support structure would be unfavorable since it could block the pores of the substrate. During coating processes using a metal stencil and a doctor blade, the wet film very well adhered to the surface of the porous support layer due to capillary forces resulting from the absorption of the wet film's fluids by the support layer. These capillary forces were presumably weaker than the capillary forces generated by the secondary fluids in the capillary suspension of the wet film layer, so that the particle structure in the wet film and the front between these two layers were maintained during the whole manufacturing processes. The sintering process stabilized the contact between these layers, resulting in a stable bond between the thin layer and the substrate / support layer after sintering.

The properties of the cylindrical asymmetric membrane with wet film thickness of 0.2 mm are compared with two simple filter discs (d = 42 mm, h = 5 mm), all of which were made based on capillary suspensions. The first comparison filter was made of P4 powder, which was also used for the substrate of the asymmetric membranes. The other comparison filter is manufactured using F2 powder, which came into use for the coating of the asymmetric

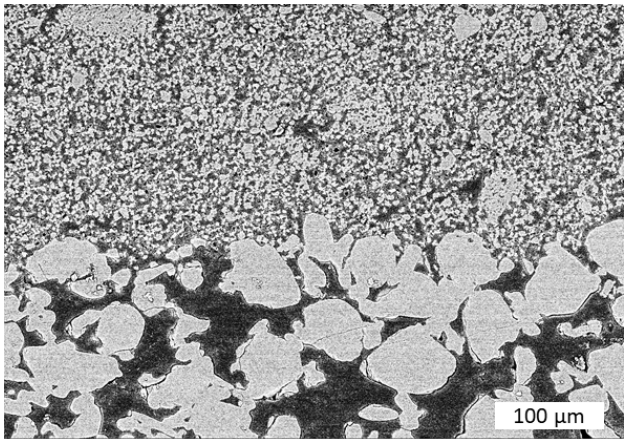

Figure 32 **Particle structure in a sintered asymmetric membrane at the transitional region between the thin membrane layer and the substrate.** The SEM cross section image shows the central section of a cylindrical asymmetric membrane sample. The loose pore structure at the bottom represents the substrate, which was made using glass powder P4, while the fine-pored structure at the top half corresponds to the thin membrane layer, prepared with glass powder F2. The thin layer was prepared using a capillary suspension with a solids content of Φ_{sol} = 20 vol% and a secondary fluid content of Φ_{sec} = 3 vol%. The substrate was prepared using a capillary suspension with a solids content of Φ_{sol} = 35 vol% and a secondary fluid content Φ_{sec} = 5 vol%.

Table 3 **Filtering properties of asymmetric membranes (AM).** Comparison of the asymmetric membrane (AM) with the P4 and F2 filters, which were designed to represent the substrate and thin layer of AM, respectively. Both the thin layer of the asymmetric membrane and the F2 filter were prepared using a capillary suspension with a solids content of Φ_{sol} = 20 vol% and a secondary fluid content of Φ_{sec} = 3 vol%. The substrate of the asymmetric membrane and the P4 filter were prepared using a capillary suspension with a solids content of Φ_{sol} = 35 vol% and a secondary fluid content Φ_{sec} = 5 vol%.

	P4 Filter	F2 Filter	AM
Pore size d_{pore}/ µm	15.5 ± 1.6	1.2 ± 0.1	1.0 ± 0.1
Open porosity ε_o / %	43 ± 1	54 ± 1	40 ± 1
Specific permeability $\varkappa$ / 10^{-15} m^2	1556 ± 56	49 ± 1,4	150 ± 95

membranes. The compositions and sintering conditions of the respective comparison filters were based on the sintering conditions used to produce the respective layers in the asymmetric membrane to be compared. Thus, both comparison filters are to represent the substrate and the thin layer, respectively. The asymmetric membrane combines the filter properties of the respective layers. In Table 3 it is obvious that the pore size of the asymmetric membrane is similar to that of the F2 filter. The porosity, on the other hand, is similar to that of the P4 filter. So overall, the pore size and porosity of asymmetric membrane are controlled by the thin film and substrate, respectively. The bubble point method used to measure the pore size is sensitive to detect cracks in the filter. Thus, the similarity of the pore size of the asymmetric membrane and the F2 filter also implies that the thin layer is crack free. In general, the specific permeability depends strongly on the pore size. The small pore size of the F2 filter results also in a low specific permeability. Contrastingly, the specific permeability of the asymmetric membrane with similar pore size is about 3 times higher. To conclude, a significant increase in permeability can be achieved with the asymmetric structure while maintaining the same pore size.

6 Filter & Filtration

6.1 Filter properties

Filter properties such as porosity, pore size, and flexural strength are critical to the efficiency and reliability of filtration processes. Porosity represents the volume of voids within the filter, which facilitates fluid flow. Higher porosity increases flux by providing more pathways for fluid passage. Pore size primarily determines the filter's cut-off point and filtration efficiency, directly influencing its ability to retain particles of a specific size while maintaining adequate flux. To ensure effective filtration, the pore size must be appropriately matched to the particle size of the material being filtered. Filtration pressure serves as the driving force for the process, overcoming both the filter's inherent resistance and the additional resistance caused by particle accumulation. This pressure acts tangentially to the filter surface, making the flexural strength of the filter essential to maintaining structural integrity under operating conditions. Proper alignment between filtration pressure and the filter's flexural strength ensures that the filter can withstand the applied forces while efficiently retaining particles and allowing fluid flow. The interplay of porosity, pore size, filtration pressure, and flexural strength is fundamental to designing filters capable of achieving optimal filtration performance and durability.

Measuring pore size in porous materials can be accomplished through various techniques, including mercury porosimetry, image analysis from cross-sections of porous samples, and the bubble point method (see Chapter 3.2). While mercury porosimetry and image analysis provide pore size distributions, the bubble point method yields only a specific pore size value. In Figure 33, a comparison of pore size measurements obtained using these three methods is presented. Notably, the pore size determined via the bubble point method closely aligns with the average pore size at Q_3 = 50 % determined by mercury porosimetry. This concurrence can be attributed to the working principle of these methods, which relies on capillary intrusion. Thus, the pore size measured here corresponds to the size of the pore neck at its narrowest point. Furthermore, both methods measure the sizes of open pores, since only open pores can be intruded by mercury or air for mercury porosimetry and the bubble point method, respectively. However, there is a distinction: the bubble point method measures the pore size at the surface, whereas the pore size from mercury porosimetry corresponds to the average size of open pores throughout the entire sample. In contrast, the pore size determined using image analysis via the line intercept method is significantly larger than the values obtained through the other techniques. This discrepancy is due to the fact that the pore size measured here corresponds to the average size of pores throughout

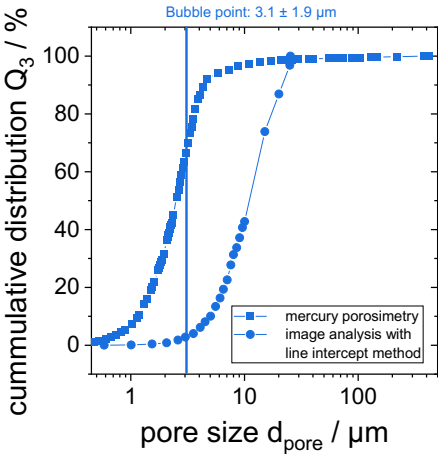

Figure 33 **Comparison of pore sizes determined using different measurement methods.** The three methods employed include bubble point, mercury porosimetry, and image analysis using the line intercept method. The samples were prepared from a capillary suspension with a solids content of Φ_{sol} = 20 vol% and a secondary fluid content of Φ_{sec} = 3 vol%. Sintering of the samples was performed at a temperature of T_{sin} = 670 °C with a heating rate of r_{sin} = 4 °C/min and a holding time of $t_{hold,sin}$ = 3 min.

the entire pore volume, encompassing not only the dimensions of pore necks but also the broader pore bodies. Additionally, this method measures pores within the sample, not only on the surface, and accounts for both open and closed pores. For filtration applications, both mercury porosimetry and the bubble point method are advantageous for pore size determination. They provide valuable insights into open pores, which allow the flow of liquids, and into the dimensions of pore necks, a critical factor in a filter's retention behavior.

To investigate the influence of pore structure on filter properties, the characterization of filters made from three different glass powders (P5, P5+30F2 and F2) was conducted (see Figure 34). The filters are named after the glass powder used. It is to be noted that all filter discs used in the characterization of the filter properties were sintered with a quartz frit as sintering setter and covered with a quartz frit during sintering, according to the setup in Figure 14b, to obtain porosity-gradient-free filter discs. Figure 34a shows the dependence of the pore size determined using the bubble point method on the open porosity. The difference in porosity for filters made from the same glass powder is induced by varying the sintering temperature. The pore size shows a strong dependence on the particle diameter of the glass powder used, with larger particles giving larger pore sizes. However, the pore size hardly depends on the porosity and hence on the sintering temperature for ε_o ranging from 10% to 50%. Based on this, it can be deduced that as the sintering temperature is raised, and consequently, the densification process is accelerated, the formation of sintering necks increases. This leads to more open pores becoming enclosed and transitioning into closed pores, which are no longer accessible to liquids. However, this transition doesn't

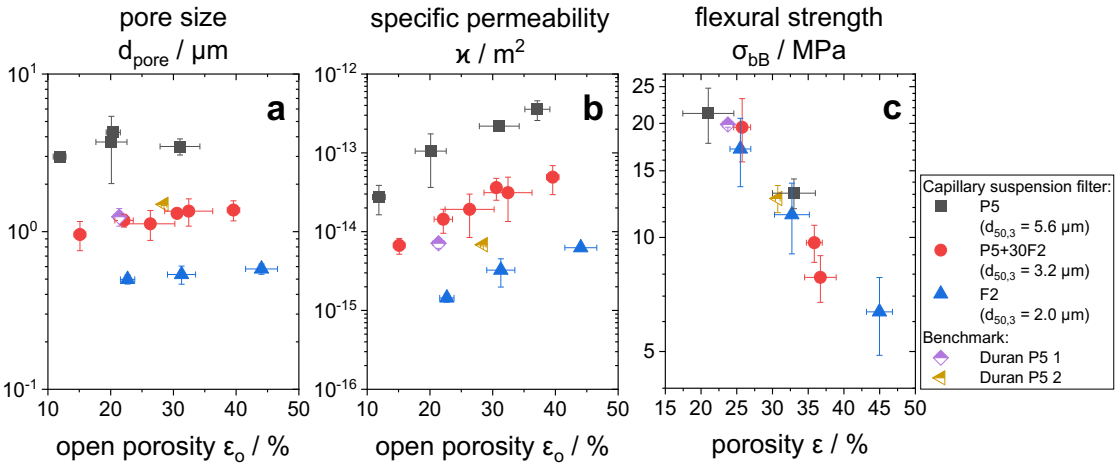

Figure 34 **Glass filter properties**. Pore size d_{pore} (**a**), specific permeability ϰ (**b**) and coaxial double ring flexural strength σ_{bB} (**c**) as a function of open porosity ε_o. All glass filter sample based on capillary suspensions had an initial solids content of Φ_{sol} of 40 vol% and were sintered with r = 4 °C/min and t_{hold} = 15 min. The sintering temperature was varied between T_{sin} = 690 °C-750 °C.

significantly alter the size of the remaining accessible open pores, which explains the constant behavior of pore size as open porosity decreases.

The specific permeability (ϰ) is a critical filter parameter that is closely related to the particle structure and is normalized to the filter thickness. For filters made of the same glass powder, permeability decreases with decreasing porosity. This confirms the previous conclusion regarding the open-to-closed pore transition at high sintering temperatures. As a consequence, there are fewer voids available for fluid flow, resulting in lower permeability. In addition, the permeability is also influenced by the particle size of the glass powder and thus the pore size. For a given open porosity, larger pores have a lower specific hydrodynamic resistance, allowing easier fluid flow through the pores, resulting in higher permeability. Figure 34c shows the dependence of the double ring bending strength on the porosity. The flexural strength decreases with increasing porosity independent of the particle size used and thus of the pore size. Due to the opposing effects of porosity, filters have to be designed according to the desired application. Porosity should be as high as possible to achieve a good permeability, but on the other hand porosity must be limited to a level still providing sufficient mechanical strength depending on the point of use.

6.2 Filtration tests

The filtration mechanism, efficiency and performance depend not only on the filter properties but also on the operating filtration condition and interaction of particle-fluid-filter material system [124–127]. Therefore, conducting filtration tests is crucial in the development and evaluation of filters. Table 4 lists all tested simple filter discs along with their manufacturing parameters and filter properties. All symmetrical filter discs used in the filtration tests were sintered with a quartz frit as sintering setter and covered with a quartz frit during sintering, according to the setup in Figure 14b, to obtain porosity-gradient-free filter discs. Three types of glass powders (P5, P5+30F2 and F2) were used and the porosity was adjusted by varying the sintering temperature. For a given powder this does not affect the pore size as already discussed above (see Figure 34a). In addition to the uniform filter discs, the asymmetric membrane (AM) listed in Table 3 as well as two commercial filters Duran P5_1

Table 4 **Overview of glass filters used in the filtration tests**. All capillary suspension-based filters were manufactured with Φ_{sol} = 40 vol% and sintered with r = 4 °C/min and t_{hold} = 3 min. Data for two commercial filters Duran P5_1 and Duran P5_2 are also included.

Filter	Manufacturing parameters		Filter properties			
	Glass powder	Sintering temperature	Pore size	Open porosity	Specific permeability	Flexural strength
		T_{sin} / °C	d_{pore} / µm	ε_o / %	$\varkappa$ / 10^{-15} m^2	σ_{bB} / MPa
P5_E715/3	P5	715	3.5 ± 0.5	32 ± 3	218 ± 23	13.1 ± 1.2
P5_E750/3	P5	750	3.4 ± 1.1	15 ± 3	66 ± 15	21.2 ± 3.5
P5+30F2_S710/3	P5+30F2	710	1.4 ± 0.2	40 ± 1	49 ± 10	6.5 ± 1.1
P5+30F2_S725/3	P5+30F2	725	1.4 ± 0.3	32 ± 3	31 ± 18	9.7 ± 1.1
P5+30F2_S735/3	P5+30F2	735	1.2 ± 0.3	22 ± 1	14 ± 1	19.5 ± 3.7
F2_S710/3	F2	710	0.5 ± 0.1	22 ± 2	1.5 ± 0.2	17.1 ± 3.5
Duran P5 1			1.2 ± 0.2	21 ± 1	31.3 ± 17.8	19.9 ± 0.3
Duran P5 2			1.5 ± 0.1	29 ± 1	6.8 ± 0.3	12.7 ± 1.0

and Duran P5_2 were also tested. Turbidity measurements of the filtrate were performed during filtration.

Turbidity data from dead-end filtration experiments using different types of filters are presented in Figure 35. Lower turbidity of the filtrate indicates that more particles were separated by the filter. It should be noted that the three particle types tested have different concentrations, as already shown in Table 2. Irrespective of that, complete retention of the particles is to be assumed for a filtrate turbidity of less than 1 ntu, considering the measurement inaccuracy of the turbidity device of approx. ± 0.5 ntu.

All filters tested show good separation efficiency for filtering the PS1 particles. For MSB particles, only filter types P5+30F2, F2 and AM showed good separation efficiency and were able to reliably separate the particles. Partial filtration was observed for both P5 filters, which could be explained by the larger pores of P5 compared to the size of MSB particles. In addition, MSB particles are elongated deformable objects, thus they can easily squeeze through the pores and could additionally impair the separation efficiency for filtration using P5 filters. Similar results can be seen for the PS0.5 particle type, where partial retention occurred only for both P5 filters. In this case, the rigid PS0.5 particles are much smaller than the pores of the P5 filters. The pore size of the P5 filters is approximately nine times the particle diameter of PS0.5, resulting in only partial separation of the particles. Since the pores of the P5 filters are larger compared to the size of all the particles tested, it can be assumed that these particles were separated by depth filtration, where the particles are deposited on the pore walls inside the filter, rather than by sieving or cake formation on the surface of the filter. In depth filtration, the difference in porosity also affects the separation efficiency. Filter P5_E750/3 with an open porosity of ε_o = 15% could retain particles better

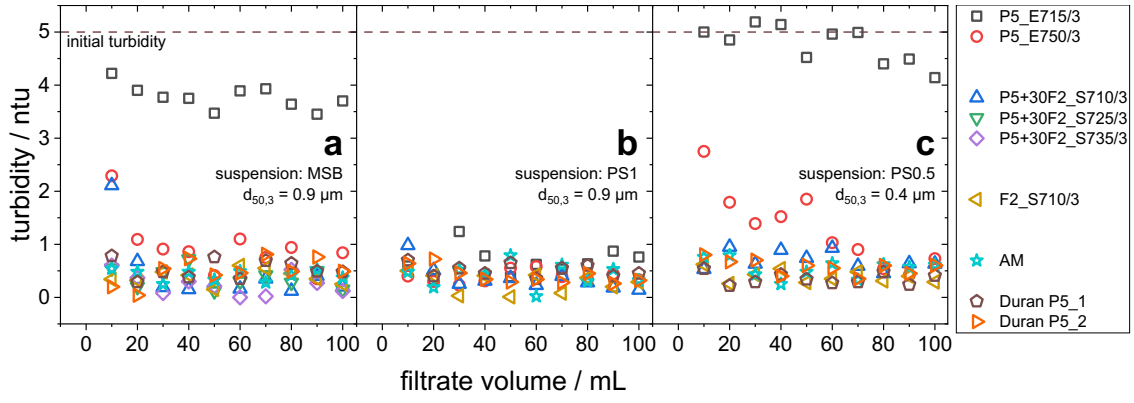

Figure 35 **Separation efficiency of glass filter.** Turbidity of filtrate from filtration tests in dead-end mode using the asymmetric membrane (AM) listed in **Fehler! Verweisquelle konnte nicht gefunden werden.**, three types of symmetrical filter discs: P5, P5+30F2 and F2 and two commercial filters Duran P5_1 and Duran P5_2. The corresponding filter properties are presented in Table 4. The suspensions used for the tests were MSB (**a**), PS1 (**b**) and PS0.5 (**c**).

than P5_E715/3 with ε_o = 32% (see Figure 35a and Figure 35c). As shown in Figure 34b, permeability and flux depend on the porosity of the filter. Lower porosity, and thus lower flux, results in a longer residence time of the particles inside the filters and increases the probability of particle retention. In this case, low porosity has a positive effect on the separation efficiency of the filter.

In the following, the results of the filtration tests are shown. It should be noted that all the filters used for the filtration tests can completely retain the particles during filtration, as shown in the turbidity measurements in Figure 35. Figure 36 presents a comparative analysis of dead-end and cross-flow filtration, focusing on filters AM and F2_S710/3. It is to be noted, that both filtration configurations were performed with the same filtration pressure of 0.8 bar. The specific water permeability of AM at $\varkappa = 150 \cdot 10^{-15}$ m², is approximately 100 times higher than that of F2_S710/3 at $\varkappa = 1.5 \cdot 10^{-15}$ m². This variance in permeability is evident in the initial flux J_0 levels at the start of filtration. Following the initial flux, both

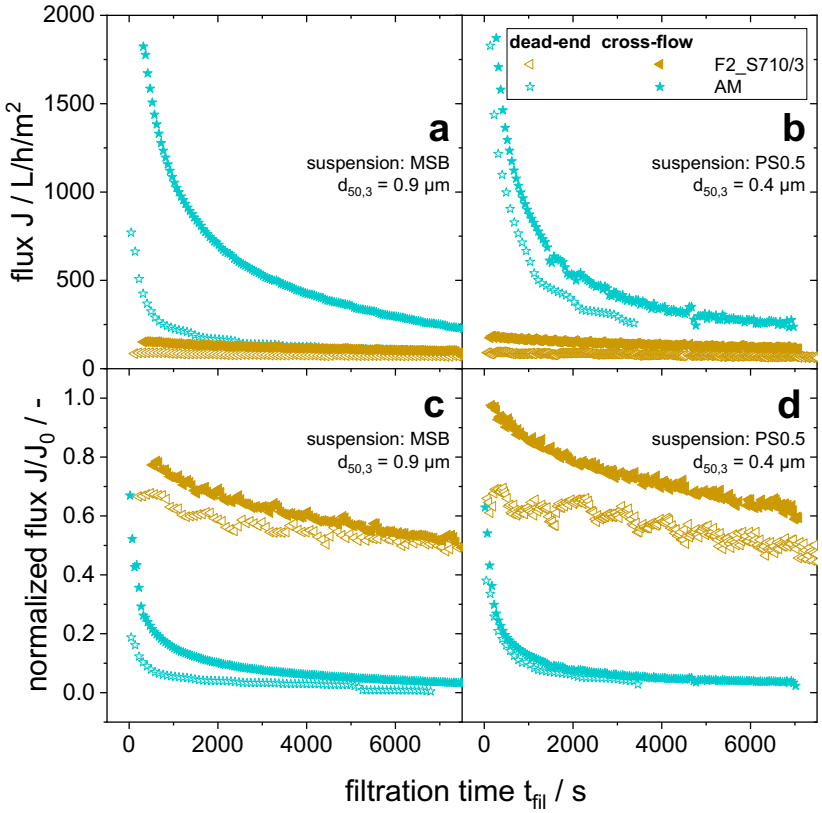

Figure 36 **Comparison of filtration performance in dead-end and cross-flow setups:** The filtrate flux is shown as a function of time during the filtration of selected filters in both dead-end and cross-flow configurations for the suspensions MSB (**a**) and PS0.5 (**b**). The normalized flux, defined as the ratio of the filtrate flux to the initial flux at the start of filtration (t_{fil} = 0 s), is shown for MSB and PS0.5 in (**c**) and (**d**), respectively. The corresponding filter properties are presented in Table 4.

filters experience a significant reduction in flux within the first 1000 s of filtration time due to fouling. The extent of flux reduction is influenced by the permeability and, consequently, the initial flux. AM, with its high permeability, exhibits a much more pronounced reduction in flux compared to F2_S710/3. Higher initial flux values result in a greater number of particles deposited on the filter within the same filtration time. This may lead to increased particle penetration into the pores or the formation of filtration cakes, thereby accelerating the rise in filtration resistance and ultimately intensifying the extent of flux reduction [128].

The dead-end configuration, characterized by a flow direction perpendicular to the filter surface, results in denser particle deposition compared to the cross-flow configuration. In the cross-flow configuration, where the flow is parallel to the filter surface, adherent particles can be efficiently flushed away. As a result, particle deposition on the filter surface is reduced, resulting in less flux reduction and consequently higher overall flux. This phenomenon is observed for both AM and F2_S710/3 filters with the MSB particle system. The AM and F2_S710/3 filters have pore sizes of 1.0 and 0.5 µm, respectively, while the MSB particles have a diameter of 0.9 µm. Since the pore sizes of AM and F2 are approximately equal to or smaller than the MSB particles, it is reasonable to assume that particles are primarily deposited on the filter surface due to a sieve effect. The cross-flow effectively sweeps the particles away from the surface, resulting in a reduced filtration resistance and a consequent increase in total flux compared to dead-end filtration.

In the case of the PS0.5 particle system, only the F2 filter shows improvement with cross-flow configuration. The AM filter shows a similar reduction in flux in both dead-end and cross-flow. PS0.5 consists of particles with a diameter of 0.4 µm, which is half the pore size of the AM filter. It can be assumed that these particles are primarily deposited within the filter pores due to interactions with the pore walls. Consequently, cross-flow does not have a significant effect. In other words, the potential for flux improvement through the use of cross-flow exists when particles are predominantly deposited on the filter surface.

Figure 37 shows the filtrate flux over time in cross-flow filtration of MSB and PS0.5 for three selected symmetrical filters (P5+30F2_S725/3, P5+30F2_S735/3, F2_S710/3) and asymmetric membrane. The initial flux depends strongly on the specific water permeability of the filter, which already discussed before. The permeability itself is directly correlated to the pore size of the filters. For instance, for both MSB and PS0.5 particle systems, filter F2_S710/3 with d_{pore} = 0.5 µm has a lower flux than filter P5+30F2_S735/3 with d_{pore} = 1.2 µm, which in turn has a lower flux than P5+30F2_S725/3 with d_{pore} = 1.4 µm. Due to its asymmetric design, the filter AM with d_{pore} = 1.0 µm has a much higher flux at the beginning of filtration than the symmetrical filter P5+30F2_S735/3, despite the same pore size. The extent of flux reduction over time due to fouling varies depending on the initial flux J_0, in accordance with the results before (see Figure 36), with higher initial flux resulting in more pronounced fouling behavior.

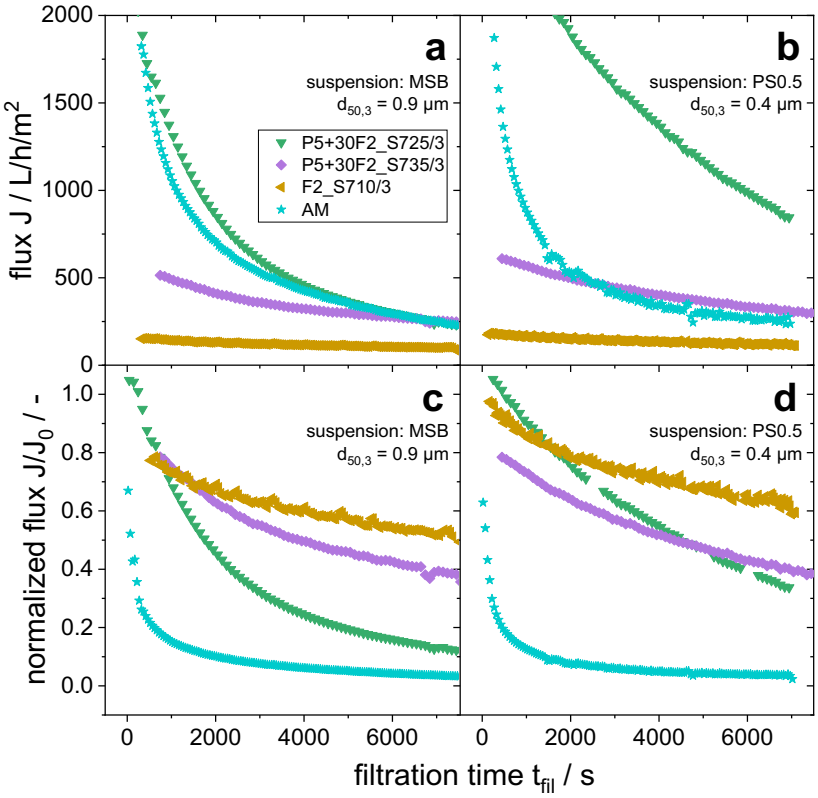

Figure 37 **Filtration performance of selected filters in a cross-flow filtration**. The filtrate flux is shown as a function of time of filters P5+30f, F2 and asymmetric membrane (AM) for the suspensions MSB (**a**) and PS0.5 (**b**). The normalized flux, defined as the ratio of the filtrate flux to the initial flux at the start of filtration (t_{fil} = 0 s), is shown for MSB and PS0.5 in (**c**) and (**d**), respectively. The corresponding filter properties are presented in Table 4.

6.3 Benchmark tests

In the glass filter market, a common and simple manufacturing method is the sintering of glass powder. As discussed in Chapter 2.2.2, this process involves pouring glass particles of various sizes—depending on the desired pore size—into molds. The particles may be compacted into tablets to create a denser pore structure, particularly for filters with smaller pores. The molded glass powder is then subjected to a controlled heating process, causing the glass grains to soften and sinter together at their contact points. Benchmark tests have been conducted to compare glass filters produced by the so-called dry processing route with filters made from capillary suspensions. The purpose of this comparative analysis is to objectively evaluate the filter characteristics and overall filtration performance of capillary suspension glass filters in comparison to similar products available on the market.

In Figure 34 the characteristic specifications of glass filters made from three different glass powders P5, P5+30F2 and F2 using the capillary suspension based wet processing route are compared to two commercial glass filters Duran P5_1 and Duran P5_2 with different porosity (see Table 4) fabricated using a dry processing route. The two benchmark filters were made from the powder P5 also used in this work. Figure 34a shows that the capillary suspension based processing route yields a higher pore size compared to the commercial glass filters. On average, the P5 filters made from capillary suspensions have 2.5 times larger pore size. The effect of the larger pore size can be seen in the separation efficiency (Figure 35). For MSB and PS0.5 particle types, the benchmark filters showed a better separation

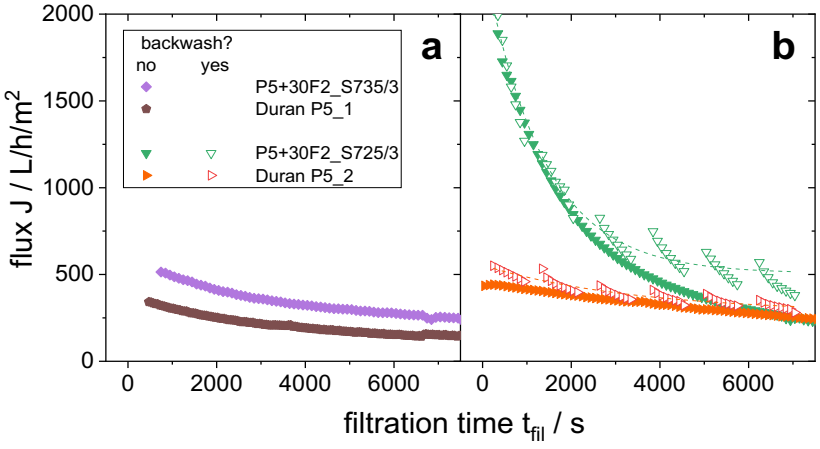

Figure 38 **Comparison of filtration curves of commercial products with filters based on capillary suspensions.** Cross flow filtration of MSB was performed. Each graph shows pairwise the evolution of the flux over time and each pair of compared filters features similar open porosity and pore size: (**a**) P5+30F2_S735/3 & Duran P5_2 – $d_{pore} \approx 1.2$ µm, $\varepsilon_o \approx 21\%$; (**b**) P5+30F2_S725/3 & Duran P5_1 – $d_{pore} \approx 1.5$ µm, $\varepsilon_o \approx 30\%$. For P5+30F2_S725/3 and Duran P5_1, filtration experiments with backwash were conducted. The dotted line represents the exponential curve fitting of the filtration data with backwash.

efficiency and resulted in a lower filtrate turbidity in comparison to P5 filters. However, the larger pore size consequently manifests in the higher permeability. At the same porosity, the specific permeability of the P5 filters is approximately a decade higher than that of the benchmark filters (Figure 34b). In terms of flexural strength, the capillary suspension filters do not differ from the benchmark filters (Figure 34c), as expected, the flexural strength depends only on the porosity and not on the pore size or manufacturing method used.

Next, the P5+30F2_S735/3 filter is compared with the benchmark Duran P5 1 filter. Table 4 indicates that the two filters have similar porosity ($\varepsilon_o \approx 21\%$) and pore size ($d_{pore} \approx 1.2$ µm). Due to the same porosity, the two filters also share the same flexural strength. Nevertheless, the P5+30F2_S735/3 filter has twice the specific permeability of the benchmark filter, which is also reflected in the filtration performance, as shown in Figure 38a. In cross-flow filtration of the MSB suspension, the capillary suspension filter exhibits a flux almost 2 times higher than the benchmark filter over the entire filtration time. The difference in filtration performance between capillary suspension and benchmark filters is more evident at a higher porosity. Figure 38b compares the P5+30F2_S725/3 and Duran P5 2 filters, both with $\varepsilon_o \approx 30\%$. Despite similar porosity and pore size ($d_{pore} \approx 1.5$ µm), the specific permeability of the capillary suspension filter is approximately 4.5 times higher. This is also reflected in the significantly high flux of the capillary suspension filter in cross flow filtration. Further filtration tests with backwash conducted on the P5+30F2_S725/3 and Duran P5_2 filters provided additional evidence of the capillary suspension filter's enhanced flux performance relative to the commercial counterpart.

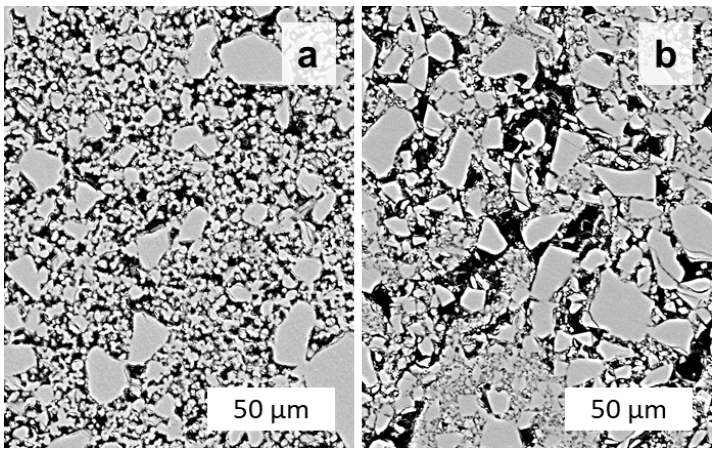

Figure 39 **Comparison of the microstructure of commercial products with filters based on capillary suspensions.** Scanning electron microscopy (SEM) cross-section images of filters P5+30F2_S725/3 (**a**) and Duran P5_1 (**b**) reveal the differences in pore structure between the two filters.

The strong difference in the filtration performance could be associated with the microstructure of the filters itself (see Figure 39a and Figure 39b). The capillary suspension filter shows more uniform pore structure compared to the benchmark filter, which is assumed to contribute to the higher permeability and flux during filtration. Similar results regarding the difference in permeability have also been reported in a previous study [2]. In summary, the use of the capillary suspension method to produce glass filters has demonstrated significant improvements in filtration performance while maintaining constant filter properties, including pore size and porosity, compared to benchmark filters. This result underscores the competitive advantage of capillary suspension glass filters.

7 Conclusion

This study focused on the development of borosilicate glass 3.3 filters based on capillary suspensions. The first part of the study investigated critical aspects of the manufacturing process, including the shrinkage behavior of green bodies, the control of porosity gradients during sintering, and the impact of material composition and sintering parameters on the pore structure of the final filters. Based on these findings, glass filter discs were produced, exhibiting minimal shrinkage and a uniform pore structure free of porosity gradients. In the second part, these filters underwent comprehensive characterization and testing.

The use of capillary suspensions significantly reduced shrinkage during the debinding process, resulting in a 20% decrease compared to green bodies produced from conventional pure suspensions. It was observed that green bodies with higher solids content experienced less shrinkage during debinding compared to those with lower solids content. However, during the subsequent sintering process, the solids content showed no notable effect on shrinkage at a given sintering temperature. Higher sintering temperatures led to greater solidification and thus increased shrinkage, regardless of whether the suspension was pure suspension or capillary suspension. To sum up, shrinkage during both debinding and sintering could be minimized by using a lower solids content and employing lower sintering temperatures. The particle network formed in the capillary suspensions provided enhanced stability to the green bodies, leading to isotropic shrinkage in both diameter and height in disc-shaped samples, even at lower solids content. This behavior contrasts with that of pure suspensions, where low solids content resulted in anisotropic shrinkage.

Sintering conditions play a critical role in the development of porosity gradients in glass filters. Spatially uneven heat transfer to the sintered body can lead to localized variations in sintering activity, accelerating the process in specific areas and resulting in an inhomogeneous pore structure. In this study, a porosity gradient was observed under unfavorable conditions, where the top side of the sample exhibited a denser pore structure compared to the bottom. This effect is attributed to the configuration of the sintering process, in which samples were positioned relatively low in the sintering chamber, with heat predominantly radiating from the upper section of the furnace. Under severe conditions, this setup led to a porosity difference of up to 40% between the top and bottom of the samples. Longer residence times in the furnace further exacerbated the formation of these gradients. However, implementing measures to ensure more uniform heat distribution, such as shielding the samples from direct heat sources, significantly reduced the extent of the porosity gradient.

The pore architecture of filters produced from capillary suspensions can be controlled by adjusting the composition of the suspension and modifying the sintering conditions. Pore size is heavily influenced by the particle size of the glass powder, with finer particles leading to smaller pores. Porosity, on the other hand, is largely governed by the solids content and sintering parameters. Lower solids content results in a looser particle arrangement, creating a more porous structure and thus higher porosity. Conversely, higher sintering temperatures increase sintering activity, promoting densification and reducing porosity. In addition, the particle size can also be a determinant of porosity. Due to their greater surface area, smaller particles exhibit higher sintering activity under identical sintering conditions, resulting in a denser structure and lower porosity compared to their larger counterparts. The water permeability of the filters is strongly influenced by both pore size and open porosity, with larger pores and higher open porosity resulting in greater permeability. The mechanical strength of the filter, on the other hand, shows a strong dependence on porosity, but is independent of the pore size, the glass particle used and the manufacturing methods employed.

Building on the findings from the first part of the study, glass filter discs were manufactured with minimal shrinkage and no porosity gradients. These filters were subjected to comprehensive filtration tests in the second part of the study. To evaluate the performance of the capillary suspension-based glass filters, filtration experiments were conducted using *Oenococcus oeni* (MSB), a lactic acid bacterium, and spherical polystyrene particles (PS) with diameters ranging from 0.5 µm to 1 µm. The separation efficiency and filtration performance were determined by a combination of filter properties, particle characteristics, and the interaction between the particles and the filter media. Pore size proved to be a key factor in determining separation efficiency. Particles could be reliably retained when the pore size of the filter was sufficiently small. In cases where the pore size was significantly larger than the particle diameter, depth filtration occurred, with particles being trapped within the filter's internal structure. In such instances, lower filter porosity contributed to better separation efficiency, as the reduced flux allowed more particles to be retained within the filter. Additionally, MSB was more difficult to filter compared to PS of the same size due to its deformability, which allowed it to pass through pores smaller than its rigid dimensions would suggest. Filtrate flux was also closely linked to pore size, with smaller pores resulting in lower flux. When comparing dead-end and cross-flow filtration setups, cross-flow filtration resulted in higher filtrate flux, but only when particle separation occurred through surface deposition on the filter. In contrast, no significant improvement in flux was observed when particles were trapped within the filter's internal structure. By carefully tuning the pore size and porosity, capillary suspension-based glass filters with high flux at small pore sizes were successfully developed, enabling reliable filtration of both MSB and PS.

In addition to developing symmetrical glass filter discs, asymmetric membranes were produced, which demonstrated significantly enhanced permeability compared to symmetrical filters with equivalent pore size. A critical factor in the manufacturing process was the thickness of the wet film layer, as excessive thickness can lead to increased stress during the drying phase, resulting in crack formation. By optimizing the wet film thickness to 0.2 mm, crack-free membranes were successfully produced. During filtration tests, especially at the early stages, these asymmetric membranes exhibited superior performance, delivering substantially higher filtrate flux compared to their symmetrical counterparts.

Finally, a benchmarking comparison was conducted between the glass filters produced via capillary suspensions in a wet processing route and commercially available filters manufactured through a dry processing method. The capillary suspension-based filters, made from the same glass powder as the commercial benchmarks, exhibited larger pore sizes, which resulted in a higher cutoff and increased permeability due to the looser arrangement of particles. However, the most notable outcome was that capillary suspension-based filters with the same pore size and porosity as the commercial filters demonstrated significantly higher filtrate flux. This performance boost was attributed to the more uniform pore structure of the capillary suspension filters, which enhanced fluid flow and filtration efficiency.

Appendix

Table 5 Characteristic values of borosilicate glass 3.3 [61]

α		10^{-6}/K	3.3
Transformation temperature T_g		°C	525
Glass temperature at viscosities	10^{13} dPa · s	°C	560
	$10^{7.6}$ dPa · s	°C	825
	10^{4} dPa · s	°C	1260
Density at 25 °C			2.23
Young's modulus		10^{3} N/mm²	63
Poisson's ratio		μ	0.20
Heat conductivity λ at 90 °C)		W/(m K)	1.2
t_{k100}		°C	250
Logarithm of the electric volume resistance in Ω cm at	250 °C		8.0
	350 °C		6.5
Dielectric properties for 1 MHz at 25 °C	ε_r		4.6
	tan δ	10^{-4}	37
Refractive index nd (λ_d= 587.6 nm)			1473
Stress optical coefficient K		10^{-6} mm²/N	4.0
Classes of chemical stability	Water		1
	Acid		1
	Alkaline solution		2

Notations

d	Diameter
$d_{50,3}$	Volume-based median diameter
d_{pore}	Pore diameter
h	Height
J	Flux
J_0	Initial flux
l	Length
m	Slope of the linearly fitted curve
q_3	Volume density distribution
Q_3	Cumulative volume distribution
r_{deb}	Heating rate in debinding process
$r_{deb,0}$	Initial heating rate in debinding process
r_{shrink}	Volumetric shrinkage ratio
r_{sin}	Heating rate in sintering process
$r_{sin,0}$	Initial heating rate in sintering process
$r_{d,shrink}$	Diameter shrinkage ratio
$r_{h,shrink}$	Height shrinkage ratio
$r_{V,shrink}$	Shrinkage ratio
$t_{hold,deb}$	Hold time in debinding process
$t_{hold,sin}$	Hold time in sintering process
T_{deb}	Debinding temperature
T_{sin}	Sintering temperature
V	Volume

ε	Total porosity
ε_o	Open porosity
Θ	Three-phase contact angle
$\varkappa$	Specific permeability
σ_{bB}	Flexural strength
σ_y	Yield stress
Φ_{sec}	Secondary fluid content
Φ_{sol}	Solids content
Φ_{sur}	Surfactant content

bbII	Brown body II
MSB	*Milchsäurebakterien* (German for "lactic acid bacteria")
MVM	*Institut für Mechanische Verfahrenstechnik und Mechanik* (German for „Institute of Mechanical Process Engineering and Mechanics”)
PS	Polystyrene
sb	Sintered body
SEM	Scanning electron microscope

References

[1] K. Tedjokusuma, W. Lauth, N. Willenbacher, Manufacture and filtration performance of glass filters made from capillary suspensions, Separation and Purification Technology 329 (2024) 125097.

[2] J. Maurath, J. Dittmann, N. Schultz, N. Willenbacher, Fabrication of highly porous glass filters using capillary suspension processing, Separation and Purification Technology 149 (2015) 470–478.

[3] R.J. Wakeman, C.J. Williams, Additional techniques to improve microfiltration, Separation and Purification Technology 26 (2002) 3–18.

[4] R.W. Baker, Membrane technology and applications, John Wiley & Sons, 2012.

[5] A. Bottino, C. Capannelli, A. Del Borghi, M. Colombino, O. Conio, Water treatment for drinking purpose: ceramic microfiltration application, Desalination 141 (2001) 75–79.

[6] B. Han, T. Runnells, J. Zimbron, R. Wickramasinghe, Arsenic removal from drinking water by flocculation and microfiltration, Desalination 145 (2002) 293–298.

[7] T.E. Doll, F.H. Frimmel, Cross-flow microfiltration with periodical back-washing for photocatalytic degradation of pharmaceutical and diagnostic residues-evaluation of the long-term stability of the photocatalytic activity of TiO2, Water Research 39 (2005) 847–854.

[8] Y. Wang, J. Zhu, H. Huang, H.-H. Cho, Carbon nanotube composite membranes for microfiltration of pharmaceuticals and personal care products: Capabilities and potential mechanisms, Journal of Membrane Science 479 (2015) 165–174.

[9] Y. El Rayess, C. Albasi, P. Bacchin, P. Taillandier, J. Raynal, M. Mietton-Peuchot, A. Devatine, Cross-flow microfiltration applied to oenology: A review, Journal of Membrane Science 382 (2011) 1–19.

[10] H.C. van der Horst, J.H. Hanemaaijer, Cross-flow microfiltration in the food industry. State of the art, Desalination 77 (1990) 235–258.

[11] F.L. Hua, Y.F. Tsang, Y.J. Wang, S.Y. Chan, H. Chua, S.N. Sin, Performance study of ceramic microfiltration membrane for oily wastewater treatment, Chemical Engineering Journal 128 (2007) 169–175.

[12] A. Lim, Membrane fouling and cleaning in microfiltration of activated sludge wastewater, Journal of Membrane Science 216 (2003) 279–290.

[13] S.F. Anis, R. Hashaikeh, N. Hilal, Microfiltration membrane processes: A review of research trends over the past decade, Journal of Water Process Engineering 32 (2019) 100941.

[14] B. Hofs, J. Ogier, D. Vries, E.F. Beerendonk, E.R. Cornelissen, Comparison of ceramic and polymeric membrane permeability and fouling using surface water, Separation and Purification Technology 79 (2011) 365–374.

[15] F. Klocke, A. McClung, C. Ader, Direct laser sintering of borosilicate glass, 2004 International Solid Freeform Fabrication Symposium (2004).

[16] N. Bouras, M.A. Madjoubi, M. Kolli, S. Benterki, M. Hamidouche, Thermal and mechanical characterization of borosilicate glass, Physics Procedia 2 (2009) 1135–1140.

[17] M.M. Lima, R. Monteiro, Characterisation and thermal behaviour of a borosilicate glass, Thermochimica Acta 373 (2001) 69–74.

[18] D. Enke, F. Janowski, W. Schwieger, Porous glasses in the 21st century-a short review, Microporous and Mesoporous Materials 60 (2003) 19–30.
[19] A. Inayat, B. Reinhardt, J. Herwig, C. Küster, H. Uhlig, S. Krenkel, E. Raedlein, D. Enke, Recent advances in the synthesis of hierarchically porous silica materials on the basis of porous glasses, New Journal of Chemistry 40 (2016).
[20] L.C. Klein, R.H. Woodmann, Porous Silica by the Sol-Gel Process, Key Engineering Materials 115 (1995) 109–124.
[21] J. Lin, C.W. Brown, Sol-gel glass as a matrix for chemical and biochemical sensing, TrAC Trends in Analytical Chemistry 16 (1997) 200–211.
[22] P.L. Kirk, R. Craig, R.S. Rosenfels, Preparation of Sintered Pyrex Glass Filters, Industrial and Engineering Chemistry - Analytical Edition 6 (1934) 154–155.
[23] F.B. Siebers, N. Greulich, W. Kiefer, Manufacture, properties and application of open-pore sintered glasses and open-pore sintered glass-ceramics, Glastech. Ber.;(Germany, Federal Republic Of) 62:2 (1989).
[24] E. Fiume, S. Ciavattini, E. Verné, F. Baino, Foam Replica Method in the Manufacturing of Bioactive Glass Scaffolds: Out-of-Date Technology or Still Underexploited Potential?, Materials 14 (2021).
[25] H. Fu, Q. Fu, N. Zhou, W. Huang, M.N. Rahaman, D. Wang, X. Liu, In vitro evaluation of borate-based bioactive glass scaffolds prepared by a polymer foam replication method, Materials Science and Engineering: C 29 (2009) 2275–2281.
[26] L.J. Gauckler, T. Graule, F. Baader, Ceramic forming using enzyme catalyzed reactions, Materials Chemistry and Physics 61 (1999) 78–102.
[27] E. Koos, N. Willenbacher, Capillary Forces in Suspension Rheology, Science 331 (2011) 897–900.
[28] J. Dittmann, E. Koos, N. Willenbacher, Ceramic Capillary Suspensions: Novel Processing Route for Macroporous Ceramic Materials, Journal of the American Ceramic Society 96 (2013) 391–397.
[29] J. Dittmann, N. Willenbacher, Micro structural investigations and mechanical properties of macro porous ceramic materials from capillary suspensions, Journal of the American Ceramic Society 97 (2014) 3787–3792.
[30] M. Weiß, J. Maurath, N. Willenbacher, E. Koos, Shrinkage and dimensional accuracy of porous ceramics derived from capillary suspensions, Journal of the European Ceramic Society 39 (2019) 1887–1892.
[31] Z.P. Baănt, W.J. Raftshol, Effect of cracking in drying and shrinkage specimens, Cement and Concrete Research 12 (1982) 209–226.
[32] T. Shiotani, J. Bisschop, J.G.M. van Mier, Temporal and spatial development of drying shrinkage cracking in cement-based materials, Engineering Fracture Mechanics 70 (2003) 1509–1525.
[33] V. Slowik, M. Schmidt, R. Fritzsch, Capillary pressure in fresh cement-based materials and identification of the air entry value, Cement and Concrete Composites 30 (2008) 557–565.
[34] J. Yang, J. Yu, Y. Huang, Recent developments in gelcasting of ceramics, Journal of the European Ceramic Society 31 (2011) 2569–2591.
[35] T.S. Yeh, M.D. Sacks, Effect of particle size distribution on the sintering of alumina, Journal of the American Ceramic Society 71 (1988) 484.
[36] M. Pfaffinger, G. Mitteramskogler, R. Gmeiner, J. Stampfl, Thermal debinding of ceramic-filled photopolymers, Materials Science Forum 825 (2015) 75–81.
[37] D.E. García, D. Hotza, R. Janssen, Building a sintering front through fast firing, International Journal of Applied Ceramic Technology 8 (2011) 1486–1493.

[38] I. Gueven, S. Frijters, J. Harting, S. Luding, H. Steeb, Hydraulic properties of porous sintered glass bead systems, Granular Matter 19 (2017) 1–21.
[39] M.G. Kutty, S. Bhaduri, S.B. Bhaduri, Gradient surface porosity in titanium dental implants: Relation between processing parameters and microstructure, Journal of Materials Science: Materials in Medicine 15 (2004) 145–150.
[40] M.J. Suk, S.I. Choi, J.S. Kim, Y.D. Kim, Y.S. Kwon, Fabrication of a porous material with a porosity gradient by a pulsed electric current sintering process, Metals and Materials International 9 (2003) 599–603.
[41] M.H.P. Teixeira, V. Skorych, R. Janssen, S.Y.G. González, A. Noni Jr, J.B.R. Neto, D. Hotza, M. Dosta, High heating rate sintering and microstructural evolution assessment using the discrete element method, Open Ceramics 8 (2021) 100182.
[42] M. Schneider, J. Maurath, S.B. Fischer, M. Weiß, N. Willenbacher, E. Koos, Suppressing crack formation in particulate systems by utilizing capillary forces, ACS Applied Materials and Interfaces 9 (2017) 11095–11105.
[43] E.R. Dufresne, D.J. Stark, N.A. Greenblatt, J.X. Cheng, J.W. Hutchinson, L. Mahadevan, D.A. Weitz, Dynamics of fracture in drying suspensions, Langmuir 22 (2006) 7144–7147.
[44] W. Man, W.B. Russel, Direct measurements of critical stresses and cracking in thin films of colloid dispersions, Physical Review Letters 100 (2008) 198302.
[45] C. Allain, L. Limat, Regular patterns of cracks formed by directional drying of a collodial suspension, Physical Review Letters 74 (1995) 2981.
[46] K.B. Singh, M.S. Tirumkudulu, Cracking in Drying Colloidal Films, Physical Review Letters 98 (2007) 218302.
[47] B.C. Bonekamp, Preparation of asymmetric ceramic membrane supports by dip-coating, Membrane Science and Technology 4 (1996) 141–225.
[48] J.D. Musgraves, J. Hu, L. Calvez, eds., Springer Handbook of Glass, Springer, Cham, Switzerland, 2019.
[49] H. Scholze, Glass: Nature, Structure, and Properties, Springer New York, New York, NY, 1991.
[50] S.J. Ikhmayies, ed., Advances in Glass Research, 1st ed. 2023, Springer International Publishing, Cham, 2023.
[51] J.M.D. Lane, Cooling rate and stress relaxation in silica melts and glasses via microsecond molecular dynamics, Phys Rev E Stat Nonlin Soft Matter Phys 92 (2015) 012320.
[52] H. Warlimont, W. Martienssen, Springer Handbook of Materials Data, 2nd Edition, Springer International Publishing, Cham, 2018.
[53] European Commission. Joint Research Centre. Institute for Prospective Technological Studies., Best available techniques (BAT) reference document for the manufacture of glass: industrial emissions Directive 2010/75/EU: integrated pollution prevention and control, Publications Office, 2013.
[54] M.M. Smedskjaer, J.C. Mauro, R.E. Youngman, C.L. Hogue, M. Potuzak, Y. Yue, Topological principles of borosilicate glass chemistry, J Phys Chem B 115 (2011) 12930–46.
[55] H. Schaeffer, Scientific and technological challenges of industrial glass melting, Solid State Ionics 105 (1998) 265–270.
[56] Mathieu Hubert, Anne Jans Faber, On the structural role of boron in borosilicate glasses, Physics and Chemistry of Glasses-European Journal of Glass Science and Technology Part B 55 (2014) 136–158.

[57] N. Favaro, Van Houte F., European Glass Industry Review, Glass Worldwide (2011) 28–32.
[58] Willem Leendert Konijnendijk, The Structure of Borosilicate Glasses, Journal of the Ceramic Association, Japan 59 (1975) 474–481.
[59] R.H. Doremus, G.H. Sigel, Glass Science, Physics Today 47 (1994) 63–63.
[60] Schott AG, SCHOTT Technical Glasses (Physical and Technical Properties), 2007.
[61] DIN ISO 3585:1999-10, Borosilicatglas 3.3 - Eigenschaften (ISO 3585:1998), Beuth Verlag GmbH, Berlin, 1999.
[62] A. Marzocchi, F. Lachut, W.H. Willis JR., Glass Fibers and Their Use as Filter Media, Journal of the Air Pollution Control Association 12 (1962) 38–42.
[63] R.P. Donovan, Fabric filtration for combustion sources: Fundamentals and basic technology, Dekker, New York, 1985.
[64] T.M. Singh, Introduction to HEPA filtration systems, Tappi Journal 73 (1990) 123–125.
[65] A. van Wente, R.T. Lucas, Formation of Filter Materials from Glass Fibers, Ind. Eng. Chem. 48 (1956) 219–222.
[66] D. Purchas, K. Sutherland, Handbook of Filter Media, Elsevier Science, 2002.
[67] N. Lifshutz, On the 'Mean Flow' Pore Size Distribution of Microfiber and Nanofiber Webs, International Nonwovens Journal (2005) 1558925005os--1400103.
[68] G. Toquer, C. Delchet, M. Nemec, A. Grandjean, Effect of leaching concentration and time on the morphology of pores in porous glasses, Journal of Non-Crystalline Solids 357 (2011) 1552–1557.
[69] V.A. Kreisberg, T.V. Antropova, Changing the relation between micro- and mesoporosity in porous glasses: The effect of different factors, Microporous and Mesoporous Materials 190 (2014) 128–138.
[70] V.A. Kreisberg, V.P. Rakcheev, T.V. Antropova, Influence of the acid concentration on the morphology of micropores and mesopores in porous glasses, Glass Phys Chem 32 (2006) 615–622.
[71] H. Tanaka, T. Yazawa, K. Eguchi, H. Nagasawa, N. Matsuda, T. Einishi, Precipitation of colloidal silica and pore size distribution in high silica porous glass, Journal of Non-Crystalline Solids 65 (1984) 301–309.
[72] O.V. Mazurin, E.A. Poraĭ-Koshitś, N.S. Andreev, Phase separation in glass, North-Holland, Amsterdam; New York, 1984.
[73] A.M. Siouffi, Silica gel-based monoliths prepared by the sol-gel method: facts and figures, J Chromatogr A 1000 (2003) 801–18.
[74] K. Deshmukh, T. Kovářík, T. Křenek, D. Docheva, T. Stich, J. Pola, Recent advances and future perspectives of sol–gel derived porous bioactive glasses: a review, RSC Advances 10 (2020) 33782–33835.
[75] A.M.M. Santos, W.L. Vasconcelos, Properties of porous silica glasses prepared via sol–gel process, Journal of Non-Crystalline Solids 273 (2000) 145–149.
[76] K. Sumida, K. Liang, J. Reboul, I.A. Ibarra, S. Furukawa, P. Falcaro, Sol–Gel Processing of Metal–Organic Frameworks, Chem. Mater. 29 (2017) 2626–2645.
[77] L.M. Muresan, Corrosion protective coatings for Ti and Ti alloys used for biomedical implants, in: Intelligent Coatings for Corrosion Control, Elsevier, 2015: pp. 585–602.
[78] D. Bokov, A. Turki Jalil, S. Chupradit, W. Suksatan, M. Javed Ansari, I.H. Shewael, G.H. Valiev, E. Kianfar, Nanomaterial by Sol-Gel Method: Synthesis and Application, Advances in Materials Science and Engineering 2021 (2021) 1–21.
[79] S.N. Tan, W. Wang, L. Ge, Biosensors based on Sol–Gel-derived materials, (2011).
[80] G. Kickelbick, Introduction to sol-gel nanocomposites, in: Sol-Gel Nanocomposites, Springer, 2014: pp. 1–19.

[81] K. Nakanishi, R. Takahashi, T. Nagakane, K. Kitayama, N. Koheiya, H. Shikata, N. Soga, Formation of Hierarchical Pore Structure in Silica Gel, Journal of Sol-Gel Science and Technology 17 (2000) 191–210.
[82] G.J. Owens, R.K. Singh, F. Foroutan, M. Alqaysi, C.-M. Han, C. Mahapatra, H.-W. Kim, J.C. Knowles, Sol–gel based materials for biomedical applications, Progress in Materials Science 77 (2016) 1–79.
[83] B. Reinhardt, D. Enke, G. Bienhaus, Hierarchically structured silica via combination of salt sintering process and phase separation, Optica Applicata 42 (2012) 265–270.
[84] A. Inayat, B. Reinhardt, H. Uhlig, W.-D. Einicke, D. Enke, Silica monoliths with hierarchical porosity obtained from porous glasses, Chem Soc Rev 42 (2013) 3753–64.
[85] J. Vogel, C. Russel, Open-pore glasses and glass-ceramics by sintering of modified pyrogenic silicic acids, CERAMICS SILIKATY 44 (2000) 9–13.
[86] B. Reinhardt, J. Herwig, S. Rannabauer, M. Scheffler, D. Enke, Hierarchically structured glass monoliths based on polyurethane foams as template, Journal of the European Ceramic Society 34 (2014) 1465–1470.
[87] E. Boccardi, A. Philippart, J.A. Juhasz-Bortuzzo, G. Novajra, C. Vitale-Brovarone, A.R. Boccaccini, Characterisation of Bioglass based foams developed via replication of natural marine sponges, Advances in Applied Ceramics 114 (2015) 56–62.
[88] O. Bretcanu, S. Misra, I. Roy, C. Renghini, F. Fiori, A.R. Boccaccini, V. Salih, In vitro biocompatibility of 45S5 Bioglass®-derived glass–ceramic scaffolds coated with poly(3-hydroxybutyrate), Journal of Tissue Engineering and Regenerative Medicine 3 (2009) 139–148.
[89] S.C. Hu, K.S. Hwang, Dilatometric analysis of thermal debinding of injection moulded iron compacts, Powder Metallurgy 43 (2000) 239–244.
[90] K. Wang, M. Qiu, C. Jiao, J. Gu, D. Xie, C. Wang, X. Tang, Z. Wei, L. Shen, Study on defect-free debinding green body of ceramic formed by DLP technology, Ceramics International 46 (2020) 2438–2446.
[91] E. Koos, Capillary suspensions: Particle networks formed through the capillary force, Current Opinion in Colloid & Interface Science 19 (2014) 575–584.
[92] F. Bossler, Structural Investigations of Capillary Suspensions using Rheology and Confocal Microscopy, Dissertation, Karlsruher Institut für Technologie (KIT), 2018.
[93] E. Koos, J. Johannsmeier, L. Schwebler, N. Willenbacher, Tuning suspension rheology using capillary forces, Soft Matter 8 (2012) 6620.
[94] M. Weiß, P. Sälzler, N. Willenbacher, E. Koos, 3D-Printed lightweight ceramics using capillary suspensions with incorporated nanoparticles, Journal of the European Ceramic Society 40 (2020) 3140–3147.
[95] J. Maurath, N. Willenbacher, 3D printing of open-porous cellular ceramics with high specific strength, Journal of the European Ceramic Society 37 (2017) 4833–4842.
[96] T. Fuchigami, M. Toki, K. Nakanishi, Membrane Emulsification Using Sol-Gel Derived Macroporous Silica Glass, Journal of Sol-Gel Science and Technology (2000) 337--341.
[97] D. Enke, F. Friedel, F. Janowski, T. Hahn, W. Gille, R. Müller, H. Kaden, Ultrathin porous glass membranes with controlled texture properties, in: F. Rodriguez-Reinoso, B. McEnaney, J. Rouquerol, K. Unger (Eds.), Studies in Surface Science and Catalysis, Elsevier, 2002: pp. 347–354.
[98] E. Mercadelli, D. Montaleone, A. Gondolini, P. Pinasco, A. Sanson, Tape-cast asymmetric membranes for hydrogen separation, Ceramics International 43 (2017) 8010–8017.

[99] R.K. Nishihora, P.L. Rachadel, M.G.N. Quadri, D. Hotza, Manufacturing porous ceramic materials by tape casting—A review, Journal of the European Ceramic Society 38 (2018) 988–1001.
[100] T.C.A. Ng, Z. Lyu, Q. Gu, L. Zhang, W.J. Poh, Z. Zhang, J. Wang, H.Y. Ng, Effect of gradient profile in ceramic membranes on filtration characteristics: Implications for membrane development, Journal of Membrane Science 595 (2020) 117576
[101] L. Angelis, M.M.F. Cortalezzi, Ceramic membrane filtration of organic compounds: Effect of concentration, pH, and mixtures interactions on fouling, Separation and Purification Technology 118 (2013) 762–775.
[102] O. Şan, C. Özgür, Fabrication of glassy ceramic membrane filters for filtration of spring water with clogging phenomena, Journal of Membrane Science 305 (2007) 169–175.
[103] J. Kiennemann, T. Chartier, C. Pagnoux, J.F. Baumard, M. Huger, J.M. Lamérant, Drying mechanisms and stress development in aqueous alumina tape casting, Journal of the European Ceramic Society 25 (2005) 1551–1564.
[104] H. Salmang, H. Scholze, Keramik, Springer, 2006.
[105] E.M. Rabinovich, Preparation of glass by sintering, Journal of Materials Science 20 (1985) 4259–4297.
[106] M. Stevens, W.M. Carty, The role of heating rate on the sintering of glass powders, Int J of Appl Glass Sci 13 (2022) 620–628.
[107] J. Frenkel, Viscous flow of crystalline bodies under the action of surface tension, J. Phys.(USS R) 9 (1945) 385.
[108] M.N. Rahaman, Ceramic processing, Second edition, Taylor & Francis, CRC Press, Boca Raton, 2017.
[109] M. Oscar Prado, E. Dutra Zanotto, R. Müller, Model for sintering polydispersed glass particles, Journal of Non-Crystalline Solids 279 (2001) 169–178.
[110] G.W. Scherer, Sintering of Low-Density Glasses: I, Theory, Journal of the American Ceramic Society 60 (1977) 236–239.
[111] J. Mackenzie, R. Shuttleworth, A phenomenological theory of sintering, Proceedings of the Physical Society. Section B 62 (1949) 833.
[112] A. Simchi, The role of particle size on the laser sintering of iron powder, Metallurgical and Materials Transactions B 35 (2004) 937–948.
[113] W.H. Rhodes, Agglomerate and particle size effects on sintering yttria-stabilized zirconia, Journal of the American Ceramic Society 64 (1981) 19–22.
[114] C. Herring, Effect of change of scale on sintering phenomena, Journal of Applied Physics 21 (1950) 301–303.
[115] R. Wakeman, The influence of particle properties on filtration, Separation and Purification Technology 58 (2007) 234–241.
[116] S. Nakao, Determination of pore size and pore size distribution 3. Filtration membranes, Journal of Membrane Science 96 (1994) 131–165.
[117] P. H. Hermans, H. L. Bredée, Zur Kenntnis der Filtrationsgesetze, Recueil Des Travaux Chimiques Des Pays-Bas 54 (1935).
[118] J. Hermia, Etude analytique des lois de filtration à pression constante, Rev. Univ. Mines 2 (1966).
[119] A.Y. Kirschner, Y.-H. Cheng, D.R. Paul, R.W. Field, B.D. Freeman, Fouling mechanisms in constant flux crossflow ultrafiltration, Journal of Membrane Science 574 (2019) 65–75.
[120] J.C. Russ, Practical stereology, Springer, 2013.

[121] J. Dittmann, Verwendung von Kapillarsuspensionen als Precursor für die Herstellung hochporöser Sinterwerkstoffe, Dissertation, Karlsruher Institut für Technologie (KIT), 2015.
[122] J.A. Alvarado-Contreras, E.A. Olevsky, R.M. German, Modeling of gravity-induced shape distortions during sintering of cylindrical specimens, Mechanics Research Communications 50 (2013) 8–11.
[123] J. Li, A.K. Dozier, Y. Li, F. Yang, Y.T. Cheng, Crack pattern formation in thin film lithium-ion battery electrodes, Journal of the Electrochemical Society 158 (2011) 689.
[124] R. Barhate, S. Ramakrishna, Nanofibrous filtering media: Filtration problems and solutions from tiny materials, Journal of Membrane Science 296 (2007) 1–8.
[125] D. Grant, B. Liu, W. Fisher, R. Bowling, Particle capture mechanisms in gases and liquids: an analysis of operative mechanisms in membrane/fibrous filters, The Journal of Environmental Sciences 32 (1989) 43–51.
[126] J.K. Lee, Particulate retention by microporous membrane filters in liquid filtration, University of Minnesota, 1992.
[127] J.A. Destephen, K.J. Choi, Modelling of filtration processes of fibrous filter media, Separations Technology 6 (1996) 55–67.
[128] E. Aoustin, A.I. Schäfer, A.G. Fane, T.D. Waite, Ultrafiltration of natural organic matter, Separation and Purification Technology 22 (2001) 63–78.